Mathematisches Forschungsinstitut Oberwolfach

Report No. 34/2006

Mathematical Methods in Tomography

Organised by
Alfred K. Louis (Saarbrücken)
Frank Natterer (Münster)
Eric Todd Quinto (Medford)

July 30th – August 5th, 2006

Abstract. This is the seventh Oberwolfach conference on the mathematics of tomography, the first one taking place in 1980. Tomography is the most popular of a series of medical and scientific imaging techniques that have been developed since the mid seventies of the last century.

Mathematics Subject Classification (2000): 65R32 , 44A12 , 92C55.

Introduction by the Organisers

Mathematically, the original problem of tomography consisted in reconstructing a function in R^2 from the set of integrals over straight lines. This problem was essentially solved by Radon in 1917, who gave an explicit formula for a function in terms of its line integrals, the famous Radon inversion formula. The numerical implementation of Radon's inversion formula is in no way obvious. Deep results from sampling theory are needed. Also, the problem of tomography is ill-posed, meaning that the result doesn't depend continuously on the data. Besides, in many cases of practical interest the solution is not uniquely determined. Problems like this were on the agenda of the first Oberwolfach conference in 1980, and they still played a role in the present conference.

In recent years, imaging must be seen in a much broader sense. The original straight line paradigm still plays a role, but other imaging techniques based on completely different principles are nowadays at the center of interest. In particular imaging techniques based on partial differential equations play an important role. This tendency is clearly reflected by the participants and the speakers of the present conference.

One of the promising recent developments is thermoacoustic tomography. This is a combination of microwave and acoustic imaging. The object is illuminated by

microwaves. In this way tumors and other abnormalities are heated and generate pressure waves that are measured by acoustic transducers. Various mathematical, physical, numerical and applied aspects of thermoacoustic tomography are discussed in the talks of Kuchment, Agranovsky, Finch, Kunyansky, Palamodov and Patch.

Ritman's talk is dedicated to one of the classical problems in imaging: the trade off between exposure and resolution. Grünbaum's talk is an example of the application of techniques originally developed for medical imaging to completely different fields, namely the imaging on directed graphs, the underlying mathematics being Markov chains. Candès and Ramlau put sampling in tomography into the framework of wavelets, in particular the theory of sparseness. This makes it possible to reconstruct piecewise constant functions with a fraction of the data needed for general functions. Noo's and Clackdoyle's talks deal with an old problem in tomography, namely with incomplete data. Using elegant mathematics they are able so solve truncated projections and region of interest problems that were inaccessible to previous methods. Maaß applies methods of the modern theory of mathematical imaging, in particular non-convex optimization, to emission tomography. Nolan's talk is an example for imaging with the wave equation and the application of microlocal analysis to imaging. Katsevich's talk is on a problem in present day's clinical tomography, namely on true 3D reconstruction from cone beam projections. This topic is also covered in the talk of Louis, who presents a general theory of approximate inverses for problems of this type. Oeckl applies the highly successful technique of multi-resolution analysis to imaging problems from nondestructive testing. Sabatier applies a general inverse scattering transform to derive global solutions of linear pde's, and he analyzes the resolving power of electrical impedance tomography. The talks of Rieder, Faridani, Desbat and Izen are concerned with details of sampling and discretization for the filtered backprojection algorithm, which is the most important algorithm in clinical tomography. Mair's talk deals with the parameter choice in iterative algorithms for emission tomography. Another new and promising medical imaging technique is optical tomography, often referred to as molecular imaging. This topic is dealt with in the talks of Dorn, Schotland and Jiang, providing examples for imaging with the diffusion and the transport equation. The vectorial extension of tomography, with exciting applications in industry, is covered by Schuster.

Summing up, tomography is a lively branch of science with an inexhaustable supply of mathematical problems. Every new imaging modality poses new mathematical problems. The conference can be viewed as a snapshot of this lively development.

Workshop: Mathematical Methods in Tomography

Table of Contents

Abstracts

Medical X-ray CT-Resolution/Radiation Exposure Trade-offs

Erik L. Ritman

Background

X-ray imaging is a common and powerful technique for noninvasive evaluation of internal damage or disease. It is, however, a technique that has been perfected to the point where potential for radiation damage constrains its breadth of clinical utility beyond current applications. Currently x-ray images are generated by virtue of a proportion of the x-rays being stopped from passing through tissues [1]. This results in the signal being actually the absence of photons. Hence, many (may be a million) photons are needed to "illuminate" a selected location (i.e., pixel) in the body (e.g., 1 mm^2) in order to be sure that there is a certain fractional reduction in the number of transmitted photons [2]. The dilemma of current attenuation-based x-ray imaging is that the more contrast (i.e., detail) we want to have in the image the more we need to stop the x-rays, and it is the stopped x-rays that do the damage! Hence, there is tight coupling between the image quality and the radiation damage.

To put the effects of radiation into perspective, the following statistics are provided. The Gray (Gy) is the measure of absorbed dose in tissue and the Sievert (Sv) is the effective dose to the subject. The Sv takes into account radio-sensitivity of different tissues. An 0.1 Gy (10 Rad) absorbed dose [3,4] increases cancer incidence from 20 to 20.01%, and an 18 Gy dose results in tissue necrosis. Patient size, age and anatomic region, the scan protocol used, and quality of the x-ray beam, all affect the dose. Dose decreases with increased kVp and filtration, but increases with mA and number of slices (or duration of helical scan). A 64 channel helical CT scan results in 14.4 mGy for head, 23.7 mGy for coronary calcium and 58.9 mGy for coronary angiogram [5]. The effective dose in children is greater than in adults (6 mSv in the head of new-born and 1.5 mSv in the head of an adult). In 2000, 93 million CT exams were performed world wide [6].

Methods for reducing radiation exposure by attenuation-based x-ray imaging

Unfortunately, methods used for reduction of radiation exposure by current x-ray imaging have proven to be of limited impact. Methods include use of modulation of x-ray mA with angle around the patient [7], use of monochromatic, rather than bremsstrahlung radiation [8], K-edge subtraction imaging [9,10] and photon counting methods [11]. Monochromatic x-ray reduces chest effective dose by 18.7%, dose to the head by 1.2%, but intra-abdominal organs by 35-47% [12]. Imaging of different tissue components by virtue of how they scatter x-ray would increase the contrast between those tissue components [13], but it is less likely that this allows for reducing the patients' absorbed dose.

Based on increasing experience (especially with synchrotron x-ray-based imaging),

x-ray imaging based on differences in refractive index (i.e., consequences of different velocity of x-ray in different tissues) rather than attenuation, has potential for greatly decreasing the x-ray exposure needed to make useful images. There are three potential advantages of use of tissue refractive index to generate images. Foremost is that each transmitted photon is the signal (as compared to its absence in attenuation x-ray imaging), which is the basis for potential reduction of x-ray exposure. The second reason is that the greater differences in refractive index (than differences of attenuation) by the different tissues at clinical x-ray photon energies would generate images with soft tissue discrimination comparable to MRI. Finally, because of the increased inherent contrast, the need for administered contrast agents to provide useful images might also be reduced.

The x-ray photon velocity-based imaging approach, however, presents formidable technological problems. One approach is to scale up the refraction and phase contrast imaging methods, developed for small-specimen imaging, so as to be suitable for whole-body imaging. These approaches are faced, however, with the problem of "unraveling" the many changes in refraction (as expressed as a phase shift which results in a Moiré pattern) that would occur as the photon passes through some 30 cm of tissue. At 17.5 keV, 50 μm of water causes a 180° phase shift, hence for a 30 cm abdomen we would expect 6000 phase shifts! The Bonse Hart interferometer [14] has been used effectively for phase imaging of small specimens. The method involves use of a reference beam against which the beam transmitted through the object is compared. The optic path length of that beam should be stable to within 0.1 nm, another major technological problem.

Another approach involves use of an x-ray Talbot interferometer [15]. An object is imaged using coherent illumination passing through a phase grating. This approach is probably more practical in a clinical setting compared to the Bonse Hart approach. Momose et al. [16] used this method to show that 10^{-9}g/cm^3 sensitivity can be achieved in small specimens. Use of a small x-ray source instead of parallel radiation has been explored [17,18], hence this approach appears to also have potential for clinical application.

A third method is called "Diffraction Enhanced Imaging" (DEI) [19]. It generates a transmission image with edge enhancement effect caused by the slight refraction of the x-ray in regions with rapid change of refractive index, such as occurs at the surface of collagen fibers and blood vessels. Use of a "rocking curve" analysis of that signal can separate out several components of the x-ray information by virtue of the shape of the "rocking curve." This method may have potential for application to imaging the breast or limbs.

Conclusion

Clinical x-ray tomographic imaging based on tissues' x-ray refractive indices will require major technological developments and implementation of reconstruction algorithms similar to those developed for ultrasound [20]. However, the potential for increased contrast and reduced radiation may favor this option.

References

[1] D. J. Dowseth, P. A. Kenny, R. E. Johnston, *The physics of diagnostic imaging*, London, Chapman and Hall Med. (1988).

[2] J. W. Motz, M. Danos, *Image information content and patient exposure*, Med. Phys. **5** (1978), 8–22.

[3] http://srab.cancer.gov/devcan.

[4] L. K. Wagner, P. J. Eifel, R. A. Geise, *Potential biological effects following high x-ray dose interventional procedures*, J. Vasc. Interv. Radiol. **5** (1994), 71–84.

[5] J. J. DeMarco, C. H. Cagnon, D. D. Cody, D. M. Stevens, C. H. McCollough, J. O'Daniel, M. F. McNitt-Gray, *A Monte Carlo based method to estimate radiation dose from multidetector CT(MDCT): Cylindrical and anthropomorphic phantoms*, Phys. Med. Biol. **50** (2005), 3989–4004.

[6] http://www.fda.gov/cdrh/ct/risks/html.

[7] W. A. Kalender, H. Wolf, C. Seuss, M. Giess, H. Greess, W. A. Bautz, *Dose reduction in CT by on-line tube current control; principles and validation on phantom and cadavers*, Eur. Radiol. **9** (1999), 323–328.

[8] F. A. Dilmanian, *Computed tomography with monochromatic x-rays*, Am. J. Physiol. Imaging **7** (1992), 175–193.

[9] A. M. Laval-Jeantet, C. E. Cann, B. Roger, P. Dallant, *A post processing dual energy technique for vertebral CT densitometry*, J. Comput. Assist. Tomogr. **8** (1984), 1164–1167.

[10] E. Rubenstein, R. Hofstadter, H. D. Zeman, A. C. Thompson, J. N. Otis, G. S. Brown, J. S. Giacomini, H. J. Gordon, R. S. Kerkhoff, D. C. Harrison, W. Thomlisson, *Transvenous coronary angiography in humans using synchrotron radiation*, Proc. Natl. Acad. Sci. USA **83** (1986), 9724–9728.

[11] P. M. Shikhaliev, T. Xu, H. Le, S. Molloi, *Photon counting, decrease noise, energy resolution*, Med. Phys. **31** (2004), 1061–1071.

[12] P. Baldelli, A. Taibi, A. Tuffanelli, M. Gambaccini, *Dose comparison between conventional and quasi-monochromatic systems for diagnostic radiology*, Phys. Med. Biol. **49** (2004), 4135–4146.

[13] J. P. Schlomka, J. Delfs, H. Barschdorf, A. Thran, U. van Stevendaal, *Experimental feasility study of energy-resolved fan-beam coherent scatter computed tomography*, In: Developments in X-ray Tomography IV, U. Bonse (ed). Proc SPIE **5535** (2004), 410–423.

[14] F. Beckman, U. Bonse, F. Busch, O. Gunnewig, *X-ray micro tomography (mCT) by phase contrast for the investigation of organic matter*, J. Comput. Assist. Tomogr. **21** (1997), 539–553.

[15] T. Weitkamp, A. Diaz, B. Nohammer, F. Pfeiffer, T. Rohbeck, P. Cloetens, M. Stampanoni, C. David, *Hard x-ray phase imaging and tomography with a grating interferometer*, In: Developments in X-Ray Tomography IV, U. Bonse (ed). Proc SPIE **5535** (2004), 137–142.

[16] A. Momose, S. Kawamoto, I. Koyama, *Phase tomography using an x-ray Talbot interferometer*, In: Developments in X-Ray Tomography IV, U. Bonse (ed). Proc SPIE **5535** (2004), 352–360.

[17] T. E. Gureyev, C. Raven, A. Snigirev, I. Snigireva, S. W. Wilkins, *Hard x-ray quantitative non-interferometric phase-contrast microscopy*, J. Phys. D: Appl. Phys. **32** (1999), 563–567.

[18] T. Davis, D. Gao, T. Gureyev, A. Stevenson, S. Wilkins, *Phase contrast imaging of weakly absorbing materials using hard x-rays*, Nature **373** (1996), 335–338.

[19] M. O. Hasnah, C. Parham, E. D. Pisano, Z. Zhong, O. Oltulu, D. Chapman, *Mass density images from diffraction enhanced imaging technique*, Med. Phys. **32** (2005), 549–552.

[20] J. F. Greenleaf, S. A. Johnson, A. H. Lent, *Measurement of spatial distribution of refractive index in tissues by ultrasonic computer assisted tomography*, Ultrasound Med. Biol. **3** (1978), 327–339.

An inverse problem for multiterminal networks

F. Alberto Grünbaum

1. The inverse problem

All the networks that we consider are instances of directed graphs. Let $G = (V, E)$ be a directed graph with node set V and directed-edge set E. Let I be the set of sources of D, O its set of sinks, and $Ht = E\backslash(I \cup O)$, the set of "intermediate" or "hidden" nodes. We think of each node of G as a state in a Markov chain, and call the elements of I input terminals, the elements of O output terminals, and the elements of H intermediate terminals. To each directed edge (a, b) of G, we associate an indeterminate $p_{(a,b)}$. This indeterminate represents the one-step transition probability of going from terminal a to terminal b. We refer to these graphs as "multi-terminal networks".

We consider four matrices P_{IO}, P_{IH}, P_{HH} and P_{HO}. The rows of P_{IO} are indexed by the input terminals, its columns are indexed by the output terminals, and the a, b entry of P_{IO} is $p_{(a,b)}$ if (a, b) is a directed edge in G. All other entries are zero. The other matrices are defined analogously and either rows or columns (or both) are indexed by the hidden terminals. These matrices are the blocks in the one-step transition probability matrix of our Markov chain. We allow for all input and hidden terminals to be *absorbing states*, that is, we do not insist that the sum $\sum_b p_{(a,b)}$ be unity when a is either an input or an intermediate terminal.

We consider the problem of recovering the matrices P_{IO}, P_{IH}, P_{HH} and P_{HO} from the distribution of a random variable called "travel time" for **any pair** made up of an input and an output terminal. If we had access to the complete distribution of this *collection of* random variables we would have access to the matrices $\delta_1 = P_{IO}$, $\delta_2 = P_{IH}P_{HO}$, $\delta_3 = P_{IH}P_{HH}P_{HO}, \ldots \delta_j = P_{IH}P_{HH}^{j-2}P_{HO}, \ldots$. These matrices give the probability of making a transition in one, two, three,.. units of time from an arbitrary input terminal to an arbitrary output terminal. Notice that, under appropriate conditions, this information is mathematically equivalent to the knowledge of the *moments* of "travel time", which are given by the matrices $Q_{IO}^{(j)} = P_{IO} + \sum_{m=0}^{\infty}(m+2)^j P_{IH}P_{HH}^m P_{HO}$. From a practical standpoint, a few of the moments $Q_{IO}^{(j)}$ can be measured, but measuring the matrices δ_j may not be practical.

In view of this we will take the position that the only available information are the zero-th and first order moments of "travel time". We compute now these two moments in terms of our *unknowns*

$$P_{IO}, P_{IH}, P_{HH}, P_{HO}.$$

From the definition of the zero-th moment of travel time we obtain (after an appropriate summation of the corresponding geometric series) the following expression for $Q_{IO} \equiv Q_{IO}^{(0)}$:

$$Q_{IO} = P_{IO} + P_{IH}(I - P_{HH})^{-1}P_{HO}, \tag{1}$$

where I is the identity matrix.

If we denote the expression

$$P_{IH}(I - P_{HH})^{-2}P_{HO}$$

by R, then one can see that the first moment of the "travel time" can be expressed as

$$Q_{IO} + R.$$

Proof. Recall that the j-th moment of the travel time is given by

$$Q_{IO}^{(j)} = P_{IO} + \sum_{k=0}^{\infty} P_{IH}P_{HH}^{k}P_{HO}(k+2)^{j}.$$

For $j = 1$ we get

$$\begin{aligned} Q_{IO}^{(1)} &= P_{IO} + 2P_{IH}(I - P_{HH})^{-1}P_{HO} + P_{IH}P_{HH}(I - P_{HH})^{-2}P_{HO} \\ &= Q_{IO}^{(0)} + P_{IH}(I - P_{HH})^{-2}[I - P_{HH} + P_{HH}]P_{HO} \\ &= Q_{IO}^{(0)} + R. \end{aligned}$$

□

Since Q_{IO} is taken as data we can consider R as the extra information provided by the expected value of travel time.

In a number of papers mentioned below we have explored the general program outlined above.

References

[1] M. Muster, *Computing certain invariants of topological spaces of dimension three*, Topology **32** (1990), 100–120.

[2] M. Muster, *Computing other invariants of topological spaces of dimension three*, Topology **32** (1990), 120–140.

[3] F.A. Grünbaum, *Tomography with diffusion*, in "Inverse Problems in Action", P. C. Sabatier (ed.), Springer-Verlag, Berlin, pp. 16–21.

[4] F.A. Grünbaum, *Diffuse tomography: The isotropic case*, Inverse Problems **8** (1992), 409–419.

[5] F.A. Grünbaum, *Diffuse tomography: Using time-of-flight information in a two-dimensional model*, International J. of Imaging Technology **11** (2001) 283–286.

[6] F.A. Grünbaum, *A nonlinear inverse problem inspired by three-dimensional diffuse tomography*, Inverse Problems **17** (2001), 1907–1922.

[7] J. Singer, F.A. Grünbaum, P. Kohn and J. Zubelli, *Image reconstruction of the interior of bodies that diffuse radiation*, Science **248** (1990), 990–993.

[8] F.A. Grünbaum and S. Patch, *The use of Grassmann identities for inversion of a general model in diffuse tomography*, Proceedings of the Lapland Conference on Inverse Problems, Saariselka, Finland, June 1992.

[9] F.A. Grünbaum and S. Patch, *Simplification of a general model in diffuse tomography*, in "Inverse Problems in Scattering and Imaging", M. A. Fiddy (ed.), Proc. SPIE **176**, 744–754.

[10] F.A. Grünbaum and L.F. Matusevich, *Explicit inversion formulas for a model in diffuse tomography*, Advances in Applied Mathematics, **29** (2002) 172–183

[11] F.A. Grünbaum and L.F. Matusevich, *A nonlinear inverse problem inspired by 3-dimensional diffuse tomography*, Int. J. Imaging Technology, **12** (2002), 198–203.

[12] F.A. Grünbaum and L.F. Matusevich, *A network tomography problem related to the hypercube*, in "Contemporary Mathematics" (2004) Volume **362** 189–197 AMS, Providence, RI.
[13] F. Natterer and F. Wubbeling, *Mathematical methods in image reconstruction*, SIAM (2001).
[14] S. Patch, *Recursive recovery of a family of Markov transition probabilities from boundary value data*, J. Math. Phys. **36**(7) (July 1995), 3395–3412.
[15] S. Patch, *A recursive algorithm for diffuse planar tomography*, Chapter 20 in "Discrete Tomography: Foundations, Algorithms, and Applications", G. Herman and A. Kuba (eds.), Birkhauser, Boston, 1999.
[16] S. Patch, *Consistency conditions in Diffuse Tomography*, Inverse problems, **10**, 1 , (1994) , 199–212.
[17] J. Vardi, *Network tomography: Estimating Source-Destination Traffic Intensities From Link Data*Journal of the Statistical Association, **91**(1996) , 365–377.

This abstract gives a summary of some of my recent joint work with Laura Matusevich.

We consider the general problem of determining the unknown characteristics of a **random routing strategy** from **end-to-end** measurements. More specifically, we construct a Markov chain that models the traffic of messages in a multiterminal network consisting of *input*, *intermediate* and *output* terminals. The topology of the network is assumed to be known, but the Markovian routing strategy is not known. We solve the problem of determining the unknown one-step transition probability matrix of our random walk from input-output measurements of "travel time". In several cases we give explicit inversion formulas (up to a natural gauge). This kind of result holds for a large (but not arbitrary) class of multiterminal networks.

A large open problem is to characterize those networks that allow for this "ideal" situation, where one can solve explicitly a complicated set of **nonlinear equations** by first reducing them **analyically** to an equivalent set of **linear equations** and them solving them up to a natural gauge.

Compressive Sampling

Emmanuel J. Candès
(joint work with Justin Romberg and Terence Tao)

Conventional wisdom and common practice in acquisition and reconstruction of images from frequency data follows the basic principle of the Nyquist density sampling theory. This principle states that to reconstruct an image, the number of Fourier samples we need to acquire must match the desired resolution of the image, i.e. the number of pixels in the image.

This talk introduces a newly emerged sampling theory which shows that this conventional wisdom is inaccurate. Perhaps surprisingly, images or signals of scientific interest can be recovered accurately and sometimes even exactly from a limited number of nonadaptive random measurements. For example, we prove that one can recover a k-sparse signal in dimension n (an n-dimensional real or complex valued vector with at most k nonzero entries) from just about $k \log n$ of its Fourier coefficients. If one uses a random projection in which the plane is sampled uniformly at random, then one only needs about $k \log(n/k)$ pieces of information (the dimension of the plane needs only be about $k \log(n/k)$). Such results extend to signals that are not sparse but compressible. In a nutshell, compressible signals

are those signals which are well-approximated by sparse signals. This is interesting because signals and images of scientific interest are usually highly compressible, i.e. approximately sparse in a convenient basis; for example, a wavelet basis. The consequence is that we need far fewer measurements than the number of pixels, say, to reconstruct these signals accurately.

The key element here is that the reconstruction algorithms are very concrete; in fact, they only involve solving convenient convex optimization programs. A typical result is as follows: suppose we measure $y = \Phi x$ where $x \in \mathbb{R}^m$ and $y \in \mathbb{R}^m$ so that Φ is a "long" m by n matrix. We assume we have undersampled data, i.e. $m \ll n$. Then we prove that if Φ is a suitable sensing matrix—i.e. obeys a so called restricted isometry property [5]—and the unknown vector $x \in \mathbb{R}^n$ we wish to recover is sufficiently sparse, then x is the unique solution of the ℓ_1-minimization problem

$$(P_1) \qquad \min_{\tilde{x} \in \mathbb{R}^n} \|\tilde{x}\|_{\ell_1} \quad \text{subject to} \quad y = \Phi \tilde{x}.$$

There exist variations of the algorithm (P_1) to deal with undersampled *and* noisy data, which again miminize an ℓ_1 norm subject to convex inequality constraints. A somewhat unexpected feature is that these algorithms are also very stable. For example, the accuracy of the reconstruction degrades smoothly as the noise level increases. This is surprising in the sense that the inversion of Φ is stable even though the large majority of the singular values vanish.

In effect, the talk introduces a theory suggesting "the possibility of compressed data acquisition protocols which perform as if it were possible to directly acquire just the important information about the image of interest." In other words, by collecting a comparably small number of measurements rather than pixel values, one could in principle reconstruct an image with essentially the same resolution as that one would obtain by measuring all the pixels, a phenomenon with perhaps far reaching implications. I will try to explain why this theory gives us a new vantage point for a diverse set of applications including accelerated tomographic imaging, analog-to-digital conversion, and digital photography.

There are significant interactions between compressive sampling and other fields such as coding theory, and statistics.

References

[1] E. J. Candès and J. Romberg. Quantitative robust uncertainty principles and optimally sparse decompositions. *Found. of Comput. Math.* 6, 227-254, 2006.

[2] E. J. Candès, J. Romberg, and T. Tao. Robust uncertainty principles: Exact signal reconstruction from highly incomplete frequency information. *IEEE Trans. Inform. Theory* 52, 489-509, 2006.

[3] E. J. Candès, J. Romberg, and T. Tao. Stable signal recovery from incomplete and inaccurate measurements. *Comm. Pure Appl. Math.* 59, 1207-1223, 2006.

[4] E. J. Candès and T. Tao. Near-optimal signal recovery from random projections and universal encoding strategies, 2004. To appear in *IEEE Trans. Inform. Theory.*

[5] E. J. Candès and T. Tao. Decoding by linear programming. *IEEE Trans. Inf. Theory* 2005; 51:4203-4215.

[6] E. .J. Candès and J. Romberg. Practical signal recovery from random projections. *Wavelet Applications in Signal and Image Processing XI, Proc. SPIE Conf. 5914*, 2005.

[7] E. .J. Candès and T. Tao. The Dantzig selector: statistical estimation when p is much larger than n, 2005. To appear in *Annals of Statistics*.
[8] E. J. Candès, M. Rudelson, T. Tao and R. Vershynin. "Error correction via linear programming." In *Foundations of Computer Science 2005 (FOCS'05)*, 2005.
[9] E. J. Candès. Compressive sampling. In *Proceedings of the International Congress of Mathematicians, Madrid, Spain, 2006*, 2006.
[10] R. A. DeVore. Optimal computation. In *Proceedings of the International Congress of Mathematicians, Madrid, Spain, 2006*, 2006.
[11] D. L. Donoho. For Most Large Underdetermined Systems of Linear Equations the Minimal ℓ_1-norm Solution is also the Sparsest Solution. *Comm. Pure Appl. Math.* 59(6):797–829, 2006.
[12] D. L. Donoho. Compressed sensing. *IEEE Trans. Inform. Theory* 52(4): 1289–1306, 2006.

Two-Dimensional Region-of-Interest Tomography

Rolf Clackdoyle
(joint work with Michel Defrise, Frédéric Noo, Hiroyuki Kudo)

1. Problem Definition

In this presentation we describe, at least in broad terms, what is currently known about the region-of-interest (ROI) problem in two-dimensional (i.e. classical) tomography. To define this problem we first introduce some notation.

The 2D Radon transform of a smooth function f with known compact support Ω is defined as $\mathcal{R}f(\phi, s) = \int f(r\alpha + s\alpha^{\perp})dr$ where $\alpha = (\cos\phi, \sin\phi)$ and $\alpha^{\perp} = (-\sin\phi, \cos\phi)$. We use L to denote a line in the plane, and more specifically $L^{(\phi,s)} = \{x |\, x \cdot \alpha^{\perp} = s\}$. We let Ω^{+} be a fixed neighborhood of the support of the unknown function f, and we consider the set of all lines intersecting Ω^{+}: $\mathcal{L} = \{L |\, L \cap \Omega^{+} \neq \emptyset\}$, and let $\mathcal{N} \subset \mathcal{L}$ be an open set of *unavailable* lines and $\mathcal{M} = \mathcal{L} \backslash \mathcal{N}$ be the set of *measured* (or *available*) lines. The 2D ROI problem is: *given $\mathcal{R}f(\phi, s)$ for all $L^{(\phi,s)} \in \mathcal{M}$, what is the maximal region $R \subset \Omega$ such that $f(x)$ can be (stably) reconstructed for all $x \in R$?*

The region R is considered to be the ROI. In practical terms it would be more logical to begin with the ROI and to ask which sets $\mathcal{M}$ need to be measured in order to recover the ROI. However, the formulation above is more conveniently analyzed.

By "stable reconstruction" we mean that between suitable function spaces there is a continuous inverse that maps $\mathcal{R}f|_{\mathcal{M}}$ to $f|_R$.

2. Regions A and B

It will be useful to split Ω^{+} into two regions; we define region A to be $\Omega^{+} \backslash B$, and region B to be $B = \{x \in \Omega^{+} |\, x \in L \text{ for some } L \in \mathcal{N}\}$. Region A therefore consists precisely of that part of Ω^{+} that is completely illuminated by rays from all directions. Region B consists of points that each have a missing range of lines,

and therefore cannot be stably reconstructed, so $B \cap R = \emptyset$. Thus we only need consider region A when looking for ROIs that can be reconstructed.

Henceforth we assume that both Ω and Ω^+ are convex. We now observe that each connected component of region A is also convex. For a proof, let x lie in the convex hull of some connected component A_c of A and let $\bar{L}$ be a line segment containing x with endpoints y_1 and y_2 lying in A_c. Note that by convexity of Ω^+, the line segment $\bar{L}$ lies entirely in Ω^+. Now since A_c is connected there is a path lying entirely in A_c and joining y_1 to y_2. Every line that passes through x must intersect this path, and since the path lies in region A, these lines are all measured (are all in the set $\mathcal{M}$). Thus x lies in region A, and since the argument can be repeated for all points lying on $\bar{L}$, the point x must lie in the component A_c which is therefore convex.

Knowledge of Ω^+ and regions A and B is not enough to determine the measured and non-measured sets $\mathcal{M}$ and $\mathcal{N}$, because there is considerable freedom as to which lines pass through region B. We say that region B is *minimally illuminated* if the only measured lines passing through region B also intersect region A, i.e. if $\{L \in \mathcal{M} |\, L \cap B \neq \emptyset \text{ and } L \cap A = \emptyset\} = \emptyset$. If B is minimally illuminated, then regions A and B do determine $\mathcal{M}$ and $\mathcal{N}$.

By the *frontier* of Ω we mean the open set $\Omega^F = \Omega^+ \backslash \Omega$. We say that region A is *internal* if it does not intersect the frontier of the support of f, (i.e. if $A \cap \Omega^F = \emptyset$). Note that if A is internal and B is minimally illuminated, then we are in the situation of the classical interior problem [1], and we know that no unique solution exists for any $R \subset A$. With B not minimally illuminated, an example has been published of $R = A$ with A internal, for which an explicit stable inversion formula was given [2].

3. Differentiated Backprojection and Finite Hilbert Transforms

Almost all that is currently known about the 2D ROI problem is based on the machinery of differentiated backprojection (DBP), which effectively converts the 2D problem into a collection of one-dimensional (1D) problems involving inversion of the Hilbert transform.

Differentiated backprojection $\mathcal{D}$, refers to the operation of taking a derivative of the Radon transform data, followed the backprojection, so $\mathcal{DR}f(x) = \int_0^\pi \frac{\partial}{\partial s}\mathcal{R}f(\phi, s)|_{s=x\cdot\alpha^\perp} d\phi$. It is important to note that $\mathcal{DR}f(x)$ can only be evaluated for those values of x for which all lines that pass through a neighborhood of x lie in $\mathcal{M}$, equivalently, for just those x lying in the interior of region A.

A straightforward calculation shows that $\mathcal{DR}f(x) = 2\pi\mathcal{H}_0 f(x)$ where $\mathcal{H}_0 f(x) = \int 1/(\pi r)\, f(x_1 - r, x_2)\, dr$ is the Hilbert transform of $f(x) = f(x_1, x_2)$ with respect to the first variable. To achieve a similar Hilbert transform $\mathcal{H}_\theta f(x) = \int 1/(\pi r)\, f(x - r\beta)\, dr$ along a direction at an angle of θ to the x_1-axis (here $\beta = (\cos\theta, \sin\theta)$), the integration limits of the DBP are simply shifted: $\mathcal{D}_\theta\mathcal{R}f(x) = \int_\theta^{\theta+\pi} \frac{\partial}{\partial s}\mathcal{R}f(\phi, s)|_{s=x\cdot\alpha^\perp} d\phi$ to yield $\mathcal{D}_\theta\mathcal{R}f(x) = 2\pi\mathcal{H}_\theta f(x)$. See [3], [4] for more.

We digress to discuss the finite Hilbert transform. Suppose $g(r)$ is a function of a scalar variable with known support $[P_1, P_2]$, and suppose the Hilbert transform

$\mathcal{H}g$ of g is known on the interval (Q_1, Q_2). If $(Q_1, Q_2) = (-\infty, \infty)$ then g can easily be recovered from complete information of its Hilbert transform. The question is, to what extent can g be recovered from $\mathcal{H}g$ for various finite intervals (Q_1, Q_2)? An explicit formula for g has long been known (for example [5]) for the case $[P_1, P_2] \subset (Q_1, Q_2)$, and this result has applications for the 2D ROI problem. An even more significant result, recently published in [4], established stable recovery of $g(r)$ for $r \in (Q_1, P_2]$ provided $Q_1 < P_2 < Q_2$, and similarly for $r \in [P_1, Q_2)$ provided $Q_1 < P_1 < Q_2$.

4. Partial Solution to the 2D ROI Tomography Problem

We are now ready to apply this machinery to establish the following partial result on the 2D ROI problem. *Stable reconstruction of f can be achieved on the interior of each non-internal connected component of region A (i.e. on the interior of each connected component A_c that satisfies $A_c \cap \Omega^F \neq \emptyset$).*

Consider a non-internal connected component A_c of region A, and denote the interior of A_c by A_c°. We take A_c° to be non-empty. Noting that we only need concern ourselves with $A_c^\circ \cap \Omega$ because f is known to be zero outside Ω, we let y be any point in $A_c^\circ \cap \Omega$. Now let L be a line passing through y and any point in $A_c \cap \Omega^F$. This line lies at say, angle θ to the x_1-axis so $L = L^{(\theta,s)}$ where $s = y \cdot \beta^\perp$ (with $\beta^\perp = (-\sin\theta, \cos\theta)$). We know that $L^{(\theta,s)} \cap \Omega$ is a single closed line segment in Ω because Ω is convex and compact, and we label the endpoints of this segment u_1 and u_2, ordered such that $u_1 \cdot \beta \leq u_2 \cdot \beta$. Similarly, $L^{(\theta,s)} \cap A_c^\circ$ is a single open line segment in A_c° bounded by endpoints v_1 and v_2 satisfying $v_1 \cdot \beta < v_2 \cdot \beta$. The definition of L ensures that at least one of v_1, v_2 lies in Ω^F (because for A_c convex, every line segment joining a point in A_c to a point in A_c° has at most one point outside A_c°; see for example theorem 3 of [6]).

We now convert to the 1D problem by letting $g = f|_{L^{(\theta,s)}}$, specifically $g(r) = f(r\beta + s\beta^\perp)$, and defining $P_i = u_i \cdot \beta$ and $Q_i = v_i \cdot \beta$ for $i = 1, 2$. The point $Y = y \cdot \beta$ lies in the support $[P_1, P_2]$ of g, and we also have $Y \in (Q_1, Q_2)$ since this interval corresponds to region A_c°. We note that $\mathcal{H}g(r) = \mathcal{H}_\theta f(r\beta + s\beta^\perp)$ is known for $r \in (Q_1, Q_2)$ because this interval corresponds to those x along the line $L^{(\theta,s)}$ that lie in A_c°, and so $\mathcal{H}_\theta f(x)$ is known. Now either $v_1 \in \Omega^F$ in which case $Q_1 < P_1$ and $Y \in [P_1, Q_2)$, or $v_2 \in \Omega^F$ which would force $P_2 < Q_2$ and $Y \in (Q_1, P_2]$ (or both $v_1, v_2 \in \Omega^F$ forcing $Y \in [P_1, P_2] \subset (Q_1, Q_2)$). In any event, we are assured by [4] that $g(Y)$ can be stably reconstructed, as discussed in section 3 above. Thus $f(y)$ can be stably reconstructed for all such $y \in A_c^\circ$ in the interior of a general non-internal component of region A.

5. Remarks

For the case of internal components of region A, no corresponding general statement can yet be made. Any such statement will need to at least distinguish the case of a minimally illuminated region B, so something more will be needed than the DBP and finite Hilbert machinery described here.

On the other hand, for non-internal components in the presence of a non-convex support Ω, it appears reasonable that small extensions of the approach described here will provide a similar result.

As a practical application of the results presented here, we consider a single-slice medical CT scanner which would illuminate a circular field-of-view (FOV) with rays which after suitable processing would be good estimates of the Radon transform of the unknown linear attenuation coefficient. A fair approximation of the support Ω would be an ellipse or similar convex shape. In this example, region A is the intersection of the FOV with Ω and region B is minimally illuminated. The results presented here show that either no stable reconstruction is possible anywhere because region A is internal, or reconstruction is possible everywhere in region A because it is intersects the frontier of the support. The second part of this statement was unknown prior to the publication of [4].

In three dimensions, the Radon transform has a local inverse in the sense described in [1]), which means that the straightforward generalizations of sets $\mathcal{M}$, $\mathcal{N}$, and regions A, B would immediately yield the ROI solution $R = A^{\circ}$ in all circumstances. For the x-ray transform (the line-integral transform), the three-dimensional (3D) case differs from two-dimensions in several aspects, which we summarize here (without providing demonstrations). Here, we consider the general fully 3D case, not just cone-beam geometries. We let $L_{x,\gamma} = \{y \,|\, y = x + t\gamma, t \in (-\infty, \infty)\}$ be the line in the direction $\gamma \in S^2$ passing through the point x. Now define Γ_x to be the directions of all measured lines passing through x: $\Gamma_x = \{\gamma \in S^2 \,|\, L_{x,\gamma} \in \mathcal{M}\}$. Loosely speaking, region A would be defined in three-dimensions by $x \in A$ if Γ_x satisfies Orlov's condition [7], that every great circle on S^2 intersects Γ_x. (Equivalently, in the language of Tuy [8], $x \in A$ if for every plane Π containing x, there exists a measured line in Π passing through x) We note that in the 3D case, connected components of region A are not necessarily convex. Now, for x in the interior of region A, a 3D DBP process can be applied to yield $\mathcal{H}_\gamma f(x)$ only if Γ_x contains a path on the unit sphere connecting $-\gamma$ to γ. The collection of directions for which $\mathcal{H}_\gamma f(x)$ is available could be empty (if no such path exists), could be 1D (because the central symmetry of Γ_x allows γ to be any element along the path), could be a 2D subset of S^2, or even could be the set of all directions S^2 if x were fully illuminated from all directions (i.e. if $\Gamma_x = S^2$). Note that in the 2D case treated here, we are always in this latter situation of all possible Hilbert directions $H_\theta f(x)$. So in three-dimensions it is not enough to simply consider a line $L_{y,\gamma}$ passing through the interior of region A, because we would also need some assurance that the Hilbert transform of f could be found in the γ-direction for all points on the line $L_{y,\gamma}$. Therefore, more structure needs to be placed on the measurement set $\mathcal{M}$ before attempting to apply the DBP and finite-Hilbert method to 3D ROI tomography. One example where the necessary structure is present involves a single-turn helical path lying outside the (extended) support Ω^+, and where $\mathcal{M}$ is some subset of all lines intersecting this helix. In this case, non-internal convex components of region A can be stably reconstructed according to the DBP and finite-Hilbert method.

Acknowledgement

This work was partially supported by the Agence Nationale pour la Recherche (ANR) under grant NT05-1 45428 and partially supported by the National Institutes of Health (NIH) under grant R01 EB000627.

References

[1] F. Natterer, The Mathematics of Computerized Tomography (New York: Wiley), 1986.
[2] F. Noo, M. Defrise, R. Clackdoyle, H. Kudo, *Image reconstruction from fan-beam projections on less than a short-scan*, Phys. Med. Biol. **47** (2002), 2525–2546.
[3] I. M. Gel'fand, M. I. Graev, *Crofton's function and inversion formulas in real integral geometry*, Func. Anal. Appl. **25** (1991), 1-5.
[4] M. Defrise, F. Noo, R. Clackdoyle, H. Kudo, *Truncated Hilbert transform and image reconstruction from limited tomographic data*, Inverse Problems **22** (2006), 1037–1053.
[5] F. G. Tricomi, Integral Equations (New York: Dover), 1957.
[6] H. G. Eggleston, Convexity (Cambridge: Cambridge University Press), 1958.
[7] S. S. Orlov, *Theory of three-dimensional reconstruction. 1. Conditions of a complete set of projections*, Sov. Phys. Crystallography, **20** (1976), 312–314.
[8] H. K. Tuy. *An inversion formula for cone beam reconstruction*, SIAM J. Appl. Math. **43** (1983), 546–552.

Image reconstruction from truncated data in SPECT

Frédéric Noo

(joint work with Michel Defrise, Jed D. Pack, Rolf Clackdoyle)

Recently, several works (see [1], [2], [3], [4]) have shown that classical two-dimensional (2D) tomography is not "all or nothing" contrary to long-standing folklore. That is, the measured data need not cover the whole object for accurate reconstruction to be possible in some regions-of-interest (ROIs). This statement holds for any finite-size object, and this work investigates how they may be extended to single-photon emission computed tomography (SPECT).

The attenuation map is assumed to be known and a constant μ_o within a bounded convex region Ω that includes the support of the unkown tracer-activity function p. Under this assumption, the data from which p must be reconstructed may be viewed as the exponential Radon transform of p:

$$(E_{\mu_o} p)(\phi, s) = \int_{-\infty}^{\infty} p(s\,\underline{\theta} + t\,\underline{\theta}^{\perp})\, e^{\mu_o t}\, dt\,. \tag{1}$$

where $\underline{\theta} = (\cos\phi, \sin\phi)$ and $\underline{\theta}^{\perp} = (-\sin\phi, \cos\phi)$. For a fixed ϕ, the values of $(E_{\mu_o} p)(\phi, s)$ obtained by varying s define an exponential parallel-beam projection of p. If these values are only known for a limited range of s, the projection is said to be truncated. For example, if Ω is the centered disk of radius R, the projection is truncated as long as $(E_{\mu_o} p)(\phi, s)$ is not known for all $s \in [-R, R]$.

We investigate image reconstruction from exponential parallel-beam projections that are only known over 180 degrees and may each be truncated. We build this investigation on results by Rullgård [5]. The angular range over which the

projections are known is seen as a single interval, not a union of disjoint intervals, and, for convenience, this interval is chosen as $\phi \in [0, \pi]$. Given a truncation pattern, we examine where accurate (exact and stable) reconstruction is possible inside Ω. We note that remarkable findings have been published recently on the more general problem of inverting the attenuated Radon transform. However, they assume the projections are non-truncated.

To achieve reconstruction with truncation, we introduce a differentiated back-projection (DBP) operation and show that this DBP yields a one-dimensional (1D) integral equation for the unknown p. Then, we investigate the inversion of this integral equation. We define the DBP for the exponential Radon transform as

$$b(\underline{x}) = \int_0^\pi e^{-\mu_o \underline{x}\cdot\underline{\theta}^\perp} \left(\frac{\partial}{\partial s}(E_{\mu_o} p)\right)(\phi, \underline{x}\cdot\underline{\theta})\, d\phi \tag{2}$$

Assuming that p is continuously differentiable, this DBP is well-defined, and following steps by Rullgård [5] we find that

$$b(x,y) \quad = \quad -2\pi \int_{-\infty}^{\infty} \frac{\cosh \mu_o(y-y')}{\pi(y-y')}\, p(x,y')\, dy' \tag{3}$$

where the singularity is handled as a Cauchy principal value. In practice, (3) is only of interest for $(x, y) \in \Omega$, the bounded and convex region outside which p is known to be zero. Let (x, L_x) and (x, U_x) be the end points of the intersection of Ω with the line parallel to the y-axis through a point $(x, y) \in \Omega$. Then,

$$b(x,y) \quad = \quad -2\pi \int_{L_x}^{U_x} \frac{\cosh \mu_o(y-y')}{\pi(y-y')}\, p(x,y')\, dy' \quad \text{for } (x,y) \in \Omega\,. \tag{4}$$

This expression explicitly shows that the integral in y' has finite bounds.

Equation (4) reduces the reconstruction problem to a 1D integral equation with convolution kernel. Rullgård showed there exists a distribution ρ such that

$$p(x,y) = \int_{y-D_x}^{y+D_x} \rho(y-y')\, b(x,y')\, dy' \qquad \text{for } (x,y) \in \Omega\,, \tag{5}$$

where $D_x = U_x - L_x$. Although not pointed out by Rullgård, (5) represents a first proof that reconstruction of a ROI in SPECT with uniform attenuation does not require knowing $E_{\mu_o} p$ on all lines passing through the region Ω where the activity lies. To obtain p at a given location $(x, y) \in \Omega$ according to (5), only the values of $E_{\mu_o} p$ required to compute $b(x, y')$ with $|y' - y| < D_x$ are needed. These values correspond to the lines that meet a neighbourhood of the line segment connecting $(x, y - D_x)$ to $(x, y + D_x)$, hence $E_{\mu_o} p$ need not be available for all lines passing through the activity region. See figure 1a for an illustration of this assertion and figure 1b for its extension to an ROI.

We improve on Rullgård's result, equation (5), by discarding the convolution and relaxing the measurement requirement. Specifically, we show that

> *A function p that is continuously differentiable on Ω can be accurately reconstructed at a given location $(x, y) \in \Omega$, if for each $\phi \in [0, \pi]$ the values of $E_{\mu_o} p$ are known (measured) for just those lines*

that intersect a neighbourhood of the line segment from (x, L_x) *to* (x, U_x).

This statement holds for any value of μ_o that satisfies a specific condition. Numerical evaluation of this condition reveals that it is satisfied for a fine sampling of a wide range of values of μ_o that effectively covers all medical applications of SPECT. See figure 1c for a visual illustration of the statement in comparison with truncation allowed by Rullgård's formula. More details on the condition and a proof of the statement may be found in [6].

Acknowledgement

This work was supported by the National Institutes of Health (NIH) under grants R21 EB002526 and R01 EB000627. Its contents are solely the responsibility of the authors and do not necessarily represent the official views of NIH.

References

[1] R. Clackdoyle, F. Noo, J. Guo and J. A. Roberts, *Quantitative reconstruction from truncated projections in classical tomography*, IEEE Trans. Nuc. Sci. **51(5)** (2004), 2570–78.
[2] F. Noo, R. Clackdoyle, J. D. Pack, *A two-step Hilbert transform method for 2D image reconstruction*, Phys. Med. Biol. **49** (2004), 3903–23.
[3] Y. Zou, X. Pan and E. Y. Sidky, *Image reconstruction in regions-of-interest from truncated projections in a reduced fan-beam scan*, Phys. Med. Biol **50** (2005), 13–28.
[4] I. M. Gelfand and M. I. Graev, *Crofton's function and inversion formulas in real integral geometry*, Funct. Anal. Appl. (1991) 1–5.
[5] H. Rullgård, *An explicit inversion formula for the exponential Radon transform using data from* 180°, Ark. Mat. **42** (2004), 353–62.
[6] F. Noo, M. Defrise, J. D. Pack, R. Clackdoyle, *Image reconstruction from truncated data in SPECT with uniform attenuation*, Inverse Problems, (submitted) (2006).

On the minimization of non-convex, non-differentiable functionals with an application to SPECT

Peter Maass

(joint work with T. Bonesky, K. Bredies, D. Lorenz)

This exposition is concerned with analyzing the convergence properties of a generalized conditional gradient method for solving

$$\min F(u) + \Phi(u), \tag{1}$$

where F is non-convex but differentiable and Φ is non-differentiable but convex. The interest in such functionals arises from two different points of view: First of all, Tikhonov-regularization techniques for non-linear operator equations with Besov penalty terms, where

$$F(u) = \|K(u) - g^\delta\|^2 \quad , \quad \Phi(u) = \|u\|^p_{B^s_{pp}}.$$

Such functionals have recently investigated intensively in the context of image processing (in particular $K = I$ or K a convolution operator, see e.g. [ChL]),

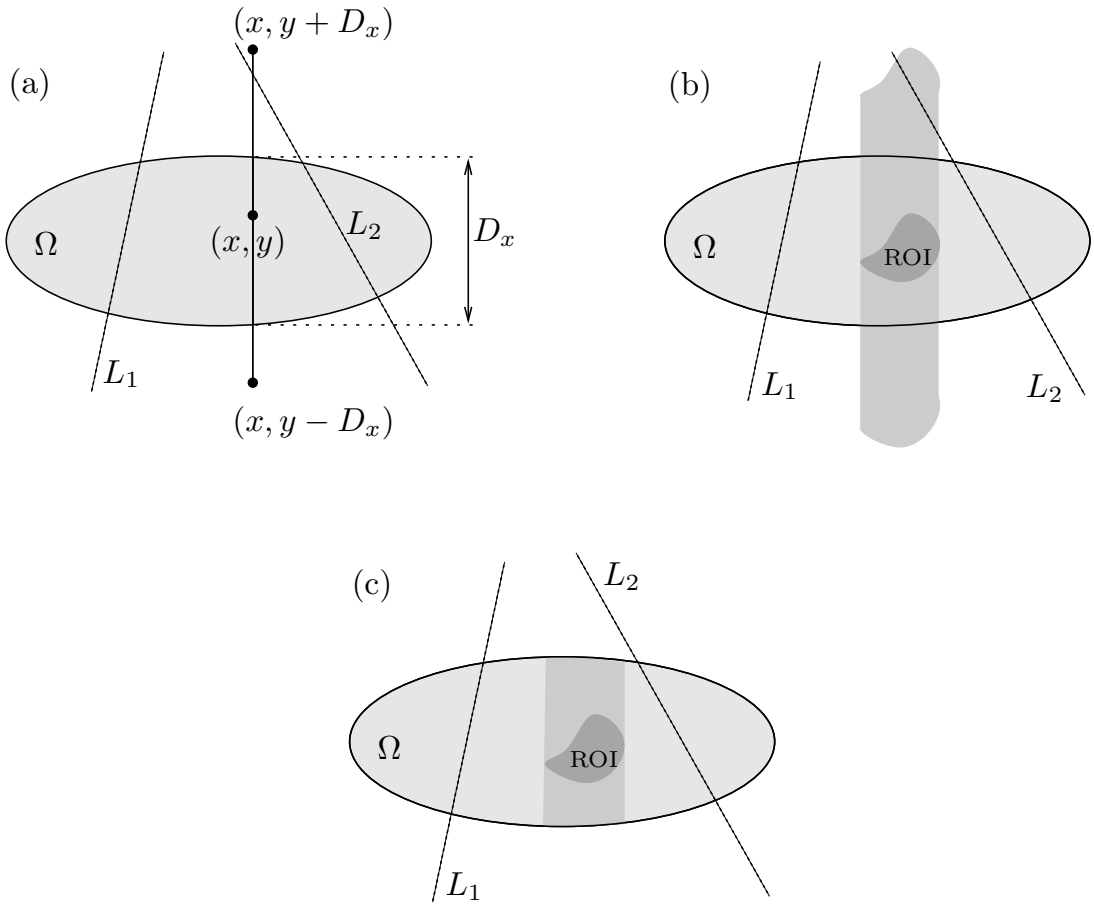

FIGURE 1. Illustration of allowed data truncation. The activity sources are within the ellipse Ω. (a) According to Rullgård's results, accurate reconstruction at (x, y) only requires the data on the lines that cross a neighborhood of the vertical line segment through (x, y). Line L_2 is thus needed but not line L_1. (b) According to Rullgård's results, accurate reconstruction within the depicted ROI requires the data on all lines passing through the shaded vertical strip. (c) According to our results, accurate reconstruction within the depicted ROI only requires the data on all lines passing through the intersection of the shaded vertical strip with Ω. In particular, line L_2 is not needed.

which also was the starting point for analyzing surrogate techniques (K a linear compact operator, see [DDD]). This second paper has triggered some follow up papers, which also included non-linear K, see [BLM], [RaT]. Finally, a full chapter in [ChS] is devoted to 'Besov images' and the minimization of related functionals. Secondly, such functionals are a natural generalization of a particular type of

constrained minimization problems

$$\min_{u\in U_{ad}} F(u)$$

which can be equivalently reformulated with the help of the indicator function

$$I_{U_{ad}}(u) = \begin{cases} 0 & : \quad u \in U_{ad} \\ \infty & : \quad u \notin U_{ad} \end{cases} \qquad \text{as} \qquad \min F(u) + I_{U_{ad}}(u).$$

Because of the non-differentiability of the functional in problem (1) usual gradient methods can not be applied. For minimizing $F + \Phi$ in [BLM] a generalized conditional gradient method is introduced. It proceeds as follows:

(1) Choose $u_0 \in H$, such that $\Phi(u_0) < \infty$ and set n=0.
(2) Determine a descent direction v_n as a solution of

$$\min_{v\in H} \langle F'(u_n), v\rangle + \Phi(u_n).$$

(3) Determine a stepsize s_n as a solution of

$$\min_{s\in[0,1]} F(u_n + s(v_n - u_n)) + \Phi(u_n + s(v_n - u_n)).$$

(4) Put $u_{n+1} = u_n + s_n(v_n - u_n)$ and $n = n + 1$, return to step 2.

In [Bon] problem (1) is treated with

$$F(u) = \frac{1}{2}\|K(u) - g^\delta\|^2 - \lambda\Theta(u) \quad , \quad \Phi(u) = \lambda\Theta(u) + \alpha\Psi(u). \tag{2}$$

It is shown, that under mild assumptions on K and with

$$\Theta(u) = \frac{1}{2}\|u\|^2 \quad , \quad \alpha\Psi(u) = \sum_k w_k |\langle u, \varphi_k\rangle|^p \tag{3}$$

where $\{\varphi_k\}$ is an orthonormal basis of the Hilbertspace H, $w_k > 0$ for all k, $w_k \to \infty$ for $k \to \infty$ and $1 \le p \le 2$, there exists a convergent subsequence of the iterates $\{u_n\}$ and that every subsequence of $\{u_n\}$ converges to a stationary point of the functional $F+\Phi$. Furthermore it is shown that if the set of stationary points consists of only one point the sequence of iterates $\{u_n\}$ converges to the unique minimizer of $F + \Phi$.

The minimization problem in the second step of the generalized conditional gradient method can be reformulated and solved with the help of results from the theory of convex analysis. One can show that the minimizer is obtained by a shrinkage procedure (see [BLM]):

$$v_n = \sum_k S_{w_k,p}(\langle u_n - \lambda^{-1}K'(u_n)^*(K(u_n) - g^\delta), \varphi_k\rangle)\varphi_k,$$

where $S_{w_k,p} : \mathbb{R} \to \mathbb{R}$ is a shrinkage function given by

$$S_{w_k,p}(y) = \begin{cases} \operatorname{sign}(y)[|y| - \frac{w_k}{\lambda}]_+ & : \quad p = 1 \\ G^{-1}_{k,\lambda,p}(y) & : \quad 1 < p < 2 \\ (1 + \frac{2w_k}{\lambda})^{-1} y & : \quad p = 2 \end{cases}$$

with

$$G_{k,\lambda,p}(x) = x + \frac{w_k p}{\lambda}\text{sign}(x)|x|^{p-1}.$$

In applications it turns out that under special assumptions on λ the stepsize can be chosen as $s = 1$ during the whole iteration. This gives a simple algorithm for solving problem (1).
This algorithm can be applied to the functional $F + \Phi$ as defined in (2) and (3) where $K = R$ is the SPECT operator

$$R(f,\mu)(s,\omega) = \int_{\mathbb{R}} f(s\omega^{\perp} + t\omega)e^{-\int_t^{\infty}\mu(s\omega^{\perp}+\tau\omega)d\tau}dt,$$

with $s \in \mathbb{R}$, $\omega \in S^1$ and $u = (f,\mu)$.
For extended numerical results see [Bon]. If the algorithm is applied to data which were generated with the help of the so called MCAT-phantom and degraded with Gaussian noise and assumed optimal weights w_k one gets for example the following results:

data error δ	w_k	number of iterations	relative error E_{rel}
5%	$2^{-\frac{1}{2}} * 2 * 10^{-6}$	3481	8.6%
10%	$2 * 10^{-6}$	1727	15.5%
20%	$2^{\frac{1}{2}} * 2 * 10^{-6}$	437	24.7%

This tabular shows that for decreasing data error the relative error

$$E_{rel} = \left\| \frac{f_{true}}{\|f_{true}\|} - \frac{f_{rec}}{\|f_{rec}\|} \right\| * 100\%$$

of the optimal reconstruction f_{rec} of the activity function f_{true} decreases as well. The observed convergence rate in this case is about $O(\delta^{0.75})$.
Figure 1 shows an example of a reconstructed activity function f.

FIGURE 1. True activity function (left) and optimal reconstruction from degraded data with 10% Gaussian noise.

References

[Bon] T. Bonesky, Ein verallgemeinertes Gradientenverfahren für nichtlineare Operatorgleichungen, diploma thesis, University Bremen, 2006.

[BLM] K. Bredies, D. A. Lorenz, P. Maaß, A Generalized Conditional Gradient Method and its Connection to an Iterative Shrinkage Method, Accepted for publication in Computational Optimization and Applications, 2005.

[ChL] A. Chambolle, B. J. Lucier, Interpreting translation-invariant wavelet shrinkage as a new image smoothing scale space, *IEEE Transactions on Image Processing*, **10**(7): 993-1000, 2001.

[ChS] T. F. Chan, J. Shen, *Image Processing and Analysis, Variational, PDE, Wavelet and Stochastic Methods*, SIAM, Philadelphia, 2005.

[DDD] I. Daubechies, M. Defrise, C. De Mol, An iterative thresholding algorithm for linear inverse problems with a sparsity constraint, *Communications in Pure and Applied Mathematics* **57**(11): 1413-1457, 2004.

[RaT] R. Ramlau, G. Teschke, Tikhonov Replacement Functionals for Iteratively Solving Nonlinear Operator Equations, *Inverse Problems* **21**(5): 1571-1592, 2005.

Enhanced angular resolution from multiple scattered waves

Clifford Nolan

(joint work with M. Cheney, T. Dowling, R. Gaburro)

This talk concerns the incorporation of a-priori known environmental scatterers into a linear scattering model for reflected radar waves. The waves reflect from the known environmental scatterer(s) as well as the unknown scatterers. The idea is to use the multiple scattering between the environmental scatterer and the unknown scatterer to obtain different views of the latter. In this way, we show how one can improve the angular resolution of unknown scatterers with the aid of the environmental scatterers.

The specific application presented in this talk concerns a known wall (environmental scatterer) in an urban setting and we wish to use this wall to obtain different views of nearby scatterers (vehicles, etc), thereby obtaining a better image than if we had only incorporated direct scattering from the nearby scatterers.

The linear scattering modelling operator consists of a sum of four Fourier integral operators $F = F_1, F_2, F_3, F_4$ which maps the reflectivity function (which we wish to recover) $V(x_1, x_2)\delta(x_3)$ to the data $d(s, t)$.

In order to recover the reflectivity function, we investigate the possibility of applying a weighted-adjoint linear operator of the same type as F^* (where the asterisk denotes the formal L^2-adjoint). It turns out that in order to successfully achieve this that we must carefully beam form with the radar. We have to avoid certain bad points on the ground, otherwise, we cannot effect inversion with the weighted-adjoint.

If we are not careful about beam-forming, or it is not practical to beamform, then we demonstrate the various kinds of artifacts that will be obtained along with true scatteres using a straight backprojection scheme.

A sub-problem in our analysis is related to the 'common-midpoint' seismology imaging problem. In particular, the operators F_2, F_3 are closely related. We show that there artifacts associated with such geometries that are not (to the authors' knowledge) (well-) known in the seismics community.

References

[1] Devaney A J and Dennison M 2003 Inverse scattering in inhomogeneous background media, Inverse problems **19(4)** 855–870.

[2] Devaney A J and Guo P 2005 Superresolution imaging from limited-aperture optical diffracted field data, J. Opt. Soc. Am. A **22** 1086–1092.

[3] P. Morse & H. Feshbach, Methods of Theoretical Physics, Vol. 1, mcGraw-Hill, 1953.

[4] C. Nolan & M. Cheney, Synthetic Aperture Inversion for Arbitrary Flight Paths and Non-Flat Topography, IEEE Trans. on Image Processing, 12 (1035-1043), 2003.

[5] J.J. Duistermaat, Fourier Integral Operators, Birkhauser, Boston, 1996.

[6] M. Cheney, "A mathematical tutorial on Synthetic Aperture Radar", SIAM Review 43 (2001) 301–312.

[7] F. Treves, Introduction to Pseudodifferential and Fourier Integral Operators, volumes I and II, Plenum Press, New York, 1980.

[8] C. Nolan & M. Cheney, Synthetic Aperture Inversion, Inverse Problems, 18 (221-236), 2002.

[9] C. Nolan & M. Cheney, Microlocal Analysis of Synthetic Aperture Radar Imaging, J. Fourier Analysis and its Applications, 10 (133-148), 2004.

[10] X. Saint Raymond, Elementary Introduction to the Theory of Pseudodifferential Operators, CRC Press, 1991.

[11] C. J. Nolan & W. W. Symes, Global solution of a linearized inverse problem for the wave equation, Comm. in PDE, Vol 22(5&6), pp. 919-952, 1997.

[12] M. Cheney & R.J. Bonneau, Imaging that exploits multipath scattering from point scatterers, Inverse Problems 20, 1691-1711, 2004.

A survey on mathematical problems of thermoacoustic tomography

Peter Kuchment

An introduction

Tomographic medical imaging methods strive to satisfy several requirements: safety, low cost, high contrast, high resolution. However, these conditions are rather contradictory. For instance, some cheap and safe methods with good contrast (like electrical impedance tomography) suffer from low resolution. Novel methods have been emerging recently that combine different physical types of signals to try to overcome this hurdle. One of the best developed examples is the **Thermoacoustic Tomography (TAT)** [14]. Here a wide short radiofrequency (RF) pulse is sent through a biological object. The resulting thermoelastic expansion creates an ultrasound signal that can be measured by transducers located around the object. The transducers essentially measure the integrals of the RF energy absorption function $f(x)$ over spheres centered at transducers' locations. In mammography, cancerous cells absorb 3 to 5 times more RF energy than the healthy ones, thus high contrast. Also, ultrasound measurements provide good resolution.

Mathematics of TAT - spherical mean Radon transform

Thus, one needs to study the spherical Radon transform of functions $f(x)$ on $\mathbb{R}^d$:

$$Rf(p,r) = \int_{|y-p|=r} f(y)d\sigma(y),$$

or its *spherical mean* version $\omega_r^{-1}Rf$, where ω is the volume of the sphere of radius r in $\mathbb{R}^d$.

The mapping $f \to Rf$ is overdetermined, since it maps functions f of d variables into functions $Rf(p,r)$ of $d+1$ variables. Thus, it is natural (both from theoretical, as well as tomographic prospective) to restrict the set of centers p (transducer locations) to a hypersurface $S \subset \mathbb{R}^d$, which leads to the transform $R_S f = Rf|_{p\in S}$.

Here is the standard set of questions one would want to ask: For what sets S is R_S injective (i.e., can f be uniquely reconstructed from $R_S f$)? If R_S is injective, what are inversion formulas? How stable is inversion? What happens if the data is incomplete? What is the range description for the operator R_S?

Uniqueness of reconstruction

Let f be compactly supported. Does $R_S f = 0$ imply that $f = 0$? If the answer is "yes," we call S - a **uniqueness set**, otherwise a **non-uniqueness set**.

Lemma [17, 18, 3, 34] *Any non-uniqueness set is a set of zeros of a harmonic polynomial. In particular, any uniqueness set for harmonic polynomials is uniqueness set for the spherical mean Radon transform.*

Corollary [3, 15] *Any closed hypersurface is uniqueness set for the spherical mean Radon transform.*

This corollary resolves the uniqueness problems for most practically used geometries. It fails if f does not decay sufficiently fast [1].

Non-uniqueness sets in $\mathbb{R}^2$ [3, 17, 18]. It is clear that any line S (hyperplane in higher dimensions) is a non-uniqueness set, examples provided by functions odd with respect to S. Analogously, a Coxeter system Σ_N of N lines passing through a point and forming equal angles is also a non-uniqueness set. Less obviously, one can add any finite set Φ of points preserving non-uniqueness.

Theorem ([3], conjectured in [17, 18]). *$S \subset \mathbb{R}^2$ is a non-uniqueness set iff $S \subset \omega\Sigma_N \cup \Phi$, where Σ_N is a Coxeter system of lines, ω is a rigid motion, and Φ is finite.*

Proof uses microlocal analysis and geometry of zeros of harmonic polynomials.

Conjecture. *$S \subset \mathbb{R}^d$ is a non-uniqueness set iff $S \subset \omega\Sigma \cup \Phi$, where Σ is the surface of zeros of a homogeneous harmonic polynomial, ω is a rigid motion, and Φ is an algebraic surface of codimension at least 2.*

The problem of injectivity of R_S has relations to a wide variety of areas of analysis [3]. In particular, the following interpretation is important:

Theorem [3, 15] *The following statements are equivalent:*

1. $S \subset \mathbb{R}^d$ is a non-uniqueness set.

2. S is a nodal set for the wave equation, i.e. there exists a compactly supported f such that the solution of the wave propagation problem $\frac{\partial^2 u}{\partial t^2} = \Delta u, u(0,x) = 0, u_t(0,x) = f(x)$ vanishes on S for any moment of time.

3. S is a nodal set for the heat equation, i.e. there exists a compactly supported f such that the solution of the problem $\frac{\partial u}{\partial t} = \Delta u, u(0,x) = f(x)$ vanishes on S for any moment of time.

This interpretation provides important PDE tools and insights. In particular, it has lead to a recent progress based on the wave equation reformulation. It has also helped to understand why curves are uniqueness sets [11, 4].

Partial data: "visible" and "invisible" singularities

Uniqueness of reconstruction does not imply practical recoverability, since the reconstruction might be severely unstable. This is the case, for instance, in incomplete data situations in X-ray tomography, and even for complete data problems in electrical impedance tomography.

Theorem [19, 28, 33] *A wavefront set point (x,ξ) of f is "stably recoverable" from $R_S f$ iff there is a circle centered on S, passing through x, and normal to ξ at this point.*

This result needs to include some precise conditions (see [19]).

Reconstruction: formulas and examples

One of the most popular inversion formulas for the standard Radon transform is the so called *filtered backprojection* [20, 21]. *Approximate inversions* for the circular Radon R_S mimic this formula for the Radon transform [29]–[33]. The results are usually good and can be improved by iterations. *Exact inversion formulas* are known for S being a sphere, cylinder, or a plane. When S is a sphere, inversions via special function expansions have been discovered [23, 24]. *Backprojection formulas* have been found when $S \subset \mathbb{R}^d$ is a sphere (for odd d in [11, 29] and results for arbitrary d were presented at this workshop by D. Finch and L. Kunyansky). In the cases of cylinders and planes see [7, 9, 21, 22, 25, 29].

Here is one of the $3D$ formulas for S being the unit sphere [11]:

$$f(x) = \frac{1}{16\pi^3}\Delta_x \int\limits_{|p|=1} \frac{Rf(p,|x-p|)}{|x-p|}dp.$$

It was implemented numerically in [6].

One of L. Kunyansky's inversion formulas [16] reads in $2D$:

$$f(x) = \frac{1}{8\pi}\operatorname{Im}\nabla \cdot \int\limits_0^{2\pi} S(\vec{\omega}(\varphi), |\vec{\omega}(\varphi) - x)|)\vec{\omega}(\varphi)d\varphi,$$

where $\vec{\omega}(\varphi) = (\cos\varphi, \sin\varphi)$ and

$$S(z,t) = \int_0^\infty \left[\int\limits_0^2 H_0^{(1)}(kr)g(z,r)dr\right] \overline{H_0^{(1)}(kt)}kdk.$$

Here $H_0^{(1)}(t) = J_0(t) + iY_0(t)$ is the zero-order Hankel function of the 1st kind, $J_0(t)$, $Y_0(t)$ are zero-order Bessel functions. Similar formulas hold in any dimension.

Range conditions

The range of Radon type transforms is usually of infinite co-dimension. Knowing

the range is useful for many theoretical and practical purposes (error corrections, incomplete data, etc.

For the standard Radon transform the range conditions are: for any integer $k \geq 0$, $G_k(\omega) = \int\limits_{-\infty}^{\infty} s^k g(\omega, s) ds$ extends to a homogeneous polynomial of ω of degree k.

Complete range descriptions for R_S when S is a sphere were discovered very recently [2, 5, 10]. *Moment conditions* [3, 17, 18, 27] on data $g(p, r) = R_S f(p, r)$ look as follows: for any integer $k \geq 0$, $G_k(\omega) = \int\limits_0^{\infty} r^{2k} g(p, r) dr$ can be extended to a (non-homogeneous) polynomial of degree at most $2k$. These conditions are incomplete. *Complete conditions* were found in $2D$ [5], odd dimensions [10], and finally in all dimensions [2]. Relations to PDEs and spectral theory are revealed.

Let $B =$ unit ball, $S =$ unit sphere, $C =$ cylinder $B \times [0, 2]$. Spherical mean operator is, as before $R_S f(x, t) = G(x, t) = \omega^{-1} \int_{|x-y|=t} f(y) dS(y), |x| = 1$. Notice that if $G(x, t)$ is defined by the same formula for all $x \in \mathbb{R}^d$, then it satisfies Darboux equation $G_{tt} + (d-1)t^{-1} G_t = \Delta_x G$. Moreover, inside C, $G(x, t)$ vanishes when $t \geq 2$.

Theorem [2] *The following four statements are equivalent:*

(1) *The function $g \in C_0^\infty(S \times [0, 2])$ is representable as Rf for some $f \in C_0^\infty(B)$.*

(2) (a) *The moment conditions are satisfied.*
(b) *The solution $G(x, t)$ of the interior Darboux problem satisfies the condition*

$$\lim_{t \to 0} \int\limits_B \frac{\partial G}{\partial t}(x, t) \phi(x) dx = 0$$

for any eigenfunction $\phi(x)$ of the Dirichlet Laplacian in B.

(3) (a) *The moment conditions are satisfied.*
(b) *Let $-\lambda^2$ be an eigenvalue of Dirichlet Laplacian in B and ψ_λ the corresponding eigenfunction. Then the following orthogonality condition is satisfied:*

$$\int\limits_{S \times [0,2]} g(x, t) \partial_\nu \psi_\lambda(x) j_{n/2-1}(\lambda t) t^{n-1} dx dt = 0. \tag{1}$$

(4) (a) *The moment conditions are satisfied.*
(b) *Let $\widehat{g}(x, \lambda) = \int g(x, t) j_{n/2-1}(\lambda t) t^{n-1} dt$. Then, for any $m \in \mathbb{Z}$, the m^{th} spherical harmonic term $\widehat{g}_m(x, \lambda)$ of $\widehat{g}(x, \lambda)$ vanishes at non-zero zeros of Bessel function $J_{m+n/2-1}(\lambda)$.*

Theorem [2]

(1) *In odd dimensions, moment conditions are not necessary. (A similar earlier result was established for a related transform in* [10]*.)*

(2) *The range descriptions work in Sobolev scale $H_s \mapsto H_{s+(d-1)/2}$ (uses a recent result by Palamodov* [26]*).*

(3) *The range conditions (except the ones using Bessel functions) are necessary in arbitrary domain.*

Some open problems

1. Describe uniqueness sets S for non-compactly supported functions. The only known result is of [1].
2. Describe uniqueness sets in dimensions > 2 (prove the Conjecture formulated above). Recent limited progress is available in [4].
3. Prove an analog of the result of [3] for the hyperbolic plane.

References

[1] M. Agranovsky, C. Berenstein, and P. Kuchment, Approximation by spherical waves in L^p-spaces, J. Geom. Anal. 6 (1996), no. 3, 365–383.

[2] M. Agranovsky, P. Kuchment, and E. T. Quinto, Range descriptions for the spherical mean Radon transform. I. Functions supported in a ball, arXiv:math.AP/0606314.

[3] M. Agranovsky and E.T. Quinto, Injectivity sets for the Radon transform over circles and complete systems of radial functions, Journal of Functional Analysis, 139 (1996), 383-414.

[4] G. Ambartsoumian and P. Kuchment, On the injectivity of the circular Radon transform, Inverse Problems 21 (2005), 473-485.

[5] G. Ambartsoumian and P. Kuchment, A range description for the planar circular Radon transform, SIAM J. Math. Anal. vol. 38, no. 2, 2006, 681-692.

[6] G. Ambartsoumian and S. Patch, Thermoacoustic tomography - implementation of exact backprojection formulas, arXiv:math.NA/0510638.

[7] L.-E. Andersson, On the determination of a function from spherical averages, SIAM J. Math. Anal. **19** (1988), no. 1, 214–232.

[8] R. Courant and D. Hilbert, Methods of mathematical physics, vol. 2, Interscience, NY 1953.

[9] J. A. Fawcett, Inversion of n-dimensional spherical averages, SIAM J. Appl. Math. **45**(1985), no. 2, 336–341.

[10] D. Finch and Rakesh, The range of the spherical mean value operator for functions supported in a ball, Inverse Problems **22** (2006), 923-938.

[11] D. Finch, S. Patch, and Rakesh, Determining a function from its mean values over a family of spheres, SIAM J. Math. Anal. **35** (2004), no. 5, 1213–1240.

[12] I. Gelfand, S. Gindikin, and M. Graev, *Selected Topics in Integral Geometry*, Transl. Math. Monogr. v. 220, Amer. Math. Soc., Providence RI, 2003.

[13] F. John, *Plane Waves and Spherical Means, Applied to Partial Differential Equations*, Dover 1971.

[14] R. A. Kruger, P. Liu, Y. R. Fang, and C. R. Appledorn, Photoacoustic ultrasound (PAUS)-reconstruction tomography, Med. Phys. **22** (1995), 1605–1609.

[15] P. Kuchment, unpublished, 1993.

[16] L. Kunyansky, A backprojection inversion formula for the spherical mean operator, preprint, May 2006.

[17] V. Lin and A. Pinkus, Fundamentality of ridge functions, J. Approx. Theory, 75(1993), 295-311.

[18] V. Lin and A. Pinkus, Approximation of multivariate functions, in Advances in computational mathematics, H. P. Dikshit and C. A. Micchelli, Eds., World Sci. Publ., 1994, 1-9.

[19] A. K. Louis and E. T. Quinto, Local tomographic methods in Sonar, in *Surveys on solution methods for inverse problems*, pp. 147-154, Springer, Vienna, 2000.

[20] F. Natterer, *The mathematics of computerized tomography*, Wiley, New York, 1986.

[21] F. Natterer and F. Wübbeling, *Mathematical Methods in Image Reconstruction*, Monographs on Mathematical Modeling and Computation v. 5, SIAM, Philadelphia, PA 2001.

[22] S. Nilsson, Application of fast backprojection techniques for some inverse problems of integral geometry, Linkoeping studies in science and technology, Dissertation 499, Dept. of Mathematics, Linkoeping university, Linkoeping, Sweden 1997.
[23] S. J. Norton, Reconstruction of a two-dimensional reflecting medium over a circular domain: exact solution, J. Acoust. Soc. Am. **67** (1980), 1266-1273.
[24] S. J. Norton and M. Linzer, Ultrasonic reflectivity imaging in three dimensions: exact inverse scattering solutions for plane, cylindrical, and spherical apertures, IEEE Transactions on Biomedical Engineering, 28(1981), 200-202.
[25] V. P. Palamodov, *Reconstruction from limited data of arc means*, J. Fourier Anal. Appl. **6** (2000), no. 1, 25–42.
[26] V. Palamodov, *Remarks on the general Funk transform*, preprint, Tel Aviv University, August 2006.
[27] S. K. Patch, *Thermoacoustic tomography - consistency conditions and the partial scan problem*, Phys. Med. Biol. **49** (2004), 1–11.
[28] E. T. Quinto, *Singularities of the X-ray transform and limited data tomography in* $\mathbf{R}^2$ *and* $\mathbf{R}^3$, SIAM J. Math. Anal. **24**(1993), 1215–1225.
[29] M. Xu and L.-H. V. Wang, Time-domain reconstruction for thermoacoustic tomography in a spherical geometry, IEEE Trans. Med. Imag. **21** (2002), 814–822.
[30] M. Xu and L.-H. V. Wang, Universal back-projection algorithm for photoacoustic computed tomography, Phys. Rev. E **71** (2005), 016706.
[31] Y. Xu, D. Feng, and L.-H. V. Wang, Exact frequency-domain reconstruction for thermoacoustic tomography: I. Planar geometry, IEEE Trans. Med. Imag. **21** (2002), 823–828.
[32] Y. Xu, M. Xu, and L.-H. V. Wang, Exact frequency-domain reconstruction for thermoacoustic tomography: II. Cylindrical geometry, IEEE Trans. Med. Imag. **21** (2002), 829–833.
[33] Y. Xu, L. Wang, G. Ambartsoumian, and P. Kuchment, Reconstructions in limited view thermoacoustic tomography, Medical Physics 31(4) April 2004, 724-733.
[34] N. Zobin, unpublished, 1993.

Range description for the spherical mean Radon transform

Mark Agranovsky
(joint work with P. Kuchment, E. T. Quinto)

The transform considered in the talk averages a function supported in a ball in $\mathbb{R}^n$ over all spheres centered at the boundary of the ball. This Radon type transform arises in several contemporary applications, e.g. in thermoacoustic tomography and sonar and radar imaging. Range descriptions for such transforms are important in all such applications, for instance when dealing with incomplete data, error correction, and other issues [16]. Several different types of complete range descriptions are provided, some of which also suggest inversion procedures.

We obtain range descriptions in arbitrary dimension for the case of centers on a sphere. Moreover, we obtain several different range descriptions that shed new light on the meaning of the range conditions (in particular, onto the appearance of two seemingly different subsets of conditions). Our approach rests on study the spherical mean transform from the point of view Darboux equation

$$(\partial_t^2 + \frac{n-1}{t}\partial_t)G(x,t) = \Delta_x G(x,t),$$

which according to the well known Asgeirsson's Theorem [5, 6, 13] describes all functions G that can be represented as the spherical mean transforms of functions f:

$$Rf(x,t) := G(x,t) = \int\limits_{|\theta|=1} f(x+t\theta)dA(\theta).$$

We consider the transform R_S that is applied to functions $f(y)$ supported in the unit ball $B = \{y \in \mathbb{R}^n | \, |y| \le 1\}$ and provides the values of $G(x,t)$ for points x on the unit sphere $S = \{x \in \mathbb{R}^n | \, |x| = 1\}$ only.

The range of this transform in the planar case $n = 2$ was described in [4] and range description in the case of odd dimension n, although for a somewhat different transform, was obtained in [7].

The following conditions [2, 14, 15, 18] are analogous to the moment conditions for the standard Radon transform [9, 10, 11, 12, 16]:

Moment conditions: For any $k = 0, 1, \cdots$, the function

$$M_k(x) = \int\limits_0^\infty g(x,t)t^{2k+n-1}dt$$

(1) extends from the unit sphere $|x| = 1$ to $\mathbb{R}^n$ as a polynomial of degree at most $2k$.

Theorem 1 *The following four statements are equivalent:*

(1) *The function $g(x,t) \in C_0^\infty(S \times [0,2])$ is representable as $R_S f$ for some $f \in C_0^\infty(B)$.*

(2) (a) *The moment conditions (1) are satisfied.*

(b) *The solution $G(x,t)$ of the interior backward initial-boundary value problem for Darboux equation in the cylinder $C = \{|x| \le 1\} \times (0,2]$ with the conditions $G(x,2) = G_t(x,2) = 0$ and $G(x,t) = g(x,t), |x| = 1$ satisfies the condition*

$$\lim_{t\to 0} \int\limits_B \frac{\partial G}{\partial t}(x,t)\phi(x)dx = 0$$

for any eigenfunction $\phi(x)$ of the Dirichlet Laplacian in B.

(3) (a) *The moment conditions (1) are satisfied.*

(b) *Let $-\lambda^2$ be an eigenvalue of Dirichlet Laplacian in B and ψ_λ be the corresponding eigenfunction. Then the following orthogonality condition is satisfied:*

$$\int\limits_{S\times[0,2]} g(x,t)\partial_\nu\psi_\lambda(x)j_{n/2-1}(\lambda t)t^{n-1}dxdt = 0. \tag{2}$$

Here ∂_ν is the exterior normal derivative at the boundary of C and $j_\nu(t) = t^{-\nu}J_\nu(t)$.

(4) (a) *The moment conditions (1) are satisfied.*

(b) *Let* $\widehat{g}(x,\lambda) = \int g(x,t) j_{n/2-1}(\lambda t) t^{n-1} dt$. *Then, for any integer* l, *the* l*th order spherical harmonic term* $\widehat{g}_l(x,\lambda)$ *of* $\widehat{g}(x,\lambda)$ *vanishes at non-zero zeros of the Bessel function* $J_{l+n/2-1}(\lambda)$.

We prove that when the dimension n is odd, the moment conditions (1) follow from any of the orthogonality conditions (2b) – (4b), which agrees with the result of [7], where the moment conditions do not appear. Thus, in odd dimensions one obtains

Theorem 2 *Let* $n \geq 3$ *be an odd integer. Then, in the notations of Theorem 1,* $g = R_S f$, *if and only if the orthogonality condition (b) in Theorem 1 is satisfied in any of its equivalent forms (2b) – (4b).*

It is also proven that the range conditions 2 and 3 of Theorem 1 are necessary for arbitrary domain B, not necessarily a ball, however their sufficiency does not always hold.

A Sobolev space (instead of C_0^∞) version of the theorems is also available, which employs the recent result of V. Palamodov [17], which was also reported at this workshop.

A preprint of this work is available in arXiv [1].

A related discussion of injectivity and inversion of the transform R_S can be found in [2, 3, 8], as well as in the reports by D. Finch and L. Kunyansky at this workshop.

References

[1] M. Agranovsky, P. Kuchment and E. T. Quinto, *Range description for the spherical mean Radon transform*, preprint arXiv:math.AP/0606314.

[2] M. L. Agranovsky, E. T. Quinto, *Injectivity sets for the Radon transform over circles and complete systems of radial functions*, J. Funct. Anal., **139** (1996), 383–413.

[3] G. Ambartsoumian and P. Kuchment, *On the injectivity of the circular Radon transform arising in thermoacoustic tomography*, Inverse Problems **21** (2005), 473–485.

[4] G. Ambartsoumian and P. Kuchment, *A range description for the planar circular Radon transform,* SIAM J. Math. Anal. **38** (2006), no. 2, 681–692.

[5] L. Asgeirsson, *Über eine Mittelwerteigenschaft von Lösungen homogener linearer partieller Differentialgleichungen zweiter Ordnung mit konstanten Koeffizienten*, Ann. Math., **113** (1937), 321–346.

[6] R. Courant and D. Hilbert, *Methods of Mathematical Physics, Volume II Partial Differential Equations*, Interscience, New York, 1962.

[7] D. Finch and Rakesh, *The range of the spherical mean value operator for functions supported in a ball*, Inverse Problems **22** (2006), 923-938.

[8] D. Finch, Rakesh, and S. Patch, *Determining a function from its mean values over a family of spheres*, SIAM J. Math. Anal. **35** (2004), no. 5, 1213–1240.

[9] I. Gelfand, S. Gindikin, and M. Graev, *Selected Topics in Integral Geometry*, Transl. Math. Monogr. v. 220, Amer. Math. Soc., Providence RI, 2003.

[10] I. Gelfand, M. Graev, and N. Vilenkin, *Generalized Functions, v. 5: Integral Geometry and Representation Theory*, Acad. Press 1965.

[11] S. Helgason, *The Radon Transform*, Birkhäuser, Basel 1980.

[12] S. Helgason, *Groups and Geometric Analysis*, Amer. Math. Soc., Providence, R.I. 2000.

[13] F. John, *Plane Waves and Spherical Means, Applied to Partial Differential Equations*, Dover 1971.

[14] V. Ya. Lin and A. Pinkus, *Fundamentality of ridge functions*, J. Approx. Theory, **75** (1993), 295–311.
[15] V. Ya. Lin and A. Pinkus, *Approximation of multivariable functions*, in *Advances in computational mathematics*, H. P. Dikshit and C. A. Micchelli, eds., World Sci. Publ., 1994, 1-9.
[16] F. Natterer, *The mathematics of computerized tomography*, Wiley, New York, 1986.
[17] V. Palamodov, *Remarks on the general Funk transform*, preprint, Tel Aviv University, August 2006.
[18] S. K. Patch, Thermoacoustic tomography - consistency conditions and the partial scan problem, Phys. Med. Biol. **49** (2004), 1–11.

Equations Governing Waves Attenuated According to a Power Law

Sarah Patch
(joint work with Allan Greenleaf)

1. Introduction

Attenuation typically comes hand-in hand with dispersion. Causality imposes consistency conditions upon attenuation and dispersion, which were first derived for xray radiation by Kramers and Krönig [1, 2]. See [4] for an excellent introduction to causality where different strengths are defined. We study attenuation according to a power law

$$e^{-\alpha|\tau|^b d} \tag{1}$$

where $[\alpha] = MHz^{-b}cm^{-1}$, d is distance traveled, and the frequency τ is dual to t [7]. For most fluids, thermoviscous dissipation corresponds to $b \equiv 2$ [3] and the Kramers-Krönig relations predict zero dispersion [6]. The governing equation is a partial differential equation (PDE). Not only is the PDE consistent with primitive causality, it can be directly related to the standard heat equation. Furthermore, the impulse response function is closely related to the standard heat kernel, highlighting the fact that this theory allows signals to propagate faster than the speed of light and is inconsistent with relativistic causality. We derive the governing PDE's in three spatial dimensions starting with the unattenuated acoustic wave equation and assuming nothing other than attenuation according to (1). Working from the Fourier domain lossy wave equation we derive the governing equations, without frequency range restrictions needed in [5].

Forgetting for a moment the frequency restrictions on the attenuation model (1) we apply it to the fundamental solution to the standard wave equation to derive a smoothed impulse response function

$$\begin{aligned} p^{\delta}_{atten}(\mathbf{x},t) &= \frac{1}{|\mathbf{x}-\mathbf{x}_o|}\int_{\mathcal{R}} e^{-\alpha\tau^2|\mathbf{x}-\mathbf{x}_o|} e^{-2\pi i|\mathbf{x}-\mathbf{x}_o|/c\tau} e^{2\pi i t\tau} d\tau \\ &= \sqrt{\frac{\pi}{\alpha\,|\mathbf{x}-\mathbf{x}_o|^3}}\, e^{-\frac{\pi^2(|\mathbf{x}-\mathbf{x}_o|/c-t)^2}{\alpha|\mathbf{x}-\mathbf{x}_o|}} \end{aligned} \tag{2}$$

This is the 1D heat kernel with variables reinterpreted. Time in the standard heat kernel is replaced by the attenuation parameter times distance and distance is replaced by "retarded time," defined in [5] as time delay from the unattenuated wave front. As $\alpha\,|\mathbf{x}-\mathbf{x}_o| \to 0$, h approaches a delta function centered on the unattenuated wave front. Notice also that $h > 0$ for $\alpha > 0$ and all finite distances $|\mathbf{x}-\mathbf{x}_o| - ct$. This agrees with *primitive* causality as discussed by Nussenzveig [4]. Like the fundamental solution to the standard heat equation, h is relativistically acausal, permitting infinite propagation speed. An impulse at the origin at time t_o generates positive signal for all finite distances, $|\mathbf{x}-\mathbf{x}_o|$, at arbitrarily small time t.

This is the 3D version of impulse response functions derived in [3, 6]. Assuming no dispersion, attenuated pressure is equal to the convolution of f against the fundamental solution

$$p^f_{att}(\mathbf{x},t) \;=\; \int_{\mathcal{R}^3} \frac{f(\mathbf{y})}{|\mathbf{x}-\mathbf{y}|}\left(\int_{\mathcal{R}} e^{-\beta(\tau)|\mathbf{x}-\mathbf{y}|}e^{2\pi i t\tau}d\tau\right)d\mathbf{y} \tag{3}$$

where we have defined

$$\beta(\tau) \;=\; -\left(\alpha\tau^2 + 2\pi i\tau/c_o\right) \leftrightarrow \left(\frac{\alpha}{4\pi^2}\frac{\partial}{\partial t} - \frac{1}{c_o}\right)\frac{\partial}{\partial t} \tag{4}$$

Multiplication by $\beta(\tau)$ in the Fourier domain corresponds to taking derivatives with respect to time. We formally compute $\Delta_{\mathbf{x}} p^f_{att}$, first noting that

$$\Delta_{\mathbf{x}}\left(\frac{e^{\beta(\tau)|\mathbf{x}-\mathbf{y}|}}{|\mathbf{x}-\mathbf{y}|}\right) \;=\; \beta(\tau)^2\left(\frac{e^{\beta(\tau)|\mathbf{x}-\mathbf{y}|}}{|\mathbf{x}-\mathbf{y}|}\right) + \delta(\mathbf{x}-\mathbf{y})\,e^{\beta(\tau)|\mathbf{x}-\mathbf{y}|} \tag{5}$$

The Laplacian of pressure is given by

$$\Delta_{\mathbf{x}} p^f_{att}(\mathbf{x},t) \;=\; \int_{\mathcal{R}^3} f(\mathbf{y})\int_{\mathcal{R}} \beta(\tau)^2\left(\frac{e^{\beta(\tau)|\mathbf{x}-\mathbf{y}|}}{|\mathbf{x}-\mathbf{y}|}\right)e^{2\pi i t\tau}d\tau d\mathbf{y} + f(\mathbf{x})\delta(t) \tag{6}$$

Combining equations (4) and (6) yields a partial differential equation for $b = 2$ that is $fourth$ order with respect to time

$$\Delta_{\mathbf{x}} p^f_{att}(\mathbf{x},t) - \left[\left(\frac{\alpha}{4\pi^2}\frac{\partial}{\partial t} - \frac{1}{c_o}\right)\frac{\partial}{\partial t}\right]^2 p^f_{att}(\mathbf{x},t) = f(\mathbf{x})\,\delta(t) \tag{7}$$

Taking spherical means of each term reduces the number of spatial dimensions to one *and* permits factorization of the differential operator into the product of two parabolic operators:

$$L_+L_-\,(r\;Mp_{att}(\mathbf{x},t,r)) = (r\;Mf)(\mathbf{x},r)\,\delta(t) \tag{8}$$

where

$$L_\pm = \frac{\partial}{\partial r} \pm \left[\left(\frac{\alpha}{4\pi^2}\frac{\partial}{\partial t} - \frac{1}{c_o}\right)\frac{\partial}{\partial t}\right] = \left(\frac{\partial}{\partial r} \mp \frac{1}{c_o}\frac{\partial}{\partial t}\right) \pm \frac{\alpha}{4\pi^2}\frac{\partial^2}{\partial t^2} \tag{9}$$

References

[1] de Krönig RL, Kramers HA, *Zur Theorie der Absorption und Dispersion in den Röntgenspektren*, pp. 174-179, (1928).

[2] de Krönig RL, *On the theory of dispersion of x-rays*," Journal of the Optical Society of America, **12**, pp. 547-557, (1926).

[3] Landau-Lefschetz, *SKP - GET THIS REFERENCE RIGHT*

[4] Nussenzveig HM, *Causality and Dispersion Relations*, Academic Press, New York, 1972.

[5] Szabo TL, *Time domain wave equations for lossy media obeying a frequency power law*, Journal of the Acoustical Society of America, **96**(1), pp. 491-500, (1994).

[6] Waters KR, Hughes MS, Mobley J, Brandenberger GH, Miller JG, *On the applicability of Kramers-Krönig relations for ultrasonic attenuation obeying a frequency power law*, Journal of the Acoustical Society of America, **108**(2), pp. 556-563, (2000).

[7] Wells PNT, *Biomedical Ultrasonics*, Academic Press, London, 1977.

Topics in Thermoacoustic Tomography

David Finch
(joint work with Markus Haltmeier, Rakesh)

I have been interested for several years in mathematical problems associated with thermoacoustic tomography. One formulation of the problem is that it is the recovery of initial data of the form $(f, 0)$ supported in a domain D from the trace of the solution of the wave equation on (a subset of) the boundary of D for some interval of time. As witness several of the presentations for this meeting, it is an area enjoying much attention at the moment.

The results discussed in this presentation concern the recovery of initial data from the trace on the boundary in even dimensions. Since the body is three dimensional and sound propagating in the body will be governed by a three dimensional wave equation, we must ask whether the results are of mathematical interest only. In fact no. While the original formulation of thermoacoustic tomography modelled the measurement process as omnidirectional point detectors on the boundary of the domain, there have been other measurement techniques investigated. The Austrian group of Burgholzer, Haltmeier, Nusler, Paltauf, and Scherzer [1, 3] have been working with integrating detectors. An integrating line detector, realized by interferometry, in effect computes the x-ray transform of a solution of the three dimensional wave equation. This is then a solution of the two dimensional wave equation, whose intial data is the x-ray transform of the initial data of the original initial data. This is done for all directions parallel to a plane by rotating the object. By this means, they reduce the three dimensional problem to many inversions of the two-dimensional wave equation, and inversion of the x-ray transform in the family of planes perpendicular to the rotation axis.

We have found an inversion formulas when D is a ball in even dimensions. An ingredient of the proof are the following inversion formulas for the circular mean

transform, $f \to Mf$, with centers on a circle S of radius ρ :

$$f(y) = \frac{1}{2\pi\rho}\Delta \int_S \int_0^{2\rho} rMf(x,r) \log|r^2 - |x-y|^2|\, dr\, ds(x)$$

or with the Laplacian inside

$$f(y) = \frac{1}{2\pi\rho} \int_S \int_0^{2\rho} \frac{\partial}{\partial r}\left(r\frac{\partial}{\partial r} Mf(x,r)\right) \log|r^2 - |x-y|^2|\, dr\, ds(x).$$

We observe that the latter expression can be also be written as

$$f(y) = \frac{1}{2\pi\rho} \int_S |x-y| \int_{-2\rho}^{2\rho} \frac{\partial}{\partial r} Mf(x,r) \frac{1}{|x-y| - r}\, dr\, ds(x),$$

if we consider Mf as an odd function in r. The inner filtering step is exactly that of the two-dimensional Radon transform, and so many good numerical implementations are known.

Let $\mathcal{P}$ denote the operator which takes initial data of the form $(0, f)$ supported in the ball B to the trace of the wave equation on the boundary of the ball (and positive time). Then $\mathcal{T} = \partial_t \mathcal{P}$ is the operator taking initial data of the form $(g, 0)$ to the trace of the solution of the initial value problem.

Theorem 1. *Let f be smooth and supported in the ball B of radius R in R^{2m}, and let $\mathcal{P}f$ and $\mathcal{T}f$ be as above. Then in B*

$$f = -\frac{2}{R}\mathcal{P}^* t \partial_t^2 \mathcal{P} f$$
$$f = \frac{2}{R}\mathcal{T} * t\mathcal{T} f = -\frac{2}{R}\mathcal{P}^* \partial_t t \partial_t \mathcal{P} f.$$

Theorem 2. *Let f, g be smooth and supported in B_R in R^{2m} ($m \geq 1$), let $S \equiv \partial B_R$, and let $u = \mathcal{P}f$, $v = \mathcal{P}g$.*

$$\int_B f(x)g(x)\, dx = -\frac{2}{R}\int_0^\infty \int_S t u_{tt}(p,t) v(p,t)\, dS_p\, dt,$$
$$\int_B f(x)g(x)\, dx = \frac{2}{R}\int_0^\infty \int_S t u_t(p,t) v_t(p,t)\, dS_p\, dt.$$

The inversion formulas and weighted integral identities above were already proved in [2] for odd dimensions, and so they hold in general. In fact, the outline of proof is very similar to that used in [2]. First, an inversion formula is proved when $n = 2$. It is then used to prove the energy identity in dimension two, and it is then seen by harmonic decomposition that it holds in all even dimensions. Finally, the energy identity implies the inversion formula completing the proof. It is in the proof of the inversion formula in dimension two that the inversion formula for the spherical means comes into play.

We should also remark that combining the standard inversion formula for an Abel type integral equation with the formula above for inversion of spherical means in dimension two gives another expression to recover the initial data from the boundary trace of the solution of the wave equation.

The relation of these formulae to the formula announced by Kunyansky at this meeting has not yet been pursued.

There are other questions of practical or of mathematical interest which arise in thermoacoustic tomography. We have not addressed range results here, but there has been recent progress in that area: the talks by Kuchment and by Agranovsky gave a good survey. In our opinion, the leading questions currently open are:

- Solve the inverse problem for non-constant wave speed.
- Find a better analysis of the situation with incomplete data.
- Incorporate a better model of transducer response.

References

[1] P. Burgholzer, C. Hofer, G. Paltauf, M. Haltmeier, and O. Scherzer, *Thermoacoustic tomography with integrating area and line detectors*, IEEE Trans. Ultrasonics, Ferroelectrics, Freq. Control, **52** (2005) 1577–1583.

[2] D. Finch, S.K. Patch, and Rakesh *Determining a function from its mean values over a family of spheres*, SIAM J. Math. Anal. **35** (2004), 1213–1240.

[3] G. Paltauf, R. Nuster, M. Haltmeier, and P. Burgholzer *Thermoacoustic computed tomography usng a Mach-Zehnder interferometer as acoustic line detector*,(2006), submitted

Improved cone beam local tomography

Alexander Katsevich

In computed tomography (CT) the goal is to reconstruct the distribution of the x-ray attenuation coefficient f inside the object being scanned. Local tomography (LT) computes not f, but $\mathcal{B}f$, where $\mathcal{B}$ is some operator that enhances singularities of f. In two dimensions (2D), $\mathcal{B}$ is an elliptic pseudo-differential operator (PDO) of order one (cf. e.g. [1, 2, 3, 4, 5, 6, 13] and references therein). In the cone beam setting (three dimensions) a LT function, which we denote here g_Λ, was introduced in [7]. It turned out that the corresponding operator $\mathcal{B} : f \to g_\Lambda$ is much more complicated than in 2D. It preserves the so-called visible (or, useful) singularities [8], but creates also non-local artifacts [9, 10]. Unfortunately, the strength of these artifacts is the same as that of the useful singularities of g_Λ [9, 10].

In this talk we describe a new cone beam LT function g, proposed recently in [12]. We show that, similarly to the LT function g_Λ, g recovers visible singularities of f. More precisely, the operator $f \to g$ is just a PDO of order one microlocally near the visible singularities of f. The principal symbol of the operator is found. As follows from [11, 10], non-local artifacts are inherent in cone beam LT. The main advantage of the new LT function is that it produces artifacts, which are one order smoother in the scale of Sobolev spaces than the artifacts produced by the previously known function g_Λ.

Next we investigate how LT works when f changes with time. We assume that f is a conormal distribution, which depends smoothly on time. The notion of visible singularities is suitably generalized, and a relationship between the wave fronts of f and g is established. Interestingly, even the visible singularities of f no

longer coincide with the corresponding singularities of g. There is a shift between them, and its size depends on the rate of change of f. We also investigate non-local artifacts in g, and they turn out to be of the same strength as in the static case (i.e., weaker than in g_Λ).

Finally, we discuss how to implement the LT function when the source trajectory is a helix and present some numerical experiments both in the static and dynamic cases. These results confirm our main theoretical conclusions.

References

[1] A. Faridani, *Results, old and new, in computed tomography*, Inverse Problems in Wave Propagation (G. Chavent, G. Papanicolaou, P. Sacks, and W. Symes, eds.), The IMA Volumes in Mathematics and its Applications, vol. 90, Springer Verlag, New York, 1997, 167–193.

[2] A. Faridani, D. Finch, E. Ritman, and K. Smith, *Local tomography II*, SIAM Journal on Applied Mathematics, **57** (1997), no. 4, 1095–1127.

[3] A. Katsevich, *Local tomography for the generalized Radon transform*, SIAM Journal on Applied Mathematics, **57** (1997), no. 4, 1128–1162.

[4] P. Kuchment, K. Lancaster, and L. Mogilevskaya, *On local tomography*, Inverse Problems, **11** (1995), 571–589.

[5] A. Ramm and A. Katsevich, *The Radon Transform and Local Tomography*, CRC Press, Boca Raton, Florida, 1996.

[6] A. Ramm, *Necessary and sufficient conditions for a PDO to be a local tomography operator*, Comptes Rend Acad Sci, Paris, **332** (1996), 613–618.

[7] A. K. Louis and P. Maass, *Contour reconstruction in 3-D X-ray CT*, IEEE Transactions on Medical Imaging, **12** (1993), 764–769.

[8] E. T. Quinto, *Singularities of the X-ray transform and limited data tomography in* $\mathbb{R}^2$ *and* $\mathbb{R}^3$, SIAM Journal of Mathematical Analysis, **24** (1993), 1215–1225.

[9] A. Katsevich, *Cone beam local tomography*, SIAM Journal on Applied Mathematics, **59** (1999), no. 6, 2224–2246.

[10] D. Finch, I.-R. Lan, and G. Uhlmann, *Microlocal analysis of the x-ray transform with sources on a curve*, Inside out: Inverse Problems and Applications (G. Uhlmann, ed.), Cambridge Univ. Press, 2003, 193–218.

[11] A. Greenleaf and G. Uhlmann, *Nonlocal inversion formulas for the X-ray transform*, Duke Mathematical Journal, **58** (1989), 205–240.

[12] A. Katsevich, *Improved cone beam local tomography*, Inverse Problems, **22** (2006), 627–643.

[13] H. Yu and G. Wang, *A General Formula for Fan-Beam Lambda Tomography*, International Journal of Biomedical Imaging (2006).

Multiresolution Analysis in Computerized Tomography and its Application to Non-Destructive Testing

Steven Oeckl

(joint work with Tobias Schön, Andreas Knauf, Alfred K. Louis)

Since wavelet analysis has become a powerful tool for signal and image processing, the multiresolution approach provides a solution for many practical applications. In X-ray computerized tomography algorithms for multiresolution two dimensional (2D) parallel beam, 2D fan-beam, and three dimensional cone-beam (Feldkamp-type) reconstruction using tensor or quincunx wavelets were introduced in [1, 2, 3].

These reconstruction formulas are based on the strong relationship between the continuous wavelet transform and the Radon transform as mentioned in [4]. In this contribution we use a different approach to achieve an algorithm for reconstructing an object at different resolutions: The approximate inverse, introduced in [5], is a method for solving first kind operator equations $Af = g$ in a stable way. Instead of determining the exact solution f, an inversion operator for f_e is calculated, where f_e is associated to f via the inner product $\langle f, e\rangle$ using a mollifier e. Applying the approximate inverse to computerized tomography yields a reconstruction algorithm of filtered backprojection type [6]. If we choose the mollifier as a wavelet, f_e represents the wavelet coefficients of f [7]. In this contribution we show a new derivation of a nonseparable multiresolution reconstruction formula using the approximate inverse. For the sake of simplicity we introduce a nonseparable multiresolution inversion formula only for the 2D parallel scanning geometry. The resulting inversion formula using the approximate inverse is equal to the formula in [1]. In case of narrow cone-beam angles we make use of the Feldkamp algorithm [8]. We replace the standard ramp filter by the proposed ramp-wavelet filter, where the 2D multiresolution acts slice by slice.

We start with a short introduction to the concept of the approximate inverse, for details see [5]. Let U, V be Hilbert spaces, where U consists of functions $f : X \to Y$, and let $A : U \to V$ be a linear, continuous Operator. Consider the problem of solving $Af = g$. For $x \in X$ we define a mollifier $e_x \in U$ and an associated approximation of f

$$\tilde{f}(x) := \langle f, e_x\rangle_U \,.$$

Let A^* denote the adjoint operator of A. If $v_x \in V$ solves $A^* v_x = e_x$, we have

$$\tilde{f}(x) = \langle f, e_x\rangle_U = \langle f, A^* v_x\rangle_U = \langle Af, v_x\rangle_V = \langle g, v_x\rangle_V =: A^\ddagger g(x)\,.$$

$A^\ddagger : V \to U$ is called the *approximate inverse* of A, v is called the *reconstruction kernel*.

The following definitions and properties related to the Radon transform can be found in [9]. For $f \in \mathcal{S}(\mathbb{R}^n)$, $\theta \in S^{n-1}$, and $s \in \mathbb{R}$ the *Radon transform* is defined $\mathcal{R}_\theta f(s) := \mathcal{R}f(\theta, s) := \int_{\theta^\perp} f(s\theta + t)\, dt$. The *Fourier transform* of f is defined $\hat{f} := (2\pi)^{-n/2} \int_{\mathbb{R}^n} f(x) e^{-i\omega x}\, dx$. For $\sigma \in \mathbb{R}$ we have $\widehat{\mathcal{R}_\theta f}(\sigma) = (2\pi)^{(n-1)/2} \hat{f}(\sigma\theta)$, and for $g = \mathcal{R}f$ the adjoint operator of $\mathcal{R}$ has the form $\mathcal{R}^* g(x) = \int_{S^{n-1}} g(\theta, x\cdot\theta)\, d\theta$. To derive an inversion formula for the Radon transform we define for $\alpha < n$ the *Riesz potential* I^α via $\widehat{I^\alpha f}(\omega) := |\omega|^{-\alpha} \hat{f}(\omega)$. For $g = \mathcal{R}f$ we have

$$f = \frac{1}{2}(2\pi)^{1-n} I^{-\alpha} \mathcal{R}^* I^{\alpha-n+1} g\,, \tag{1}$$

where the Riesz potential acts on the second variable.

Consider the problem $\mathcal{R}f = g$ in the 2D case. Choose for each $x \in \mathbb{R}^2$ a mollifier $e_x \in \mathcal{S}(\mathbb{R}^2)$, and define $v_x := \frac{1}{2}(2\pi)^{-1} I^{-1} \mathcal{R} e_x$. Due to the inversion formula (1), v_x solves the equation $\mathcal{R}^* v_x = e_x$ and is therefore the reconstruction kernel of the

approximate inverse of the Radon transform. We conclude

$$(2) \qquad \tilde{f}(x) = \mathcal{R}^{\sharp} g(x) = \langle g, v_x \rangle_{\mathcal{S}(S^1 \times \mathbb{R})} = \frac{1}{2}(2\pi)^{-1} \int_{S^1} \int_{\mathbb{R}} g(\theta, s) I^{-1} \mathcal{R}_\theta e_x(s)\, ds\, d\theta\,.$$

Since we want to make use of the approximate inverse to reconstruct the wavelet coefficients of f directly from the projection data, we introduce some results from multiresolution analysis (MRA), for details see [10, 7]. Let $D \in \mathbb{Z}^{2x2}$ be a dilation matrix and define $M := |detD|$. Let $\{\phi, \tilde{\phi}\}$ be a pair of dual scaling functions of a 2D MRA, and let $\{\psi^i, \tilde{\psi}^i\}$, $i = 1, \ldots, M$, be $M - 1$ pairs of dual mother wavelets. For a fixed $J \in \mathbb{Z}$ and $f \in L^2(\mathbb{R}^{\not\leq})$ we have the wavelet expansion

$$f = \sum_{k \in \mathbb{Z}^2} \langle f, \phi_{J,k} \rangle \tilde{\phi}_{J,k} + \sum_{i=1}^{M-1} \sum_{j<J} \sum_{k \in \mathbb{Z}^{\not\leq}} \langle f, \psi^i_{j,k} \rangle \tilde{\psi}^i_{j,k}\,,$$

where $\phi_{j,k} := |detD|^{-(j/2)}\, \phi(D^{-j} \cdot -k)\,.$

If we define $e_x := \psi_{j,x}$ for the problem $\mathcal{R}f = g$, then we have $\mathcal{R}^{\sharp}(x)g = \tilde{f}(x) = \langle f, \psi_{j,x} \rangle$. Calculating the approximate inverse at $k \in \mathbb{Z}^2$ is equal to calculating the wavelet coefficients of f, i.e. $\mathcal{R}^{\sharp} g(k) = \langle f, \psi_{j,k} \rangle$. Starting with (2), we conclude

$$\begin{aligned}
\langle f, \psi_{j,k} \rangle &= \frac{1}{2}(2\pi)^{-1} \int_{S^1} \int_{\mathbb{R}} I^{-1} g(\theta, s) \mathcal{R}_\theta \psi_{j,k}(s)\, ds\, d\theta \\
&= \frac{1}{2}(2\pi)^{-1} \int_{S^1} \int_{\mathbb{R}} I^{-1} g(\theta, s) \mathcal{R}_{-\theta} \psi_{j,0} \left(\langle D^j k, \theta \rangle - s \right)\, ds\, d\theta \\
&= \frac{1}{2}(2\pi)^{-1} \int_{S^1} \left(I^{-1} g(\theta, \cdot) * \mathcal{R}_{-\theta} \psi_{j,0} \right) \left(\langle D^j k, \theta \rangle \right)\, d\theta\,.
\end{aligned}$$

This inversion formula is of filtered backprojection type and therefore allows for a fast implementation. We are able to formulate an inversion formula to reconstruct the approximation coefficients $\langle f, \phi_{j,k} \rangle$ in the same way.

For practical applications the possibility to perform a progressive reconstruction is the main advantage of multiresolution tomographic reconstruction. Reconstructing the approximation coefficients at a high decomposition level yields a first impression of the specimen. After selecting a region of interest within the approximation only the detail coefficients of the selected region plus a certain border must be reconstructed to achieve high resolution inside the region of interest. In non-destructive testing progressive reconstruction can be used to incorporate previous knowledge about the specimen, the scanning geometry, and the inspection task efficiently into the reconstruction method.

References

[1] S. Bonnet, F. Peyrin, F. Turjman, and R. Prost, *Multiresolution Reconstruction in Fan-Beam Tomography*, IEEE Transactions on Image Processing **11(3)** (2002), 169–176.

[2] S. Bonnet, F. Peyrin, F. Turjman, and R. Prost, *Nonseparable Wavelet-Based Cone-Beam Reconstruction in 3-D Rotational Angiography*, IEEE Transactions on Medical Imaging **22(3)** (2003), 360–367.
[3] F. Rashid-Farrokhi, K. J. Ray Liu, C. A. Berenstein, and D. Walnut, *Wavelet-Based Multiresolution Local Tomography*, IEEE Transactions on Image Processing **6(10)** (1997), 1412–1430.
[4] D. Walnut, *Applications of Gabor and wavelet expansions to the Radon transform*, in J. S. Byrnes et al, editor, Probabilistic and Stochastic Methods in Analysis, With Applications, Kluwer Academic Publishers (1992), 187–205.
[5] A. K. Louis, *Approximate inverse for linear and some nonlinear problems*, Inverse Problems **12** (1996), 175–190.
[6] A. K. Louis, *Filter design in three-dimensional cone beam tomography: circular scanning geometry*, Inverse Problems **19** (2003), 31–40.
[7] A. K. Louis, P. Maaß, and A. Rieder, *Wavelets*, Teubner (1998).
[8] L. A. Feldkamp, L. C. Davis, and J. W. Kress, *Practical cone-beam algorithm*, J. Opt. Soc. Am. A **1(6)** (1984), 612–619.
[9] F. Natterer, *The Mathematics of Computerized Tomography*, John Wiley & Sons (1986).
[10] S. Mallat, *A theory for multiresolution signal decomposition: The wavelet representation*, IEEE Transactions on Pattern Analysis and Machine Intelligence **11** (1989), 674–693.

Two side topics in Inverse Theory

P.C. Sabatier
(joint work with C. Sebu)

The talk contains two parts. The first one presents results already published by PCS [1] It is shown how a Generalised Inverse Scattering Transform yields global solutions of linear partial differential equations whose coefficients are solutions of IST integrable nonlinear partial differential equations, in this sense that the solution corresponding to a boundary condition either on the full x or t axis or on the two half axes limiting the quarter-plane can be constructed. . Two simple examples are:

$$\frac{\partial a}{\partial t} + \frac{1}{4}a''' - \frac{3}{4}(aV' + a'V) = 0 \tag{1}$$

and:

$$\frac{\partial a}{\partial t} + \frac{1}{4}a''' - \frac{3}{2}(aV)' = 0 \tag{2}$$

where V is a solution of the Korteveg de Vries equation, (which is that obtained if V is relaced by a in Eq. (1)). Analogous results can be derived for equations asssociated to the Nonlinear Schrödinger Equation. and for inhomogeneous forms of these linear p.d.e.

The second part presents a simple way to estimate the resolving power of data in Electrical Impedance Tomography, where the current Φ or $\frac{\partial \Phi}{\partial \nu}$, (either one being

externally driven), and the conductivity σ are measured on the surface $\partial\Omega$ of a closed domain Ω, and an estimated value of σ is proposed inside Ω to fit these data. the EIT problem has been thoroughly studied and many reviews exist, including recent ones [2].There also exists a very refined analysis [3] of the information which can be extracted by EIT, using Gabor Analysis, and concluding that "a very limited amount of information can be extracted from any real measurements". We give here an elementary approach. Following Ciulli et al. [4], we introduce the Green functions G_D, resp. G_N, defined by:

$$\Delta_y G_{N,D}(x,y) = -\delta(x-y) \tag{3}$$

and by a condition cancelling respectively G_D and $\frac{\partial}{\partial\nu}G_N$ on $\partial\Omega$. Using them in the Potential equation:

$$\Delta\Phi(x) = -\sigma^{-1}\mathrm{grad}\,\sigma \bullet \mathrm{grad}\,\Phi(x) =: -Y(x) \tag{4}$$

we can relate to Y the following functions, that can be "measured" on $\partial\Omega$

$$\chi_D(x) = -\int_{\partial\Omega} ds(z)\frac{\partial G_D}{\partial\nu}(x,z)\Phi(z) \tag{5}$$

$$\chi_N(x) = \int_{\partial\Omega} ds(z) G_N(x,z)\frac{\partial\Phi}{\partial\nu_z}(x,z) + \frac{\int_{\partial\Omega} ds(z)\Phi(z)}{\int_\Omega ds(z)} \tag{6}$$

$$\chi_N(x) - \chi_D(x) = \int_\Omega dy\,[G_D(x,y) - G_N(x,y)]\,Y(y) \tag{7}$$

Hence Y is determined by the measurements thanks to a compact operator whose kernel, say G, is symmetric (and harmonic). For a given ratio noise over signal (say, η), the singular value decomposition, taking also care of the null space, shows the relevant eigenfunctions $w_n(x)$, the only ones to be kept: the projector constructed out of them gives a range of estimates of Y, and transfering them in the equation:

$$\Phi(x) = \chi_{N,D}(x) + \int_\Omega dy\, G_{N,D}(x,y)Y(y) \tag{8}$$

where the indices N, D, correspond to each other, we get a similar information on Φ. In [4], it is shown how σ can be determined (in C_1 cases) from its boundary value and that of Φ inside the domain. Hence we could proceed but it is simpler to linearise the conductivity equation in the neighborhood of an estimate of Φ and the corresponding calculated estimate of σ, then derive the variations of σ from those of Φ and of the boundary value by means of the following equations, obtained from Eq. (4), and by using the projector made out of all the w_n; (we assumed for simplicity that there is no error on the boundary values of σ):

$$\operatorname{div}(\sigma \operatorname{grad} \delta\Phi) = -\operatorname{div}(\delta\sigma \operatorname{grad} \Phi) \tag{9}$$

$$= -\sum_{1}^{N} w_n(y) \int\int\int_{\Omega} w_n(x) \operatorname{div}_x \left[\sigma(x) \operatorname{grad} \delta\Phi(\mathrm{x})\right] =: \left[\delta_1 \Phi\right] \tag{10}$$

$$\left[\delta_1 \Phi\right](y) = \int_{\Omega} dz \delta\sigma(z) \sum_{p=1}^{N} \sum_{n=1}^{N} w_n(y) w_p(z) \Phi_{np} \tag{11}$$

this relation can be itself analysed by the singular value decomposition. The resolving power of data is the width of the projector on relevant eigenfunctions (Backus-Gilbert style) or equivalently the half wave length of the first discarded eigenfunction. The results are of same order and show that at a given point one can only determine the integral of σ along each i coordinate on intervals of finite length, the "resolving length', centered at this point. Hence this length depends on the order of the first discarded eigenvalue, which depends itselt on η. Calculations on the example of the unit disc, with a two bumps conductity (bumps of width .2) and η as .02, show a resolving length of the order of .5 radian in the azimuthal coordinate, .1 in the radial one. The decreasing of eigenvalues of G in this particular example is as a negative power, which predicts that the resolving length decreases at most as a fractional power of η. This is consistent with the estimate of reference [3] concerning the limitations of information that can be extracted.

References

[1] P.C. Sabatier. Generalised inverse scattering transform applied to linear partial differential equations. Inverse Problems **22** (2006) 209-228

[2] G.J. Saulnier, R.S. Blue, J.C. Newell, D. Isaacson, and P.M. Edic, Electrical Impedance Tomography, IEEE Signal Processing Magazine Nov. 2001, 31-43. see also M. Hanke and M. Bruhl, Recent Progress in electrical impedance tomography. Inverse Problems **19** (2003) S65 -S90

[3] Victor P. Palamodov. Gabor analysis of the continuum model for impedance tomography. Ark. Mat. **40** (2002) 169-187

[4] S. Ciulli, M. Pidcock and C. Sebu. "An integral equation method for the inverse conductivity problem", Phys. Lett. A 325 (2004) 253-267.

Remarks on the general Funk transform

Victor Palamodov

1. Let X and Σ be n-dimensional manifolds and F is a closed hypersurface in $X \times \Sigma$ that satisfies the conditions

(i) the projections $p : F \to X$ and $\pi : F \to \Sigma$ have rank n. The sets $F(\sigma) = \pi^{-1}(\sigma), \sigma \in \Sigma$ and $F(x) = p^{-1}(x), x \in X$ are hypersurfaces in X, respectively, in Σ;

(ii) the mapping $q : F \to G^{n-1}T(X)$ is a local diffeomorphism, where $q(x,\sigma) = (x,\theta)$ and θ denotes the tangent hyperplane to $F(\sigma)$ and $G^{n-1}T(X)$ denotes the bundle of $n-1$-subspaces in the tangent bundle $T(X)$ of X.

The manifold F can be considered as a n-parameter family of hypersurfaces $F(\sigma), \sigma \in \Sigma$ in X as well as the (dual) n-parameter family of hypersurfaces $F(x), x \in X$ in Σ. The dual family also fulfils (ii).

The family F can be defined locally by the equation $I(x,\sigma) = 0$, where I is a smooth function in $X \times \Sigma$ such that $\mathrm{d}I \neq 0$. If the manifold F is cooriented, a function I can be chosen globally; we call it incidence function. If F is not cooriented, one can choose local functions $I_\alpha, \alpha \in A$ such that $I_\beta = \pm I_\alpha$ in the domain, where both functions I_α, I_β are defined.

Proposition. The conditions (i) and (ii) are equivalent to the relation $\det \Phi \neq 0$ in F,where

$$\Phi' = \left\{ \frac{\partial^2 I}{\partial x_i \partial \sigma_j} \right\}_{i,j=0}^{n}$$

where $x_1, ..., x_n$ and $\sigma_1, ..., \sigma_n$ are local coordinates in X and in Σ, respectively and $\partial/\partial x_0, \partial/\partial \sigma_0$ stand for identity operators.

2. The (generalized) Funk transform is defined for densities f in X with compact support:

$$M\mathrm{f}(\sigma) \doteq \lim_{\varepsilon \to 0} \frac{1}{2\varepsilon} \int_{|I(\cdot,\sigma)| \leq \varepsilon} \mathrm{f},\ \sigma \in \Sigma$$

It has compact support, if the following condition is fulfilled:

Example 1. Let X and Σ be unit spheres in Euclidean 3-spaces and F is defined by the global incidence function $I(x,\sigma) = x_1\sigma_1 + x_2\sigma_2 + x_3\sigma_3$. The operator M is the classical Minkowski-Funk transform for even densities. The dual operator M° is equivalent to M through the natural isomorphism $X \cong \Sigma$.

The scale of Sobolev L_2-norms $\|\cdot\|_\alpha, \alpha \in \mathbb{R}$ is defined for functions with supported in a compact set $K \subset X$ or in a set $\Lambda \subset\subset \Sigma$. Denote by $H_K^\alpha(X,\Omega)$, $H_K^\alpha(X)$ the space of distributions, respectively, of generalized functions supported in K with finite norm $\|\cdot\|_\alpha$.

Proposition. For any locally complete family F an arbitrary compact set $K \subset X$ and any real α and any function $\phi \in D(\Sigma)$ the inequality holds

$$\|\phi M\mathrm{f}\|_{\alpha+(n-1)/2} \leq C_\alpha \|\mathrm{f}\|_\alpha$$

for $\mathrm{f} \in H_K^\alpha(X,\Omega)$.

3. The dual Funk transform M° is defined as the Funk transform for the dual family of hypersurfaces. The operator $-M^\circ$ is dual to M. Fix some volume forms $\mathrm{d}X$ in X and $\mathrm{d}\Sigma$ in Σ. The *back projection* operator

$$M^* : g \mapsto M^\circ(g\mathrm{d}\Sigma)\,\mathrm{d}X$$

transforms functions g defined in Σ to densities in X.

We say that points $x, y \in X$ are conjugate with respect to a family F, if $x \neq y$ and the form $\mathrm{d}_\sigma I(x,\sigma) \wedge \mathrm{d}_\sigma I(y,\sigma)$ defined in Σ vanishes.

Theorem. Suppose that the family F has no conjugate points, then for any $\alpha > \beta$ and an arbitrary set $K \subset\subset X$ the below estimate holds for the Funk transform

$$\|\mathrm{f}\|_\alpha \leq C_\alpha \|M\mathrm{f}\|_{\alpha+(n-1)/2} + C_\beta \|\mathrm{f}\|_\beta$$

of densities f supported in K.

Corollary. The eigenvalues λ_k of the operator M^*M numbered in descreasing order satisfies the estimate

$$ck^{(1-n)/2} \leq \lambda_k \leq Ck^{(1-n)/2}.$$

Corollary. Suppose that for some $\beta < \alpha$ the equation $M\mathrm{f} = 0, \mathrm{f} \in H_K^\beta(X, \Omega)$ implies $\mathrm{f} = 0$. Then the last term can be dropped out and the two-side estimate holds:

$$c_\alpha \|\mathrm{f}\|_\alpha \leq \|M\mathrm{f}\|_{\alpha+(n-1)/2} \leq C_\alpha \|\mathrm{f}\|_\alpha .$$

4. Let $H^\alpha(X, \Omega)$ be the spaces of distributions in X that belong to $H_K^\alpha(X, \Omega)$ for any compact set K. The notation $H^\alpha(X)$ is used for the similar space of functions.

Suppose that a locally complete family F satisfies the condition (iii) the mapping $p : F \to X$ is proper. If a density f is supported in a compact set $K \subset X$, then $M\mathrm{f}$ is supported in the compact set $\Lambda \doteq \pi\left(p^{-1}(K)\right) \subset \Sigma$. Then the dual transform M° is well defined for all continuous densities in Σ and can be extended to a continuous operator $H^\alpha(X, \Omega) \to H^{\alpha+1/2}(\Sigma)$ for any α.

We say that points $x, y \in X, x \neq y$ are conjugate in the family F, if the form $\mathrm{d}_\sigma I(x, \sigma) \wedge \mathrm{d}_\sigma I(y, \sigma)$ vanishes.

Theorem. Suppose that the family F satisfies (iii) and has no conjugate points. Then for arbitrary set $K \subset\subset X$ and any α the image of the Funk operator

$$M : H_K^\alpha(X, \Omega) \to H_\Lambda^{\alpha+(n-1)/2}(\Sigma)$$

is closed and coincides with the annihilator of the space of densities φ that belong to $H^{-\alpha-(n-1)/2}(\Sigma, \Omega)$ and satisfy the equation

$$M^\circ\varphi(x) = 0, x \in X \backslash K$$

Example 2. The Radon transform in the Schwartz space is equivalent to the Funk transform as above for the class $S_0\left(P^2\right)$ of smooth densities f that are flat on the infinite projective line $P^1 \subset P^2$. The orthogonality condition as above leads to another proof of Helgason-Ludwig range conditions.

Example 3. The above results hold for the thermoacoustic acquisition geometry. The family F of circles centered on a circular arc S in the plane is locally complete in a compact set K, provided the angular length of S is $\geq \pi$.

5. The Kaczmarz method can be adopted for inversion of the Funk transform. Let F be a family of hypersurfaces in $X \times \Sigma$ that fulfils (iii) and K is a compact set in X. We want to find a solution $\mathrm{f} \in L_2(K)$ of the equation $M\mathrm{f} = \varphi$ where $\varphi \in L_2(\Lambda)$. Fix an volume form $\mathrm{d}X$ in X and consider the operator $MM^* : L_2(\Lambda) \to L_2(\Lambda)$. It is non-positive; take any invertible operator R that fulfils

$R \geq -MM^*$. The operator R is positive and invertible. Take an arbitrary density f^0 and the sequence $\mathrm{f}^k, k = 1, 2, ...$ defined by the recurrent formula

$$\mathrm{f}^{k+1} = \mathrm{f}^k + \omega M^* R^{-1} \left(M\mathrm{f}^k - \varphi \right).$$

Theorem. If M is injective and φ fulfils the consistency conditions, we have $\mathrm{f}^k \to \mathrm{f}$, where f is a solution.

References

[1] P. Funk, *Über Flächen mit lauter geschlossenen geodätischen Linien.* Math Ann. **74** (1913) 278-300.

[2] V. Guillemin, *On some results of Gelfand in integral geometry,* Lecture Notes, Symposium on Global Analysis, Durham, N. C., 1976.

[3] M.M. Lavrent'ev, A.L. Bukhgeim, *On a class of operator equations of first kind.* Funk. Anal. Appl. **7** (1973) N4, 44-53.

[4] R.G. Mukhometov, *On a problem of integral geometry.* Mathematical problems of geophysics, Novosibirsk, VC SO Akad. Nauk SSSR, **6** (1975) N2, 212-243 (Russian).

[5] F. Natterer, The mathematics of computerized tomography. B.G.Teubner, John Wiley & Sons, Stuttgart, 1986.

[6] L. Pestov, G. Uhlmann, *On characterization of the range and inversion formulas for the geodesic X-ray transform.* Intern Math Research Notes **80** (2004), 4331-4347.

[7] D.A. Popov, *The generalized Radon transform on the plane, the inversion transform, and the Cavalieri conditions.* Funk. Anal. Pril. **35** (2001) N4, 38-53.

[8] E. T. Quinto, *The dependence of the generalized Radon transform on defining measures,* Trans. of the AMS, **257** (1980) N2, 331-346.

[9] H. Rullgård, *Stability of the inverse problem for the attenuated Radon transform with 180° data.* Inverse problems, **20** (2004), 787-791.

Optimality of the fully discrete filtered backprojection algorithm in 2D

Andreas Rieder

(joint work with Arne Schneck)

Although the filtered backprojection algorithm (FBA) is the standard reconstruction algorithm in 2D computerized tomography for over 30 years its convergence behavior is not completely settled so far. We study the convergence of the fully discrete FBA and show its optimality.

Let $\mathbf{R} : L^2(\Omega) \to L^2(Z)$, $Z = [-1, 1] \times [0, 2\pi]$, be the Radon transform where Ω is the unit disk in $\mathbb{R}^2$ centered about the origin:

$$\mathbf{R}f(s, \vartheta) := \int_{L(s,\vartheta)\cap\Omega} f(x)\, \mathrm{d}\sigma(x).$$

Thus, $\mathbf{R}$ maps functions to its integrals over the lines $L(s, \vartheta) = \{\tau\, \omega^\perp(\vartheta) + s\, \omega(\vartheta) \,|\, \tau \in \mathbb{R}\}$ where $\omega(\vartheta) = (\cos\vartheta, \sin\vartheta)^t$ and $\omega^\perp(\vartheta) = (-\sin\vartheta, \cos\vartheta)^t$.

The FBA may be derived from the inversion formula

$$f = \frac{1}{4\pi} \mathbf{R}^* (\Lambda \otimes I) \mathbf{R} f$$

which holds true for $f \in L^2(\Omega)$ [3, Sec. 3.2]. Here, the backprojection operator

$$\mathbf{R}^* g(x) = \int_0^{2\pi} g(x^t \omega(\vartheta), \vartheta)\, \mathrm{d}\vartheta$$

is the adjoint of $\mathbf{R}$ and Λ is defined by

$$\widehat{\Lambda u}(\xi) = |\xi| \widehat{u}(\xi)$$

mapping $H^\alpha(\mathbb{R}^d)$ boundedly to $H^{\alpha-1}(\mathbb{R}^d)$. As usual, $\widehat{w}$ denotes the Fourier transform of $w \in L^2(\mathbb{R}^d)$ and $H^\alpha(\mathbb{R}^d)$, $\alpha \in \mathbb{R}$, is the L^2-Sobolev space with norm $\|w\|_\alpha^2 = \int_{\mathbb{R}^d} (1+|\xi|^2)^\alpha |\widehat{w}(\xi)|^2 \mathrm{d}\xi$.

Assume we have observed discrete Radon data under the lateral and angular sampling rates $h = 1/q$ and $h_\vartheta = \pi/p$, respectively. Due to Rieder and Faridani [3] the FBA can then be expressed by

$$f_{\mathrm{FBA}}(x) := \mathbf{R}^*_{h_\vartheta} (\mathrm{I}_h \Lambda E_h \otimes I) \mathbf{R} f(x)$$

where

$$\mathbf{R}^*_{h_\vartheta} g(x) := h_\vartheta \sum_{j=0}^{2p-1} g(x^t \omega(\vartheta_j), \vartheta_j), \quad \vartheta_j = j h_\vartheta.$$

The operators E_h and I_h are generalized interpolation operators: For $u \in H^\alpha(\mathbb{R})$ define

$$E_h u(s) := h^{-1} \sum_{k \in \mathbb{Z}} \big\langle u, \epsilon_h(\cdot - s_k) \big\rangle\, B_h(s - s_k),$$

where $\epsilon_h(s) = \epsilon(s/h)$ and $B_h(s) = B(s/h)$. Further, $B \in L^2(\mathbb{R})$ is the 'interpolation function' and $\epsilon \in H^{-\alpha}(\mathbb{R})$ is assumed to be even with $\widehat{\epsilon}(0) = 1/\sqrt{2\pi}$. Further, $\langle \cdot, \cdot \rangle$ denotes the duality pairing in $H^\alpha(\mathbb{R}) \times H^{-\alpha}(\mathbb{R})$. For $u \in H^\alpha(\mathbb{R})$, $\alpha > 1/2$, we may choose $\epsilon = \delta$ (Dirac distribution). Thus, $h^{-1}\langle u, \epsilon_h(\cdot - s_k)\rangle = u(s_k)$. Analogously,

$$\mathrm{I}_h u(s) := h^{-1} \sum_{k \in \mathbb{Z}} \big\langle u, \eta_h(\cdot - s_k) \big\rangle\, A_h(s - s_k),$$

where η and A play the roles of ϵ and B, respectively. For more details on E_h and I_h we refer to [3, Sec. 3.2]. Observe that

$$(\mathrm{I}_h \Lambda E_h \otimes I) \mathbf{R} f(s, \vartheta) = \sum_{\ell \in \mathbb{Z}} \Big(\sum_{k \in \mathbb{Z}} w_{\ell - k} \big\langle \mathbf{R} f(\cdot, \vartheta), \epsilon_h(\cdot - s_k) \big\rangle \Big) A_h(s - s_\ell) \tag{1}$$

with $w_r = \upsilon(r)/h^2$ where

$$\upsilon(s) := \frac{1}{\pi} \int_0^\infty \sigma\, \widehat{B}(\sigma)\, \widehat{\eta}(\sigma) \cos(s\sigma) \mathrm{d}\sigma$$

is the *reconstruction filter*. Thus, the evaluation of $f_{\mathrm{FBA}}(x)$ can be implemented exactly as in [2, Chap. V.1.1]. The sum over k in (1) represents filtering.

We require the following approximation properties of E_h and I_h, respectively: There are non-negative constants $\tau_{\max}$ and $\beta_{\min} \le \beta_{\max}$ such that[1]

$$\|E_h u - u\|_\tau \le C h^{\beta-\tau} \|u\|_\beta \tag{2}$$

for $\beta_{\min} \le \beta \le \beta_{\max}$, $1/2 \le \tau \le \tau_{\max}$, $\tau \le \beta$ and any $u \in H^\beta(\mathbb{R})$ having a compact support in $[-1,1]$.

There is a constant $\alpha_{\mathrm{I}} > 0$ such that

$$\|\mathrm{I}_h - I\|_{H^{\alpha-1/2}(\mathbb{R}) \to H^{-1/2}(\mathbb{R})} \le C h^\alpha \tag{3}$$

for $0 \le \alpha \le \alpha_{\mathrm{I}}$.

Now we can formulate our asymptotic error estimate, for a proof see Rieder and Schneck [4].

Theorem *Under* (2) *and* (3) *with* $\beta_{\max}, \tau_{\max} \ge 3/2$ *we have that*

$$\Big\| f - \frac{1}{4\pi} \mathbf{R}^*_{h_\vartheta} (\mathrm{I}_h \Lambda E_h \otimes I) \mathbf{R} f \Big\|_{L^2(\Omega)} \le C(h^\alpha + h_\vartheta^\alpha) \|f\|_\alpha, \quad \alpha_{\min} \le \alpha \le \alpha_{\max},$$

where $\alpha_{\min} = \max\{1, \beta_{\min} - 1/2\}$, $\alpha_{\max} = \min\{\alpha_{\mathrm{I}}, \beta_{\max} - 1/2, \tau_{\max} - 1/2\}$, *and* $f \in H^\alpha(\mathbb{R}^2)$ *compactly supported in* Ω.

Applying the theorem to concrete settings we find that

$$\|f - f_{\mathrm{FBA}}\|_{L^2(\Omega)} \le C\big(h^{\min\{\alpha_{\max},\alpha\}} + h_\vartheta^{\min\{\alpha_{\max},\alpha\}}\big) \|f\|_\alpha, \quad \alpha \ge 1,$$

where

$$\alpha_{\max} = \begin{cases} 3/2 & \text{Shepp-Logan filter with piecewise constant interpolation,} \\ 2 & \text{Shepp-Logan filter with piecewise linear interpolation,} \\ 5/2 & \text{mod. Shepp-Logan filter with piecewise linear interpolation.} \end{cases}$$

The modified Shepp-Logan filter was introduced in [3] where also numerical experiments illustrating the convergence orders can be found.

In view our asymptotic error estimate the choice $h = h_\vartheta$ is most efficient implying the optimal sampling rate $p = \pi q$, see, e.g., Natterer [2, Table III.1]. Further, under the optimal sampling rate the convergence rate h^α as $h \to 0$ is optimal for density distributions in H^α, see Natterer [1].

References

[1] F. Natterer, *A Sobolev space analysis of picture reconstruction*, SIAM J. Appl. Math. **39** (1980), 402-411.

[2] F. Natterer, *The Mathematics of Computerized Tomography*, Teubner-Wiley (1986).

[3] A. Rieder, A. Faridani, *The semi-discrete filtered backprojection algorithm is optimal for tomographic inversion*, SIAM J. Numer. Anal. **41** (2003), 869-892.

[4] A. Rieder, A. Schneck *Optimality of the fully discrete filtered backprojection algorithm for tomographic inversion*, Preprint, Universität Karlsruhe, Fakultät für Mathematik, 76128 Karlsruhe, Germany.

[1] C always denotes a generic constant possibly attaining different values at each instance it appears.

Theoretical and Numerical Studies on Sampling in Fan Beam Tomography

Steven H. Izen

1. Introduction

An analysis[3] of the integral kernels for two well-known fan beam CT reconstruction algorithms[6] was performed. It was found theoretically that the kernel for the standard $O(\Omega^4)$ fan beam tomography reconstruction has an essential bandregion larger than prior numerical analyses had revealed. Here, Ω denotes the essential bandwidth in the reconstructed image. It was also shown that the approximate kernel used in the $O(\Omega^3)$ convolution-backprojection reconstruction algorithm has an essential bandregion which is significantly different from that of the fan beam data. Those calculations imply that properly sampled implementations of the reconstruction algorithms require the fan beam projection data to be available at higher sampling densities than is needed for the recovery of the fan beam data itself.

The results of numerical experiments on the sampling requirements for both algorithms were presented. It was demonstrated that to avoid aliasing artifacts with the $O(\Omega^3)$ algorithm, the operational sampling density must be greater than that needed to recover the fan beam data.

2. Theoretical Analysis

For fixed scan and source radii ρ and r, with $\rho < r$, and $f \in C_c^\infty(B_\rho)$, the fan beam transform is defined by

$$Df(\beta,\alpha) = \int_0^\infty f(b+tc)dt,$$

where $b = (r\cos\beta, r\sin\beta)^T$, $c = (\cos(\pi+\alpha+\beta), \sin(\pi+\alpha+\beta))^T$. Let $\theta = \rho/r$.

Let v_Ω be the classic ramp filter used for Radon inversion and V_Ω be the corresponding an Ω-bandlimited approximate delta function. The bandwidth Ω in the reconstructed image determines resolution.

The exact reconstruction formula is of complexity $O(\Omega^4)$:

$$\begin{aligned}(V_\Omega * f)(x) &= r\int_0^{2\pi}\int_{-\pi/2}^{\pi/2} \frac{v_{|b-x|\Omega}(\sin(\gamma(\beta;x)-\alpha))}{|b-x|^2}\cos\alpha Df(\beta,\alpha)d\alpha d\beta \\ &= \int_0^{2\pi}\int_{-\pi/2}^{\pi/2} h_E(\beta,\alpha;x)Df(\beta,\alpha)d\alpha d\beta.\end{aligned}$$

To obtain a reconstruction of complexity $O(\Omega^3)$, the kernel bandwidth is fixed at $r\Omega$. This gives the approximate reconstruction formula:

$$\begin{aligned}(V_\Omega * f)(x) &\approx r\int_0^{2\pi} |b-x|^{-2}\int_{-\pi/2}^{\pi/2} v_{r\Omega}(\sin(\gamma(\beta;x)-\alpha))\cos\alpha Df(\beta,\alpha)d\alpha d\beta \\ &= \int_0^{2\pi}\int_{-\pi/2}^{\pi/2} h_A(\beta,\alpha;x)Df(\beta,\alpha)d\alpha d\beta,\end{aligned}$$

where $\gamma(\beta,x)$ is the fan angle to the reconstruction point x from a source at angle β.

To study the sampling requirements for the exact or approximate reconstruction formulas, the essential supports of the Fourier transforms $\widehat{Df}(k,2a)$, $\widehat{h_A}(k,2a;x)$, and $\widehat{h_E}(k,2a;x)$ are needed.

For an essentially Ω-bandlimited $f\in C_c^\infty(B_\rho)$ and large Ω it has been determined that the essential bandregions of K_Ω of Df[5, 7], K_Ω^E[3], and K_Ω^A[3] are slightly larger than the regions

$$\begin{aligned}K_\Omega &= \left\{(k,2a)\in\mathbb{Z}\times 2\mathbb{Z}\,\middle|\,|2a-k|\le\Omega r, |k|r\le|k-2a|\rho\right\},\\ K_\Omega^A &= \left\{(k,2a)\in\mathbb{Z}\times 2\mathbb{Z}\,\middle|\,|2a|\le\Omega r, |k|r\le|k-2a|\rho\right\},\\ K_\Omega^E &\subseteq \left\{(k,2a)\in\mathbb{Z}\times 2\mathbb{Z}\,\middle|\,|2a-k|\le\Omega r, |k|\le\rho\Omega\right\}.\end{aligned}$$

In order to choose a sampling lattice L_W sufficient to recover Df, it is necessary to ensure that shifts of K_Ω by elements of the dual lattice $L_W^\perp$ do not overlap K_Ω[8]. This can be accomplished by choosing $\Delta\beta\le\frac{\pi}{r\Omega}\frac{r+\rho}{\rho}$, $\Delta\alpha\le\frac{\pi}{r\Omega}$. $L_W^\perp$ is generated by the matrix $W^\perp=\begin{pmatrix}\xi_1 & 0\\ 0 & \xi_2\end{pmatrix}$, where $\xi_1>\frac{2r\rho\Omega}{r+\rho}$, $\xi_2>2r\Omega$. The essential bandregion K_Ω^A is not the same as K_Ω. Hence, to compute an approximate reconstruction without sampling error, one of two approaches must be taken.

- Work with an essential bandregion of $K=K_\Omega\cup K_\Omega^A$. In this case, one must select $\xi_1>\frac{2r^2\rho\Omega}{r^2-\rho^2}$, $\xi_2>(2r+\rho)\Omega$. This requires a denser sampling by a factor of $\frac{2r^2\rho}{r^2-\rho^2}/\frac{2\rho r}{r+\rho}=(1-\theta)^{-1}$ finer in the β direction and a factor of $(2r+\rho)/(2r)=1+\theta/2$ in the α direction. For $\theta=1/3$, these factors are $3/2$ and $7/6$, respectively.
- Df must be interpolated, or resampled[1, 2], to a sampling lattice suitable for K_Ω^A. The requirements are $\xi_1>\frac{2r^2\rho\Omega}{r^2-\rho^2}$, $\xi_2>2r\Omega$.

3. Numerical Results

For brevity, only a small illustrative selection of the results of some numerical experiments are shown.

The Fourier transform of the approximate kernel, $\widehat{h_A}(k,2a;x)$ for $\Omega=390$, with sampling distance at Nyquist for $\Omega=400$, and $|x|=0.95$ is shown next to $|\widehat{Df}|(k,2a)$ and the reconstructed image.

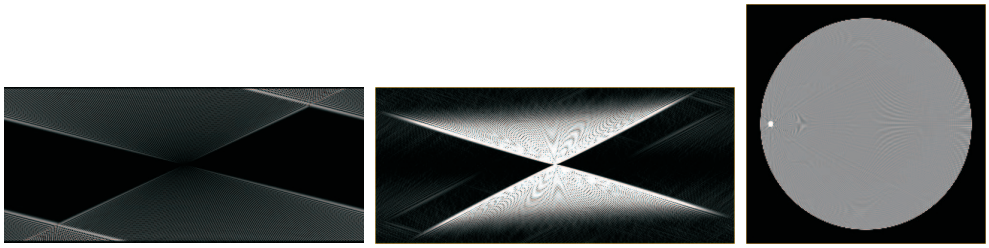

The absolute value of the Fourier transform of the approximate kernel, $\widehat{h_A}(k, 2a; x)$ for $\Omega = 390$, with two times oversampling in both β and α for $\Omega = 400$, and $|x| = 0.95$ is shown next to $|\widehat{Df}|(k, 2a)$ and the reconstructed image.

This shows $|(\widehat{h_E - h_A})(k, 2a; x)|$ for $\Omega = 390$, at ideal sampling for $\Omega = 400$ and $|x| = 0.95$. This demonstrates that the approximate kernel differs from the exact kernel primarily in high frequency content. Indeed, there is remarkable agreement in the region of $K_\Omega^E \cap K_\Omega^A$, partially explaining the good performance of the approximate reconstruction.

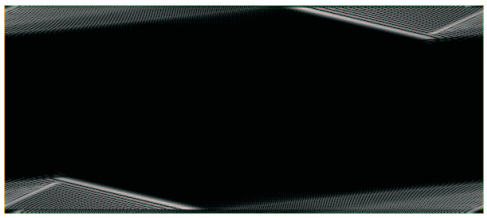

References

[1] A. Faridani, *An Application of a Multidimensional Sampling Theorem to Computed Tomography*, in Contemporary Mathematics, **113** (1990), AMS, Providence, RI, 65–80.

[2] A. Faridani, *A Generalized Sampling Theorem for Locally Compact Abelian Groups*, Math. Comp., **63** (1994), 307–327.

[3] S. Izen, *An Analysis of the Fan Beam CT Reconstruction Kernel*, Sampling Theory in Signal and Image Processing, (2006), in revision.

[4] F. Natterer, *The Mathematics of Computerized Tomography*, Wiley, New York, 1986.

[5] F. Natterer, *Sampling in Fan Beam Tomography*, SIAM J. Appl. Math, **53** (1993), 358–380.

[6] F. Natterer and F. Wübbeling, *Mathematical Methods in Image Reconstruction*, SIAM, Philadelphia, PA, 2001.

[7] V. Palamodov, *Localization of harmonic decomposition of the Radon transform*, Inverse Problems, **11** (1995), 1025–1030.

[8] D. P. Petersen and D. Middleton, *Sampling and Reconstruction of wave number-limited functions in n-dimensional Euclidean spaces*, Inform. Contr., **5** (1962), 279–323.

Shape reconstruction and structural inversion for medical, geophysical and industrial tomography

Oliver Dorn
(joint work with Rossmary Villegas)

There exist many important tomography problems in medical, geophysical and industrial applications where only few data are available and where no explicit inversion formula is available in order to reconstruct the quantities of interest from these data. One classical example is the history matching problem in petroleum engineering where the task is to recover the permeability structure of a petroleum reservoir from production data. Other examples are the detection of land mines or the monitoring of pollutant plumes in the Earth from electromagnetic data, the imaging of marker distributions in fluorescence tomography, or the early detection of breast cancer using near-infrared light or microwaves, to mention only a few.

In these very ill-posed inverse problems it is essential to be able to use additional prior information for the inversion in order to reduce non-uniqueness and to stabilize the reconstruction of the quantities of interest. Often, this prior information indicates that sharp discontinuities (e.g., between regions of different materials) are to be expected in the domain of interest. For example, when exploring a petroleum reservoir, the field engineer knows fairly well which rock or soil types are present in the reservoir (e.g., sand and shale as in our numerical examples,) such that the task can be reduced to finding the exact distributions of these different materials, as well as certain smooth variations of permeability properties inside each of these different regions (satisfying some region-dependent characteristics and limits) from the data.

In the talk, we present a novel structural inversion technique which uses a level set representation for describing the different regions and their topologies during the reconstruction. The level set technique is well known to be able to model topological changes in a completely automatic fashion. This is an important feature in our inversion scheme since the topologies of the different regions are unknown *a priori* and need to be recovered from the data. We refer for a detailed overview of different level-set based strategies for solving such structural inverse problems to the recent review articles [1, 2]. Our example will be the already mentioned history matching problem in reservoir engineering, which is outlined briefly in the following. More details regarding this example can be found in [3, 4].

In secondary oil recovery, water is injected under high pressure into so-called injection wells in order to enhance oil production at the production wells. Our simplified model for the resulting two-phase flow of oil and water in the Earth (modeled as a porous medium) is

$$-\nabla \cdot \Big[T \nabla p\Big] = Q \quad \text{in} \quad \Omega \times [0, t_f] \tag{1}$$

$$\phi \frac{\partial S_w}{\partial t} - \nabla \cdot \big[T_w \nabla p\big] = Q_w \quad \text{in} \quad \Omega \times [0, t_f] \tag{2}$$

for the two unknowns p (pressure) and S_w (water saturation). In the following, the subindices w and o will always indicate 'water' and 'oil', respectively. $\Omega \subset \mathbf{R}^n$ $(n = 2, 3)$ is the modeling domain with boundary $\partial\Omega$, and $[0, t_f]$ is the time interval for which production data is available. We denote by $\phi(\mathbf{x})$ the porosity, and by T_o, T_w and T the transmissibilities, which are known functions of the permeability K and the water saturation S_w:

$$T_w = K(\mathbf{x})\frac{K_{rw}(S_w)}{\mu_w}; \quad T_o = K(\mathbf{x})\frac{K_{ro}(S_w)}{\mu_o}; \quad T = T_w + T_o \ . \tag{3}$$

Here, the relative permeabilities $K_{rw}(S_w)$ and $K_{ro}(S_w)$ are typically available as tabulated functions, and μ_w and μ_o denote the viscosities of each phase. The quantities Q_o, Q_w and $Q = Q_o + Q_w$ represent the flows (oil, water, and total, resp.) at the few injection and production well locations in the reservoir. They define the measured data of our inverse problem. Equations (1)-(3) are solved with appropriate initial conditions, and a no-flux boundary condition on $\partial\Omega$.

In the shape inverse problem we assume now that the parameter K has the following specific form

$$K(\mathbf{x}) = \begin{cases} K_i(\mathbf{x}), & \text{where} \quad \psi(\mathbf{x}) \leq 0 \\ K_e(\mathbf{x}), & \text{where} \quad \psi(\mathbf{x}) > 0 \, . \end{cases} \tag{4}$$

In this representation, $\psi(\mathbf{x})$ is the describing level set function. The two regions D (shale) and $\Omega \backslash D$ (sand) are accordingly given as $D = \{\mathbf{x} \in \Omega \ : \ \psi(\mathbf{x}) \leq 0\}$ and $\Omega \backslash D = \{\mathbf{x} \in \Omega \ : \ \psi(\mathbf{x}) > 0\}$. The boundary of D (denoted as $\Gamma = \partial D$) is defined by the zero level set of the level set function ψ, i.e., $\partial D = \{x \ : \ \psi(x) = 0\}$.

To solve this problem, we will adopt here a time evolution approach. We write (and identify in the notation) $\psi(\mathbf{x}) = \psi(\mathbf{x}, \tau)$ (and we will use similar expressions for K_i and K_e), where τ is the artificial evolution time. The inverse problem can be stated as follows: find a level set function $\psi(\mathbf{x})$ and internal permeability profiles $K_i(\mathbf{x})$ and $K_e(\mathbf{x})$ in (4) for which a suitably chosen cost functional (here defined in (7)) is minimized. We consider the general evolution laws

$$\frac{d\psi}{d\tau} \ = \ f(\mathbf{x}, \tau, \psi, \ldots), \qquad \frac{dK_i}{d\tau} \ = \ h_i(\mathbf{x}, \tau, \psi, \ldots), \qquad \frac{dK_e}{d\tau} \ = \ h_e(\mathbf{x}, \tau, \psi, \ldots) \tag{5}$$

for the level set function ψ and for the corresponding internal permeability profiles K_i and K_e. The goal is to find forcing terms f, h_i, and h_e such that the evolution converges to the desired solution of the inverse problem. We can write (4) in the form

$$K(\psi) \ = \ K_e H(\psi) \ + \ K_i(1 - H(\psi)), \tag{6}$$

where H denotes the Heaviside function. We denote the mapping from the unknown permeability K to the corresponding data by A, and the physically measured data by g. Then, we consider the least squares cost functional

$$\mathbf{J}(K_e, K_i, \psi) \ = \ \frac{1}{2}\|R(K(K_e, K_i, \psi))\|_2^2 \tag{7}$$

with $R(K) = A(K) - g$ being the classical residual operator. Formally differentiating by the chain rule yields

$$\frac{d\mathbf{J}}{d\tau} = \int_\Omega R'(K)^* R(K) \left(\frac{\partial K}{\partial \psi}\frac{d\psi}{d\tau} + \frac{\partial K}{\partial K_e}\frac{dK_e}{d\tau} + \frac{\partial K}{\partial K_i}\frac{dK_i}{d\tau} \right) d\mathbf{x} \tag{8}$$

where $R'(K)^*$ is the formal adjoint of the linearized residual operator $R'(K)$. The expresssions $\frac{\partial K}{\partial \psi}$, $\frac{\partial K}{\partial K_e}$ and $\frac{\partial K}{\partial K_i}$ can be calculated from (6), and the expressions $\frac{d\psi}{d\tau}$, $\frac{dK_e}{d\tau}$ and $\frac{dK_i}{d\tau}$ are given by (5). Plugging this into (8) yields the descent directions

$$\begin{aligned} f_d &= -C_1(K_e - K_i)R'(K)^* R(K)\chi_\Gamma(\psi) \\ h_{i_d} &= -C_2(1 - H(\psi))R'(K)^* R(K) \\ h_{e_d} &= -C_3 H(\psi)R'(K)^* R(K), \end{aligned}$$

for the cost (7), where C_1, C_2 and C_3 are arbitrary positive constants and $\chi_\Gamma(\psi)$ is a positive valued approximation to the Dirac delta distribution $\delta(\psi) = H'(\psi)$. We will use as $\chi_\Gamma(\psi)$ a narrowband function which is one in a small neighborhood of $\Gamma = \{\mathbf{x} \ : \ \psi(\mathbf{x}) = 0\}$ and zero elsewhere. Plugging these expressions into (5), applying some additional smoothing (regularization, see [1, 2, 3, 4]) to the right hand sides and discretizing the time derivatives $\frac{d}{d\tau}$ by a straightforward finite difference scheme gives us an update rule for each step in the artificial evolution of shape and parameter values. The expressions $R'(K)^* R(K)$ are evaluated by a so-called adjoint scheme which only requires us to run one forward simulation (1)-(3) on the latest parameter distribution and one additional adjoint simulation which corresponds to the formal adjoint of the linearized forward problem. For more details regarding these simulations we refer to [3, 4], where also various numerical results for realistic situations in reservoir characterization (as presented in the talk) can be found.

References

[1] O. Dorn and D. Lesselier, *Level set methods for inverse scattering (Topical review)*, Inverse Problems **22** (2006) R67-R131.

[2] O. Dorn and D. Lesselier, *Level set techniques for structural inversion in medical imaging*, Chapter in book: "Parametric and Geometric Deformable Models: An application in Biomaterials and Medical Imagery", Volume 1, Springer Publishers, Editors (Jasjit S. Suri and Aly Farag), ISBN: 0-387-31204 8, pp. 61-90, May 2006.

[3] R. Villegas R, O. Dorn, M. Moscoso and M. Kindelan, *Shape reconstruction from two-phase incompressible flow data using level sets*, Proc. International conference on PDE-based image processing and related inverse problems, CMA, Oslo: August 2005 (Springer: *to appear*) (2006).

[4] R. Villegas R, O. Dorn, M. Moscoso, M. Kindelan and F. J. Mustieles, *Simultaneous characterization of geological shapes and permeability distributions in reservoirs using the level set method*, Proc. SPE Europec/EAGE Annual Conference and Exhibition, Vienna: June 2006 *in press* (2006).

Advances and challenges in vector field tomography

Thomas Schuster

Tensor field tomography means to recover a tensor field, or part of it, from given observations which usually are line integrals over projections of the field in direction of the line. Vector field tomography particularly deals with the problem of reconstructing a vector field, e.g. a velocity field of an incompressible moving fluid. Here, the integral data can be measured using ultrasound signals and assuming that the Doppler shift of the frequency is approximately proportional to the velocity of the particle in the fluid which causes the shift. This is a reasonable assumption when the particle velocity is significantly smaller than the speed of sound within the medium under consideration. A lot of theoretical and numerical results have been achieved over the last years for the parallel gemetry. Juhlin [4] suggested a measurement setup which is suited to get full reconstruction of solenoidal fields. Mathematical properties of this model can be found in Sparr et al. [14]. The singular value decomposition has been presented in a paper by Kazantsev and Bukgheim [5]. Desbat and Wernsdörfer [1] developed an iterative method. The author established an inversion scheme of filtered backprojection type [11, 12] relying on the method of approximate inverse and together with Rieder [10] obtained convergence with rates and stability with respect to noisy data for this method.

As in scalar 3D computerized tomography, the cone beam transform is of special interest from a practical point of view. It is defined for a tensor field of rank m by

$$\mathbf{Df}(\alpha,\omega) = \int_0^\infty \langle \mathbf{f}(\alpha+t\omega), \omega^m\rangle \,\mathrm{d}t = \int_0^\infty \mathbf{f}_{i_1\cdots i_m}(\alpha+t\omega)\,\omega^{i_1}\cdots\omega^{i_m}\,\mathrm{d}t\,, \tag{1}$$

where $\alpha \in \Gamma$ is a source point of the scanning curve $\Gamma \subset \mathbb{R}^n\backslash\overline{\Omega}$ which surrounds the object Ω, $\omega \in S^2$ is the unit vector of direction of the line and $\mathbf{f}$ is a tensor field of rank m with compact support in the open domain Ω. In (1) we use Einstein's summation convention, that means we sum up over equal indices i_j, where $1 \le i_j \le n$. For $m = 1$ (1) is the cone beam transform for vector fields. It reads

$$\mathbf{Df}(\alpha,\omega) = \int_0^\infty \langle \mathbf{f}(\alpha+t\omega), \omega\rangle \,\mathrm{d}t\,. \tag{2}$$

The space of square integrable, symmetric covariant tensor fields of rank m in $\Omega \subset \mathbb{R}^n$ is denoted by

$$L^2(\Omega, \mathcal{S}^m) := \{\mathbf{f} \in \mathcal{S}^m : \|\mathbf{f}\|_{L^2} = \langle \mathbf{f}, \mathbf{f}\rangle_{L^2}^{1/2} < \infty\}\,,$$

where the L^2-inner product of two tensor fields is given as

$$\langle \mathbf{f}, \mathbf{g}\rangle_{L^2} = \int_{\Omega^n} f_{i_1\cdots i_m}(x)\, g^{i_1\cdots i_m}(x)\,\mathrm{d}x\,.$$

Fundamental properties of (1) are summarized in the following theorem, which is the result of straightforward calculations.

Theorem 1
Let $\Omega^n := \{x \in \mathbb{R}^n : |x| < 1\}$ with $\partial\Omega^n = S^{n-1}$. The mapping $\mathbf{D} : L^2(\Omega^n, \mathcal{S}^m) \to L^2(\Gamma \times S^{n-1})$ is linear and bounded, if

$$\int_\Gamma (|\alpha| - 1)^{1-n} \, \mathrm{d}\alpha < \infty \, .$$

The adjoint (backprojection) $\mathbf{D}^* : L^2(\Gamma \times S^{n-1}) \to L^2(\Omega^n, \mathcal{S}^m)$ is given by

$$\mathbf{D}^* g(x) = \int_\Gamma \Big\{ |x-\alpha|^{1-n-m} \, g\Big(\frac{x-\alpha}{|x-\alpha|}\Big) \, (x-\alpha)^m \Big\} \, \mathrm{d}\alpha \, ,$$

where $(x-\alpha)^m = (x-\alpha) \otimes \cdots \otimes (x-\alpha) \in \mathcal{S}^m$.

For $m = 0$, $n = 3$ we obtain the well-known cone beam transform with the corresponding backprojection operator of scalar fields which is thoroughly investigated in 3D computerized tomography. For $m = 1$, $n = 3$ we have the mathematical model of 3D cone beam vector tomography and the backprojection reads

$$\mathbf{D}^* g(x) = \int_\Gamma |x-\alpha|^{-2} \, g\Big(\frac{x-\alpha}{|x-\alpha|}\Big) \, \frac{x-\alpha}{|x-\alpha|} \, \mathrm{d}\alpha$$

One of the crucial tools when computing reconstruction kernels in scalar cone beam tomography is represented by the formula of Grangeat [2]. We proved a generalization of that formula which is valid for any tensor field of rank m in n dimensions.

Theorem 2 (Sch. 2005 based on Hamaker et al. [3])
Assume $n \geq 2$ and $\mathbf{f} \in \mathcal{C}_0^{(n-2)}(\Omega^n, \mathcal{S}^m)$. Then,

$$\frac{\partial^{(n-2)}}{\partial s^{(n-2)}} \mathbf{R} f_\alpha(\omega, \langle \alpha, \omega \rangle) = (-1)^{(n-2)} \int_{S^{n-1}} \mathbf{D}\mathbf{f}(\alpha, \theta) \, \delta^{(n-2)}(\langle \omega, \theta \rangle) \, \mathrm{d}S(\theta) \, ,$$

where $\alpha \in \Gamma$, $\omega \in S^{n-1}$, $\mathbf{R}$ is the n-dimensional Radon transform and

$$\begin{aligned} f_\alpha(x) &= \langle \mathbf{f}(x), |x-\alpha|^{-m} (x-\alpha)^m \rangle \\ &= f_{i_1 \cdots i_m}(x) |x-\alpha|^{-m} (x-\alpha)^{i_1} \cdots (x-\alpha)^{i_m} \, . \end{aligned}$$

Proof. The proof is outlined in [13] and is based on a more general identity by Hamaker et al. [3]. Let $\psi(s)$ be defined on $[-1, 1]$ and $h(\theta)$ be defined on S^{n-1}.

Then, by duality

$$\begin{aligned}\int_{-1}^{1} \mathbf{R}f_\alpha(\omega,s)\,\psi(s)\,\mathrm{d}s &= \int_{\Omega^n} f_\alpha(x)\,\psi(\langle x,\omega\rangle)\,\mathrm{d}x \\ &= \int_{\Omega^n} \langle \mathbf{f}(x), |x-\alpha|^{-m}(x-\alpha)^m\rangle\,\psi(\langle x,\omega\rangle)\,\mathrm{d}x \\ &= \int_{\Omega^n} \langle \mathbf{f}(x), |x-\alpha|^{1-n-m}(x-\alpha)^m\rangle\,h\Big(\frac{x-\alpha}{|x-\alpha|}\Big)\,\mathrm{d}x \\ &= \int_{S^{n-1}} \mathbf{Df}(\alpha,\theta)\,h(\theta)\,\mathrm{d}S(\theta)\end{aligned}$$

is fulfilled, if

$$h(\theta) = \delta^{(n-2)}(\langle\theta,\omega\rangle)\,, \quad \psi(s) = \delta^{(n-2)}(s - \langle\alpha,\omega\rangle)\,,$$

where δ denotes Dirac's delta distribution. Of course, to be mathematically exact we have to replace δ by a sequence which smoothly converges to δ in L^2. □

For $m = 0$, $n = 3$ this gives the classical formula of Grangeat from which an inversion method can be deduced immediately if only Tuy's condition is satisfied, see e.g. Natterer, Wübbeling [9]. For $m = 1$, $n = 3$ we obtain the extension to the important case of cone beam vector tomography

$$\frac{\partial}{\partial s}\mathbf{R}f_\alpha(\omega,\langle\alpha,\omega\rangle) = \int_{S^2\cap\{\langle\theta,\omega\rangle=0\}} \langle\nabla_y \mathbf{D}f(\alpha,y=\theta),\omega\rangle\,\mathrm{d}S(\theta) \tag{3}$$

Unfortunately, (3) does not lead to an inversion scheme since here the function f_α depends on the source α. The construction of numerical inversion techniques for cone beam vector tomography is subject of current research. First ideas consist of using the method of approximate inverse, established by Louis, Maaß [8], Louis [6, 7], using the formula of Grangeat (3) or techniques known from the scalar case e.g. by approximating

$$\mathbf{Df}(\alpha,\omega)\omega \approx \int_0^\infty \mathbf{f}(\alpha+t\omega)\,\mathrm{d}t\,.$$

The method of approximate inverse consists of choosing a mollifier $\mathbf{e}_\gamma^j(x,\cdot) = \gamma^{-3}e((x-\cdot)/\gamma)\cdot e_j \approx \delta_x \cdot e_j$, $j = 1,2,3$, which must be seen as a smooth approximation to δ_x and aims to calculate $\mathbf{f}_j^\gamma(x) = \langle \mathbf{f}, \mathbf{e}_\gamma^j(x,\cdot)\rangle_{L^2}$. This is done by computing reconstruction kernels as solutions of

$$\mathbf{D}^* v_\gamma^j(x) = \mathbf{e}_\gamma^j(x,\cdot)$$

followed by evaluations $\mathbf{f}_j^\gamma(x) = \langle \mathbf{Df}, v_\gamma^j(x)\rangle_{L^2}$. The computation of the singular value decomposition or projection methods could also be useful tools for the development of inversion approaches.

The pictures below show reconstruction results of a solenoidal field and its curl for

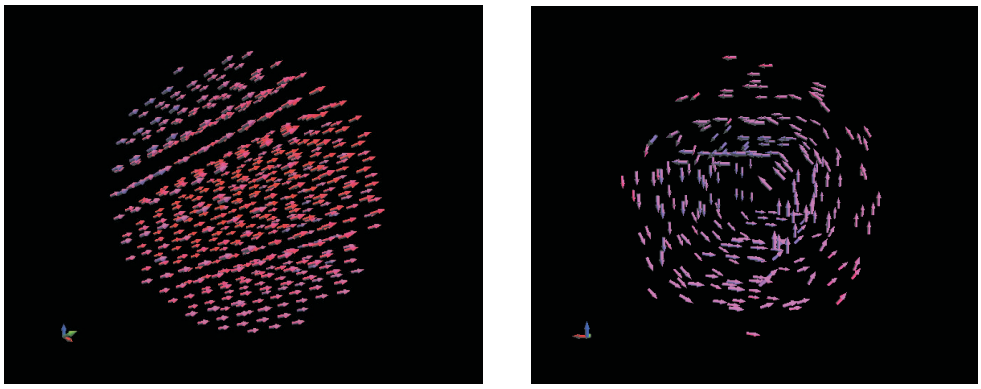

FIGURE 1. Reconstruction of $\mathbf{f}(x) = (1-x_1^2-x_2^2)\cdot e_3$ and its curl $\nabla\times\mathbf{f}(x) = 2(-x_2, x_1, 0)^\top$ by the method of approximate inverse. The pictures were generated by the software package VETOLAB created by A. Domma and the author.

the parallel geometry based on the measurement setup suggested by Juhlin. The data are given as

$$\mathbf{Pf}(x,\omega) = \int_0^\infty \langle \mathbf{f}(x+t\omega), \omega\rangle \, \mathrm{d}t \,,$$

where $\omega \in S^2 \cap \{e_j^\perp\}$, $x \in \{\omega^\perp\}$. The mollifier has been chosen as $e(x) = (1-|x|^2)_+^2$.

REFERENCES

[1] L. Desbat and A. Wernsdörfer, IEEE Trans. Trans. Signal Process. **43**:8 (1995), 1798.

[2] P. Grangeat, *Mathematical framework of cone-beam reconstruction via the first derivative of the Radon transform*, in G.T. Herman, A.K. Louis, and F. Natterer (eds.): Lecture Notes in Math. (Springer, New York) **1497** (1991), 66-97.

[3] C. Hamaker, K.T. Smith, D.C. Solmon, and S.L. Wagner, *The divergent bean X-ray transform*, Rocky Mountain J. Math. **10** (1980), 253–283.

[4] P. Juhlin, *Principles of Doppler Tomography*, technical report, Center for Mathematical Sciences, Lund Institute of technology, SE-221 00 Lund, Sweden (1992).

[5] S.G. Kazantsev and A.A. Bukgheim, *Singular value decomposition for the 2D fan-beam Radon transform of tensor fields*, J. Inv. Ill-Posed Prob. **12**:3 (2004), 245–278.

[6] A.K. Louis, *Approximate inverse for linear and some nonlinear problems*, Inverse Problems **12** (1996), 175–190.

[7] A.K. Louis, *A unified approach to regularization methods for Linear ill-posed problems*, Inverse Problems **15** (1999), 489–498.

[8] A.K. Louis and P. Maaß, *A mollifier method for linear operator equations of the first kind*, Inverse Problems **6** (1990), 427–440.

[9] F. Natterer and F. Wübbeling, *Mathematical Methods in Image Reconstruction*, SIAM, Philadelphia (2001).

[10] A. Rieder and T. Schuster, *The Approximate Inverse in Action III: 3D-Doppler Tomography*, Numerische Mathematik **97** (2004), 353–378.

[11] T. Schuster, *The 3D Doppler transform: elementary properties and computation of reconstruction kernels*, Inverse Problems **16**:3 (2000), 701–723.

[12] T. Schuster, *An efficient mollifier method for three-dimensional vector tomography: convergence analysis and implementation*, Inverse Problems **17** (2001), 739–766.

[13] T. Schuster, *The formula of Grangeat for tensor fields of arbitrary order in n dimensions*, submitted to Appl. Math. Letters (2006).

[14] G. Sparr, K. Stråhlén, K. Lindström and H.W. Persson, *Doppler tomography for vector fields*, Inverse Problems **11** (1995), 1051–1061.

On inversion of the spherical mean Radon transform

Leonid A. Kunyansky

Reconstruction of a function from its integrals over spheres (or circles in 2-D) is equivalent to inverting the so-called spherical mean (circular) Radon transform. Solution of this problem is required, in particular, in the thermoacoustic and photoacoustic tomography. In this case centers of the integration spheres (circles) lie on a closed surface surrounding the support of the function to be reconstructed. Several explicit inversion formulas are currently known for the case when the centers lie on a sphere in an odd-dimensional space [1, 2]. In the 2-D case, however, only a series solution for the circular domain is known [3]. The numerical implementation of this approach is complicated by the zeros of the Bessels functions in the denominator of the formula. We thus present a closed form exact inversion formula of the filtration/backprojection type for the circular geometry.

Given a C_0^1 function $f(\mathbf{x})$ compactly supported within the disk B let us denote by $g(\mathbf{z}, r)$ the known value of the integral from $f(\mathbf{x})$ along a circle of radius r centered at the point $\mathbf{z}$:

$$g(\mathbf{z}, r) = \int\limits_B f(\mathbf{x})\delta(r - |\mathbf{x} - \mathbf{z}|)d\mathbf{x}, \quad \mathbf{z} \in \partial B.$$

Our goal is to reconstruct $f(\mathbf{x})$ from values $g(\mathbf{z}, r)$ known for all $\mathbf{z} \in \partial B$, $0 \le r \le 2R$.

Consider functions $G_J(\mathbf{y}, k)$ and $G_Y(\mathbf{y}, k)$ defined for an arbitrary non-negative k as the following convolutions

$$G_J(\mathbf{y}, k) = \int\limits_B f(\mathbf{x})J_0(k|\mathbf{y} - \mathbf{x}|)d\mathbf{x}, \tag{1}$$

$$G_Y(\mathbf{y}, k) = \int\limits_B f(\mathbf{x})Y_0(k|\mathbf{y} - \mathbf{x}|)d\mathbf{x}.$$

If values of $G_J(\mathbf{y}, k)$ were known for all $k \ge 0$ then it would be easy to compute $f(\mathbf{y})$ using the formula

$$f(\mathbf{y}) = \frac{1}{2\pi}\int_0^\infty G_J(\mathbf{y}, k)kdk. \tag{2}$$

In turn, in order to reconstruc $G_J(\mathbf{y}, k)$ we observe that for a fixed k this function is a solution of Helmholtz equation in B, and that the boundary values of $G_J(\mathbf{y}, k)$ and $G_Y(\mathbf{y}, k)$ can be obtained from the known function $g(\mathbf{z}, r)$, namely

$$(3)\quad G_J(\mathbf{z},k)=\int_0^{2R} g(\mathbf{z},r)J_0(kr)dr,\qquad G_Y(\mathbf{z},k)=\int_0^{2R} g(\mathbf{z},r)Y_0(kr)dr,\quad \mathbf{z}\in\partial B.$$

Our derivation is based on the Helmholtz representation for $J_0(k|\mathbf{x}-\mathbf{y}|)$

$$(4)$$
$$J_0(k|\mathbf{x}-\mathbf{y}|)=-\frac{1}{4}\int_{\partial B}[Y_0(k|\mathbf{z}-\mathbf{x}|)\frac{\partial}{\partial \mathbf{n_z}}J_0(k|\mathbf{z}-\mathbf{y}|)-J_0(k|\mathbf{z}-\mathbf{y}|)\frac{\partial}{\partial \mathbf{n_z}}Y_0(k|\mathbf{z}-\mathbf{x}|)]dl_{\mathbf{z}}$$

modified as follows

$$(5)$$
$$J_0(k|\mathbf{x}-\mathbf{y}|)=-\frac{1}{4}\int_{\partial B}[Y_0(k|\mathbf{z}-\mathbf{x}|)\frac{\partial}{\partial \mathbf{n_z}}J_0(k|\mathbf{z}-\mathbf{y}|)-J_0(k|\mathbf{z}-\mathbf{x}|)\frac{\partial}{\partial \mathbf{n_z}}Y_0(k|\mathbf{z}-\mathbf{y}|)]dl_{\mathbf{z}}.$$

Unlike the standard representation (4) equation (5) is not valid for general domains. However, by harmonic decomposition one can verify that the latter formula holds in the particular case of the circulad domain B. For convinience we re-write equation (5) in the divergence form:

$$(6)$$
$$J_0(k|\mathbf{x}-\mathbf{y}|)=\frac{1}{4}\,\mathrm{div}_{\,\mathbf{y}}\int_{\partial B}[Y_0(k|\mathbf{z}-\mathbf{x}|)J_0(k|\mathbf{z}-\mathbf{y}|)-J_0(k|\mathbf{z}-\mathbf{x}|)Y_0(k|\mathbf{z}-\mathbf{y}|)]\mathbf{n_z}dl_{\mathbf{z}}.$$

Now the reconstruction formula we seek results from combining equtions (1), (2), and (6):

$$f(\mathbf{y})=\frac{1}{2\pi}\int_0^\infty G_J(\mathbf{y},k)kdk=\frac{1}{2\pi}\int_0^\infty\int_B f(\mathbf{x})J_0(k|\mathbf{y}-\mathbf{x}|)d\mathbf{x}kdk$$

$$(7)\quad =\frac{1}{8\pi}\,\mathrm{div}\int_0^\infty\int_B f(\mathbf{x})\int_{\partial B}$$
$$[Y_0(k|\mathbf{z}-\mathbf{x}|)J_0(k|\mathbf{z}-\mathbf{y}|)-J_0(k|\mathbf{z}-\mathbf{x}|)Y_0(k|\mathbf{z}-\mathbf{y}|)]\mathbf{n_z}dl_{\mathbf{z}}d\mathbf{x}kdk$$

$$(8)\quad =\frac{1}{8\pi}\,\mathrm{div}\int_{\partial B}\left(\int_0^\infty[G_Y(\mathbf{z},k)J_0(k|\mathbf{z}-\mathbf{y}|)-G_J(\mathbf{z},k)Y_0(k|\mathbf{z}-\mathbf{y}|)]kdk\right)\mathbf{n_z}dl_{\mathbf{z}},$$

where $G_Y(\mathbf{z},k)$ and $G_J(\mathbf{z},k)$ are computed from $g(\mathbf{z},r)$ using equations (3).

Alternatively, inversion formula (8) can be re-written in a more compact form by utilizing the Hankels function $H_0^{(1)}(t)=J_0(t)+iY_0(t)$:

$$f(\mathbf{y})=\frac{1}{8\pi}\,\mathrm{div}\,\mathrm{Im}\int_{\partial B}\left(\int_0^\infty\left[\int_0^{2R}g(\mathbf{z},r)H_0^{(1)}(kr)dr\right]\overline{H_0^{(1)}(k|\mathbf{z}-\mathbf{y}|)}kdk\right)\mathbf{n_z}dl_{\mathbf{z}}.$$

The above derivation of the reconstruction formula can be easily extended to higher dimensions. In the odd-dimensional case the so-obtained formulas can be further simplified. In particular, in $\mathbb{R}^3$ this approach results in the inversion formula equivalent to the one obtained in [2].

In addition to the problems with spherical data acquisition surface described above we also present a series solution for the inversion of the spherical mean Radon transform with the centers of the integration spheres supported on certain non-spherical surfaces.

References

[1] D. Finch, Rakesh, and S. Patch, *Determining a function from its mean values over a family of spheres*, SIAM J. Math. Anal. **35** no. 5 (2004), 1213–1240.

[2] M. Xu, L. V. Wang, *Universal back-projection algorithm for photoacoustic computed tomography*, Phys Review E **71** (2005), 016706.

[3] S. J. Norton, *Reconstruction of a two-dimensional reflecting medium over a circular domain: Exact solution*, J. Acoust. Soc. Amer. **67** (1980), 1266–1273.

Filter Construction in Cone Beam Tomography

Alfred K. Louis

We consider the X-ray reconstruction problem in three dimensions when the data is measured by firing an X-ray tube emitting rays to a 2D detector. We first derive an exact inversion formula, then, based on this, we derive an approximation which allows both to control the discretization error and to establish fast implementations.

The movement of the combination source - detector determines the different scanning geometries. In many real - world applications the source is moved on a circle around the object. From a mathematical point of view this has the disadvantage that the data are incomplete, the condition of Tuy-Kirillov is not fulfilled. This condition says, that essentially the data are complete for the three - dimensional Radon transform: all planes through a point x have to cut the scanning curve Γ. We base our considerations on the assumptions that this condition is fulfilled, the method also works if the data are at the end from real data given for the above described circular scanning geometry, see [Lou06].

A first theoretical presentation of the reconstruction kernel was given by Finch [Fin87], invariances were then used in the group of the author to speed-up the computation time considerably, so that real data could be handled, see [Lou03]. See also the often used algorithm from Feldkamp et al. [FDK84] and the contribution of Defrise and Clack [DC94]. The approach of Katsevich [Kat02] differs from our approach that he avoids the Crofton symbol by restricting the backprojection to a range dependent on the reconstruction point x. An overview of reconstruction formulas based on a general projection theorem is given in Zhao, Yu and Wang, [ZYW05].

The mathematical model here is the so-called X-ray transform, where we denote with $a \in \Gamma$ the source position, where $\Gamma \subset \mathbb{R}^3$ is a curve, $\theta \in S^2$ is the direction of the ray:

$$\mathbf{D}f(a,\theta) = \int_0^\infty f(a+t\theta)dt$$

The adjoint operator of $\mathbf{D}$ as mapping from $L_2(\mathbb{R}^3) \longrightarrow L_2(\Gamma \times S^2)$ is given as

$$\mathbf{D}^* g(x) = \int_\Gamma |x-a|^{-2} g\left(a, \frac{x-a}{|x-a|}\right) da$$

Most attempts to find inversion formulae are based on a relation between X-ray transform and the 3D Radon transform, the so-called *Formula of Grangeat*, first published in Grangeat's PhD thesis [Gr87], see also [Gr91] :

$$\frac{\partial}{\partial s}\mathbf{R}f(\omega, a^\top\omega) = -\int_{S^2} \mathbf{D}f(a,\theta)\delta'(\theta^\top\omega)d\theta.$$

Starting point is now the inversion formula for the 3D Radon transform

$$f(x) = -\frac{1}{8\pi^2}\int_{S^2} \frac{\partial^2}{\partial s^2}\mathbf{R}f(\omega, x^\top\omega)d\omega \tag{1}$$

rewritten as

$$f(x) = \frac{1}{8\pi^2}\int_{S^2}\int_{\mathbb{R}} \frac{\partial}{\partial s}\mathbf{R}f(\omega,s)\delta'(s-x^\top\omega)dsd\omega$$

We assume in the following that the Tuy-Kirillov condition is fulfilled. Then we can change the variables as: $s = a^\top\omega$, n is the Crofton symbol; i.e., the number of source points $a \in \Gamma$ such that $a^\top\omega = x^\top\omega$, $m = 1/n$ and get

$$\begin{aligned}
f(x) &= \frac{1}{8\pi^2}\int_{S^2}\int_\Gamma (\mathbf{R}f)'(\omega, a^\top\omega)\delta'((a-x)^\top\omega)|a'^\top\omega|m(\omega,a^\top\omega)dad\omega \\
&= -\frac{1}{8\pi^2}\int_{S^2}\int_\Gamma\int_{S^2} \mathbf{D}f(a,\theta)\delta'(\theta^\top\omega)d\theta\delta'((a-x)^\top\omega)|a'^\top\omega|m(\omega,a^\top\omega)dad\omega \\
&= -\frac{1}{8\pi^2}\int_\Gamma |x-a|^{-2}\int_{S^2}\int_{S^2} \mathbf{D}f(a,\theta)\delta'(\theta^\top\omega)d\theta\delta'(\frac{(x-a)}{|x-a|}^\top\omega) \\
&\qquad \times|a'^\top\omega|m(\omega,a^\top\omega)dad\omega
\end{aligned}$$

where we used that δ' is homogeneous of degree -2. We now introduce the following operators

$$T_1 g(\omega) = \int_{S^2} g(\theta)\delta'(\theta^\top\omega)d\theta \tag{2}$$

and we use T_1 acting on the second variable as

$$T_{1,a}g(\omega) = T_1 g(a,\omega)\,.$$

We also use the multiplication operator

$$M_{\Gamma,a}h(\omega) = |a'^\top\omega|m(\omega,a^\top\omega)h(\omega)\,. \tag{3}$$

and state the following result.

Theorem 3. *Let the condition of Tuy-Kirillov be fulfilled. Then the inversion formula for the cone beam transform is given as*

$$f = -\frac{1}{8\pi^2}\mathbf{D}^* T_1 M_{\Gamma,a} T_1 \mathbf{D} f \tag{4}$$

with the adjoint operator $\mathbf{D}^*$ *of the cone beam transform and* T_1 *and* $M_{\Gamma,a}$ *as defined above.*

Note that the operators $\mathbf{D}^*$ and M depend on the scanning curve Γ.

This form allows for computing reconstruction kernels. To this end we have to solve the equation

$$D^* \psi_\gamma = e_\gamma$$

in order to write the solution of $\mathbf{D}f = g$ as

$$f(x) =< g, \psi_\gamma(x, \cdot\,) > \ .$$

In the case of exact inversion formula e_γ is the delta distribution, in the case of the approximate inversion formula it is an approximation of this distribution, see the method of approximate inverse [Lou96]. Using that $\mathbf{D}^{-1} = -\frac{1}{8\pi^2}\mathbf{D}^* T_1 M_{\Gamma,a} T_1$ we get

$$\mathbf{D}^* \psi = \delta = -\frac{1}{8\pi^2}\mathbf{D}^* T_1 M_{\Gamma,a} T_1 \mathbf{D}\delta$$

and hence

$$\psi = -\frac{1}{8\pi^2} T_1 M_{\Gamma,a} T_1 \mathbf{D}\delta \tag{5}$$

Depending on the scanning curve Γ invariances have to be used. For the circular scanning geometry this leads to similar results as mentioned in [Lou03]. Reconstructions from real data are given in [Lou06].

References

[DC94] M. Defrise, R. Clack, *A cone-beam reconstruction algorithm using shift-invariant filtering and cone-beam backprojection.* IEEE TMI **13** (1994), 186–195.

[FDK84] L.A: Feldkamp, L.C. Davis, J.W. Kress, *Practical cone beam algorithm.* J. Opt. Soc. Am. A **6** (1984), 612–619.

[Fin87] D. Finch, *Approximate reconstruction formulae for the cone beam transform, I.* Preprint (1987).

[Gr87] P. Grangeat, *Analyse d'un Système d'Imagerie 3D par Reconstruction à partir de Radiographics X en Géométrie Conique*, Dissertation, Ecole Nationale Supérieure des Télécommunications (1987)

[Gr91] P. Grangeat, *Mathematical framework of cone beam 3-D reconstruction via the first derivative of the Radon transform* in Herman, G. T., Louis, A.K. and Natterer, F., editors, *Mathematical Methods in Tomography.* Springer, Berlin (1991) 66–97.

[Kat02] A. Katsevich, *Analysis of an exact inversion algorithm for spiral-cone beam CT.* Phys. Med. Biol. **47** (2002), 2583–2597.

[Lou89] A.K. Louis, *Inverse und schlecht gestellte Probleme* Teubner, Stuttgart (1989).

[Lou96] A.K. Louis, *The approximate inverse for linear and some nonlinear problems.* Inverse Problems **12** (1996), 175–190.

[Lou03] A.K. Louis, *Filter design in three-dimensional cone beam tomography: circular scanning geometry.* Inverse Problems **19** (2003), S31–S40.

[Lou06] A.K. Louis. *Development of algorithms in computerized tomography.* PSAPM (AMS Proceedings of Symposia in Applied Mathematics) **63** 25-42, 2006

[LMR97] A.K. Louis, P. Maass, A. Rieder *Wavelets : Theory and Applications.* Wiley, Chichester (1997).

[Nat86] F. Natterer *The mathematics of computerized tomography* Teubner-Wiley, Stuttgart (1986).

[NW01] F. Natterer, F. Wübbeling, *Mathematical Methods in Image Reconstruction*, SIAM, Philadelphia (2001).

[Qui06] E.T: Quinto, *An introduction to X-ray tomography and Radon transforms* in The Radon Transform and Applications to Inverse Problems, G. Olafsson and E.T. Quinto, eds. AMS Proceedings of Symposia in Applied Mathematics, Providence, RI, 2006, American Mathematical Society

[ZYW05] Zhao,S, Yu H, Wang G., *A* unified framework for exact cone-beam image reconstruction formula. Med. Phys. 32, 1712-1721, 2005

Tikhonov regularization with non - standard constraints for tomography

Ronny Ramlau

(joint work with Gerd Teschke, Wolfgang Ring)

1. Introduction

In Inverse and Ill - posed problems, Tikhonov regularization has frequently been used to compute a stable approximation to the solution of linear as well as nonlinear operator equations $F(x) = y$. The solution is approximated by a global minimizer of the Tikhonov functional,

$$x_\alpha^\delta = \arg\min_x J_\alpha(x) = \arg\min_x \left\{ \|y^\delta - F(x)\|^2 + \alpha\Omega(x, \bar{x}) \right\} \ , \tag{1}$$

where Ω denotes the chosen penalty term, y^δ the noisy data and $\bar{x}$ is an a priori guess to the solution. The regularization parameter α has to be chosen in dependence of the noise level such that $x^\delta_{\alpha(\delta)}$ converges to a solution of the equation as $\delta \to 0$. The penalty term has a vital influence on the features of the reconstruction. In most cases, in particular for nonlinear operators, the penalty $\Omega(x, \bar{x}) = \|x - \bar{x}\|_X^2$, with X a Hilbert space, is chosen. In the following, we will propose two different types of penalties for tomographic applications: sparsity constraints and a penalty on the perimeter of the singularity set of a function. The resulting schemes were applied to SPECT and CT data.

2. Sparsity constraints

Sparsity constraints are used to enforce a computed reconstruction to have a sparse representation with respect to some given bases or frames, but they can also be used to create Besov norm penalties. In some tomographic applications, e.g. SPECT, the function that has to be reconstructed has a sparse representation

with respect to compactly supported Wavelet bases, thus it seems useful to obtain sparse reconstructions also. For numerical illustrations, we refer to [1].

Let $\{\Phi_\lambda\}_{\lambda\in\Lambda} \subset X$ be a Frame. Then we can define the following operator and its adjoint:

$$T : X \to \ell_2 \qquad Tx = \boldsymbol{x} = \{\langle x, \Phi_\lambda\rangle\}_{\lambda\in\Lambda} \tag{2}$$

$$T^* : \ell_2 \to X \qquad T^*\boldsymbol{x} = \sum_{\lambda\in\Lambda} x_\lambda \Phi_\lambda \tag{3}$$

Denoting $x_\lambda = \langle x, \Phi_\lambda\rangle$, we introduce the functional

$$\Psi_{p,\beta}(\boldsymbol{x}) = \left(\sum_\lambda \beta_\lambda |x_\lambda|^p\right)^{1/p}$$

with some positive weights $\beta_\lambda \geq 1$, and investigate Tikhonov regularization with penalties $\Psi_{p,\beta}$ and $\Psi^p_{p,\beta}$. First, we will present a regularization result:

Theorem 1: *Let F be a strongly continuous operator and $y^\delta \in Y$ with $\|y^\delta - y\| \leq \delta$. Assume that the solution $\boldsymbol{x}^\dagger$ as well as $\bar{\boldsymbol{x}}$ have finite value of $\Psi_{p,\beta}$. Let the regularization parameter be chosen by the following rule:*

$$\left.\begin{array}{l} \alpha(\delta) \to 0 \\ \frac{\delta^2}{\alpha(\delta)} \to 0 \end{array}\right\} \text{ as } \delta \to 0 \ .$$

Then every sequence $\{\boldsymbol{x}^{\boldsymbol{\delta_k}}_{\boldsymbol{\alpha_k}}\}$ of minimizers of the functional $J_\alpha(\boldsymbol{x})$, where $\delta_k \to 0$ and $\alpha_k = \alpha(\delta_k)$ has a convergent subsequence. The limit of every convergent subsequence is a solution of $F(T^*\boldsymbol{x}) = y$ with minimal value of $\Psi_{p,\beta}(\boldsymbol{x} - \bar{\boldsymbol{x}})$. If, in addtition, the solution $\boldsymbol{x}^\dagger$ with minimal $\Psi_{p,\beta}(\boldsymbol{x} - \bar{\boldsymbol{x}})$ is unique, then we have with respect to $\Psi_{p,\beta}$

$$\lim_{\delta\to 0} \boldsymbol{x}^\delta_{\alpha(\delta)} = \boldsymbol{x}^\dagger \ . \tag{4}$$

We wish to remark that this result holds for both penalty terms. To use the method, we have to provide a minimization algorithm for the functional. We propose the so called Surrogate functionals, i.e. we introduce $J^s_\alpha(\boldsymbol{x}, \boldsymbol{a}) = J_\alpha(\boldsymbol{x}) + C\|\boldsymbol{x} - \boldsymbol{a}\|^2 - \|F(T^*\boldsymbol{x}) - F(T^*\boldsymbol{a})\|^2$, and compute the sequence

$$\boldsymbol{x_{k+1}} = \arg\min_{\boldsymbol{x}} J^s_\alpha(\boldsymbol{x}, \boldsymbol{x_k}).$$

It turns out that the surrogate functional can be minimized easily, and the sequence $\{\boldsymbol{x_k}\}$ converges towards a critical point of the Tikhonov functional. For more details, we refer to [1, 2]. A different minimization approach would be to use the generalized conditional gradient method [4]. The test computations for SPECT show that artifacts and the influence of noise is reduced by using sparsity constraints.

3. Simultaneous Segmentation and Reconstruction from Tomography Data

Some applications require a segmentation of an image obtained as a reconstruction from tomography data. This is usually done as an image postprocessing task, i.e. the segmentation process works on the reconstructed image only, the direct connection to the measured data is lost. We propose a segmentation and reconstruction algorithm that works directly on the CT data. We restrict ourself to the reconstruction of piecewise constant functions in $\mathbb{R}^2$, that is, we are looking for a solution in the space

$$PC_m(D \setminus \Gamma) := \left\{ f = \sum_{i=1}^{m} f_i \chi_{\Omega_i} : f_i \in \mathbb{R},\ \Omega_i \text{ open sets },\Omega_i \cap \Omega_j = \emptyset \text{ for } i \neq j \right\} .$$

We define the singularity set Γ where f has jumps by $\Gamma = \bigcup_{(i,j)\in I} \Gamma_{ij}$, with Γ_{ij} being a closed curve separating the sets Ω_i and Ω_j. The task is now to recover the singularity set as well as the coefficients f_i from its Radon transform data. We use a Tikhonov functional with a perimeter constraint on Γ (also well known as Mumford Shah functional),

$$\begin{aligned} J_\alpha^{MS}(f,\Gamma) &= \|y^\delta - R(f)\|^2 + \alpha|\Gamma| , \\ |\Gamma| &= \int_\Gamma 1\, dS , \\ (\mu_\alpha^\delta, \Gamma_\alpha^\delta) &= \arg \min_{\substack{\Gamma \\ f \in PC_m(D\setminus\Gamma)}} J_\alpha^{MS}(\mu,\Gamma) . \end{aligned}$$

The minimization of the functional is carried out by a shape optimization approach: First the functional variable is eliminated. Representing the shapes by a level set function, the remaining shape functional is minimized by a gradient method. For more details on the numerical realization as well as on reconstruction results, we refer to [3]. If we want to prove a regularization result, we have to define a convergence that ensures not only functional convergence but also convergence of the shapes. Using the L_1-metric for characteristic functions, defined by $d_{L_1}(\Omega,\ \tilde{\Omega}) = \|\chi_\Omega - \chi_{\tilde{\Omega}}\|_{L_1}$, we can define convergence on $PC_m(D \setminus \Gamma)$ by

$$\begin{aligned} &(f_n, \Gamma_n) \overset{PC_m(D\setminus\Gamma)}{\longrightarrow} (f,\Gamma) \\ &\quad \Longleftrightarrow f_n = \sum_{j=1}^{m} f_{j,n}\chi_{\Omega_{j,n}},\ f = \sum_{j=1}^{m} f_j \chi_{\Omega_j} \text{ with } f_{j,n} \to f_j \text{ and } \Omega_{j,n} \overset{d_{L_1}}{\longrightarrow} \Omega_j \\ &\qquad \text{for } j = 1, \cdots, m \text{ and } n \to \infty \end{aligned}$$

(modulo reordering of the sums for f_n). Based on this definition, we can prove that the functional J_α^{MS} has a minimizer in PC_m, and that the minimizer depends stable on the data. Moreover, the following regularization result holds:

Theorem 2 *Let $f^\dagger \in PC_m(D \setminus \Gamma)$ with singularity set $\Gamma^\dagger$, and $Rf^\dagger = y$. For noisy data y^δ with $\|y^\delta - y\| \le \delta$, choose the regularization parameter $\alpha(\delta)$ fulfilling*

$$\alpha(\delta) \to 0 \text{ and } \frac{\delta^2}{\alpha(\delta)} \to 0 \text{ for } \delta \to 0 \ .$$

If $(f^\delta_{\alpha(\delta)}, \Gamma^\delta_{\alpha(\delta)})$ denote the minimizer of the functional $J^{MS}_{\alpha(\delta)}$ with data y^δ, then

$$(f^\delta_{\alpha(\delta)}, \Gamma^\delta_{\alpha(\delta)}) \overset{PC_m(D\setminus\Gamma)}{\longrightarrow} (f^\dagger, \Gamma^\dagger) \quad \text{for } \delta \to 0.$$

More details will be presented in a forthcoming paper.

References

[1] R. Ramlau and G. Teschke, *A Tresholding Iteration for Nonlinear Operator Equations with Sparsity Constraints.*, Numerische Mathematik, Vol. 104, No. 2 (2006), 177 - 203.

[2] R. Ramlau, *Regularization properties of Tikhonov regularization with sparsity constraints*, submitted for publication, 2006.

[3] R. Ramlau and W. Ring, *A Mumford-Shah approach for contour tomography.* J. Comp. Phys., 2006.

[4] K. Bredies, D. Lorenz and P. Maass, *Conditional Gradient*, to appear, 2006.

Penalized image reconstruction and cardiac motion

B. A. Mair

(joint work with J. A. Zahnen)

Green's one-step-late (OSL) algorithm, and a modification by Lange, is often applied to the reconstruction of images based on the penalized maximum likelihood approach. However, these algorithms only converge under certain restrictive conditions which often do not hold in applications. In this paper we discuss a method of modifying the line search procedure in Lange's version of the OSL algorithm which maintains the positivity of the iterates and is convergent, without any restrictive conditions on the penalty or choice of parameter. The paper examines two methods for choosing the step size for the line search, one based on the bisection algorithm, and the other on Armijo's rule. Simulations in this paper show that the Armijo line search algorithm is significantly faster than the bisection method. An application to the problem of estimating both image frames and motion vector fields in gated cardiac emission tomography is also discussed.

1. Introduction

In 1990, Green [1, 2] proposed the iterative one-step-late (OSL) algorithm to reconstruct images in emission tomography from a general penalized maximum likelihood objective (PML) function. Later that same year, Lange [3] added a line search and proved, under certain conditions, that the modified algorithm was convergent and produced iterates that were non-negative, and monotonically decreased the objective function. However, the conditions restrict the choice of the penalty parameter and are not valid for the simple quadratic penalty term, since

one condition in [3] requires the penalty term to have a bounded derivative on the entire real line. As a result, many alternative algorithms have been developed for PML estimation of PET images. However, the OSL algorithm has recently been applied to recontructing images in gated emission tomography [4, 5, 6, 7]. This is due to the very general form of the penalty term, which often includes pre-estimated motion information. Since the conditions of Lange's OSL algorithm are not satisfied by the penalty term in these applications, the algorithm was further modified in [5, 6, 7] to ensure positivity of the estimates, and convergence of the objective function.

The update in Green's OSL algorithm can be expressed as the product of the current iterate with a ratio of two terms. In [5], it was observed that if the penalty parameter was too large, the term in the denominator became negative or even too large, resulting in negative iterates and a divergent algorithm. The algorithm was improved by applying a threshold to the denominator term at each iteration to ensure positivity and boundedness. In [7, 8], the performance of Green's OSL algorithm was improved by inserting a line search after each iteration. This line search was performed by using the bisection method.

In this work we investigate the effects of two numerical line search procedures, one based on the usual bisection algorithm, and another based on Armijo's rule.

2. Theory

Let the detector data be denoted by $\mathbf{d} = [d_1, d_2, \ldots, d_I]^T$. Then for each $i = 1, 2, \ldots, J$, d_i is a random sample from a Poisson distribution with mean $[H\mathbf{x}^{true}]_i$ where $\mathbf{x}^{true} = [x_1^{true}, x_2^{true}, \ldots, x_J^{true}]^T$ is the vector of true image intensity, H is the system matrix, and $[H\mathbf{x}]_i$ is the i^{th} entry in the vector $H\mathbf{x}$. . The $(i,j)^{\text{th}}$ entry of H, denoted h_{ij} is the probability that an emission in the j^{th} voxel is detected in the i^{th} detector tube. Let $U(\mathbf{x})$ be a user–defined penalty term (or potential function in a Gibbs prior), and $E(\mathbf{x}) = \sum_{i=1}^{I} ([H\mathbf{x}]_i - d_i \log[H\mathbf{x}]_i) + \alpha U(\mathbf{x})$. Then, a PML estimate $\hat{\mathbf{x}}$ of $\mathbf{x}^{true}$ is obtained by minimizing the objective function E. That is

$$\hat{\mathbf{x}} = \arg\min_{\mathbf{x}>\mathbf{0}} E(\mathbf{x}). \tag{1}$$

Proposed Algorithm: Given $\mathbf{x}^{(n)} > \mathbf{0}$, determine the update $\mathbf{x}^{(n+1)}$ as follows. Define $\lambda_j^{(n)} = \dfrac{\sum_{i=1}^{I} h_{ij} d_i / [H\mathbf{x}^{(n)}]_i}{\sum_{i=1}^{I} h_{ij} + \alpha \frac{\partial U}{\partial x_j}(\mathbf{x}^{(n)})}$. Then, Green's OSL update of $\mathbf{x}^{(n)}$ is the vector with j^{th} entry $x_j^{(n)} \lambda_j^{(n)}$. Then, in the ideal case, the objective function should decrease in the direction of the vector $v_j^{(n)} = x_j^{(n)} \lambda_j^{(n)} - x_j^{(n)}$. As in [3], we propose an update of the form $\mathbf{x}^{(n+1)}(t) = \mathbf{x}^{(n)} + t\mathbf{v}^{(n)}$ where t is a scalar to be chosen. In [3] it is assumed that the parameter α is chosen such that the OSL update is positive, which leads to a positive value for t. However, in our case, we make no such assumption, and as a result, t may be negative. To determine the step

size, first, let $a_n = [\max_j |\lambda_j^{(n)} - 1|]^{-1}$. Then, $\mathbf{x}^{(n+1)}(t) > 0$ when $|t| < a_n$. Next, to ensure that the objective function decreases, let $\psi(t) = E(\mathbf{x}^{(n+1)}) < E(\mathbf{x}^{(n)})$. Then, if $\psi'(0) < 0$, we choose $0 < t < a_n$, and if $\psi'(0) > 0$, we choose $-a_n < t < 0$. To apply the bisection rule to determine the optimal value, t_{opt}, we choose t_{opt} such that $\psi'(t)$ does not change sign for all values of t between 0 and t_{opt}, as was suggested in [3]. In applying Armijo's rule [9] to determine t_{opt}, we only require $\psi(t_{opt}) < 0$.

In [4, 7, 8], the RM algorithm was developed for the simultaneous estimation of image frames and motion in gated cardiac emission tomography. If we denote the images $f_1, f_2, \ldots, f_J$ and the displacement vectors between frames, $\mathbf{m}_1, \mathbf{m}_2, \ldots, \mathbf{m}_J$, by $\mathbf{f}$ and $\mathbf{m}$ respectively, this algorithm is based on minmizing an objective function of the form

$$E(\mathbf{f}, \mathbf{m}) = \alpha L(\mathbf{f}) + E_I(\mathbf{f}, \mathbf{m}) + \beta E_S(\mathbf{m})$$

where $L(\mathbf{f})$ is the negative log likelihood of the gated data, $E_I(\mathbf{f}, \mathbf{m})$ is the total image matching term, and $E_S(\mathbf{m})$ is the total strain energy. The RM algorithm is an iterative algorithm, in which each iterate consists of two iterative algorithms, the R step, and the M step. Given the current estimates $\mathbf{f}^{(n)}$ and $\mathbf{m}^{(n)}$, the updates are obtained by first minimizing $\alpha L(\mathbf{f}) + E_I(\mathbf{f}, \mathbf{m}^{(n)})$ subject to the constraint $\mathbf{f} \geq 0$ (R step), and then minmizing $E_I(\mathbf{f}^{(n+1)}, \mathbf{m}) + \beta E_S(\mathbf{m})$ (M step). Clearly the R step is a penalized ML problem, so we can apply the proposed algorithms to determine $\mathbf{f}^{(n+1)}$. In the previous work, the bisection method was used in [4, 8].

3. Experiments

The reconstruction algorithm was applied to simulated data with Poisson noise from a 128×128 thorax phantom with 2 million total counts. The penalty function in the objective function was $U(\mathbf{x}) = \sum_{j=1}^{J} \sum_{k \in N(j)} \omega_{jk} \log\cosh((x_j - x_k)/\delta)$ where $\delta = 50$. The alorithm was applied with the bisection and Armijo's line search options for 150 iterations, for a range of values of the penalty parameter α. The main aim of the experiments was to determine which method converged faster. Convergence was evaluated by observing how the objective function and projected gradient decreased relative to the CPU time. The projected gradient of the iterate $\mathbf{x}^{(n)}$ is a measure of how close $\mathbf{x}^{(n)}$ is to satisfying the Kuhn–Tucker optimality conditions for the PML estimate, and is defined as $\max_j |\max\{(x_j^{(n)} - \frac{\partial E}{\partial x_j}(\mathbf{x}^{(n)})), 0\} - x_j^{(n)}|$. Tests were also performed for the quadratic penalty function, using Green's algorithm.

For the quadratic function, our tests showed that the denominator in the update for Green's OSL algorithm became negative for $\alpha = 0.04$. For both the quadratic and logcosh penalties, our tests indicated that the Armijo method achieved the same or better accuracy for both the objective function and projected gradient in less than 25% of the CPU time required by the bisection method.

References

[1] P. Green, *On the use of the EM algorithm for penalized likelihood estimation*, J. Roy. Statist. Soc., B**52** (1990), 443–452.
[2] P. Green, *Bayesian reconstructions from emission tomography using a modified EM algorithm*, IEEE Trans. Med. Imag.**9** (1990), 84–93.
[3] K. Lange, *Convergence of EM image reconstruction algorithms with Gibbs smoothing*, IEEE Trans. Med. Imag.**9** (1990), 439–446.
[4] Z. Cao, D. R. Gilland, B. A. Mair and R. J. Jaszczak, *Three-dimensional motion estimation with image reconstruction for gated cardiac ECT*, IEEE Trans. Nuclear Science **50** (2003), 384–388.
[5] E. Gravier and Y. Yang, *Motion-compensated reconstruction of tomographic image sequences*, IEEE Trans. Nuclear Science **52** (2005), 51–56.
[6] D. S. Lalush and B. M. W. Tsui, *Block iterative techniques for fast 4D reconstruction using a priori motion models in gated cardiac SPECT*, Phys. Med. Biol. **43** (1998), 875–886.
[7] B. A. Mair, D. R. Gilland and Z. Cao, *Simultaneous motion estimation and image reconstruction from gated data*, Proc. 2002 IEEE Internat. Symp. Biomed. Imaging (2002), 661–664.
[8] B. A. Mair, D. R. Gilland and J. Sun, *Estimation of images and non-rigid deformations in gated emission CT*, IEEE Trans. Med. Imag. (2006), to appear.
[9] M. S. Bazaraa, H. D. Sherali and C. M. Shetty, *Nonlinear Programming: Theory and Algorithms*, 2nd ed. New York, N.Y., Wiley, 1993.

Image Reconstruction for Bioluminescence Tomography

Ming Jiang

(joint work with Tie Zhou, Jiantao Cheng, Wenxiang Cong, Ge Wang)

Gene therapy is a breakthrough in the modern medicine, which promises to cure diseases by modifying gene expression. A key for development of gene therapy is to monitor the *in vivo* gene transfer and its efficacy in the mouse model. Traditional biopsy methods are invasive, insensitive, inaccurate, inefficient, and limited in the extent. To map the distribution of the administered gene, reporter genes such as those producing luciferase are used to generate light signals within a living mouse, which can be externally measured.

Bioluminescent imaging (BLI) is an optical technique for sensing gene expression, protein functions and other biological processes in mouse models by reporters such as luciferases that generate internal biological light sources [1, 2]. The light emitted within the mouse can be captured externally using a highly sensitive CCD camera [3]. BLI has great potentials in various biomedical applications, including regenerative medicine, developmental therapeutics, treatment of residual minimal disease, and studies on cancer stem cells. BLI could be applied to study almost all diseases in small animal models [1, 2].

Although BLI is useful, it does not explore the full potential of this approach. In particular, this 2D bioluminescence imaging mode, like the traditional radiography, is incapable of 3D image reconstruction of internal source features of interest [2]. Since its first introduction in 2003 [4], the bioluminescence tomography (BLT) has been undergone a rapid development [4, 5, 6, 7, 8, 9, 10, 11, 12, 13, 2, 14, 15, 16].

BLT is being actively developed to address the needs for 3D localization and quantification of a bioluminescent source distribution in a small animal. With BLT, optimal analysis on a bioluminescent source distribution becomes feasible inside a living mouse.

Traditionally, optical tomography sends visible or near infra-red light to probe a scattering object, and reconstructs the distribution of internal optical properties, such as absorption and scattering coefficients [17, 18, 19]. In contrast to this active imaging mode, BLT reconstructs an internal bioluminescent source distribution, generated by luciferase induced by reporter genes, from external optical measures. Currently, in BLT the complete knowledge on the optical properties of involved anatomical structures is assumed to be available from an independent tomographic scan, such as a CT/micro-CT, MRI scan and/or diffuse optical tomography (DOT), by image segmentation and optical property mapping. That is, we can segment the image volume into a number of anatomical structures, and assign optical properties to each structure using a database of the optical properties compiled for this purpose or using a DOT-type technique.

Mathematically, BLT is a source inversion problem based on optical measurement on the domain boundary, utilizing detailed knowledge on the optical properties. BLT is a highly ill-posed inverse problem per se. The tomographic feasibility and the solution uniqueness were theoretically studied [5]. It was proved that the uniqueness does not hold in general. For the BLT algorithms to produce satisfactory results, *a priori* knowledge must be utilized to regularize the problem. In our previous studies, we utilized constraints such as the non-negativity and source support. Other constraints such as the range of the source intensity may be very effective as well. Another approach is to utilize spectral resolved measurement such as the hyper-spectral or multi-spectral measurement [12, 13, 15, 20] and multi-spectral source information [21] to improve the BLT reconstruction.

In previous studies, the forward imaging model is described by the diffusion approximation assuming the complete data being measured on the object boundary to reconstruct an internal bioluminescent source distribution. In practice, the measured data is often incomplete due to physical limitations as in X-ray CT [22, 18]. The available data for BLT in this situation is similar to CT image reconstruction from angle-limited data. In [16], we proposed an approach for BLT from partial boundary measurement and two iterative reconstruction algorithms based on the diffusion approximation. Moreover, We generalized the results on the solution uniqueness [5] to this partial data case. It was proved that similar results still hold given partical optical signals on the mouse body surface, although the solution characterization is more complicated. Furthermore, we extended the BLT methods in [6] to the partial data case. The first algorithm is a variant of the well-known expectation-maximization (EM) algorithm [23]. The second one is based on the projected Landweber scheme [24, 25, 26]. Either of the methods can easily incorporate knowledge-based constraints .

This work is supported in part by NKBRSF (2003CB716101) and NSFC (60325101, 60272018), Ministry of Education (306017), China, and Engineering

Research Institute of Peking University, an NIH/NIBIB grant (EB001685), a special grant for bioluminescent imaging from Department of Radiology, College of Medicine, University of Iowa.

References

[1] C. Contag and M. H. Bachmann, "Advances in bioluminescence imaging of gene expression," *Annual Review of Biomedical Engineering*, vol. 4, pp. 235 – 260, August 2002.

[2] V. Ntziachristos, J. Ripoll, L. H. V. Wang, and R. Weissleder, "Looking and listening to light: the evolution of whole-body photonic imaging," *Nature Biotechnology*, vol. 23, no. 3, pp. 313 – 320, 2005.

[3] B. W. Rice, M. D. Cable, and M. B. Nelson, "In vivo imaging of light-emitting probes," *Journal of Biomedical Optics*, vol. 6, pp. 432 – 440, 2001.

[4] G. Wang *et al*, "Development of the first bioluminescent tomography system," *Radiology Suppl. (Proceedings of the RSNA)*, vol. 229(P), December 2003.

[5] G. Wang, Y. Li, and M. Jiang, "Uniqueness theorems for bioluminescent tomography," *Medical Physics*, vol. 31, no. 8, pp. 2289 – 2299, 2004.

[6] M. Jiang and G. Wang, "Image reconstruction for bioluminescence tomography," in *Proceedings of SPIE: Developments in X-Ray Tomography*, vol. 5535, 2004, pp. 335 – 351, invited talk.

[7] ——, "Image reconstruction for bioluminescence tomography," ser. Proceedings of the RSNA, December 2004.

[8] M. Jiang, T. Zhou, J. T. Cheng, W. X. Cong, K. Durairaj, and G. Wang, "Image reconstruction for bioluminescence tomography," ser. Proceedings of the RSNA, December 2005.

[9] W. X. Cong, G. Wang, D. Kumar, Y. Liu, M. Jiang, L. V. Wang, E. A. Hoffman, G. McLennan, P. B. McCray, J. Zabner, and A. Cong, "Practical reconstruction method for bioluminescence tomography," *Optics Express*, vol. 13, no. 18, pp. 6756–6771, 2005.

[10] A. X. Cong and G. Wang, "A finite-element-based reconstruction method for 3d fluorescence tomography," *Optics Express*, vol. 13, no. 24, pp. 9847–9857, 2005.

[11] C. Kuo, O. Coquoz, T. Troy, N. Zhang, D. Zwarg, and B. Rice, "Bioluminescent tomography for in vivo localization and quantification of luminescent sources from a multiple-view imaging system," in *SMI Fourth Conference*, Cologne, Germany, 2005.

[12] G. Alexandrakis, F. R. Rannou, and A. F. Chatziioannou, "Tomographic bioluminescence imaging by use of a combined optical-PET (OPET) system: a computer simulation feasibility study," *Physics In Medicine And Biology*, vol. 50, no. 17, pp. 4225 – 4241, 2005.

[13] A. J. Chaudhari, F. Darvas, J. R. Bading, R. A. Moats, P. S. Conti, D. J. Smith, S. R. Cherry, and R. M. Leahy, "Hyperspectral and multispectral bioluminescence optical tomography for small animal imaging," *Physics In Medicine And Biology*, vol. 50, no. 23, pp. 5421 – 5441, 2005.

[14] N. V. Slavine, M. A. Lewis, E. Richer, and P. P. Antich, "Iterative reconstruction method for light emitting sources based on the diffusion equation," *Medical Physics*, vol. 33, no. 1, pp. 61 – 68, 2006.

[15] H. Dehghani, S. Davis, S. D. Jiang, B. Pogue, K. Paulsen, and M. Patterson, "Spectrally resolved bioluminescence optical tomography," *Optics Letters*, vol. 31, no. 3, pp. 365 – 367, February 2005.

[16] M. Jiang, T. Zhou, J. T. Chen, W. X. Cong, and G. Wang, "Development of bioluminescence tomography," in *Proceedings of SPIE: Developments in X-Ray Tomography*, 2006 (in press), invited talk.

[17] S. R. Arridge, "Optical tomography in medical imaging," *Inverse Problems*, vol. 15, pp. R41 – R93, 1999.

[18] F. Natterer and F. Wübbeling, *Mathematical Methods in Image Reconstruction*. Philadelphia, PA: SIAM, 2001.

[19] A. P. Gibson, J. C. Hebden, and S. R. Arridge, "Recent advances in diffuse optical imaging," *Physics in Medicine and Biology*, vol. 50, no. 4, pp. R1–R43, 2005.
[20] A. X. Cong and G. Wang, "Multispectral bioluminescence tomography: Methodology and simulation," *International Journal of Biomedical Imaging*, vol. 2006, article ID 57614. doi:10.1155/IJBI/2006/57614.
[21] C. Q. Li and H. B. Jiang, "Imaging of particle size and concentration in heterogeneous turbid media with multispectral diffuse optical tomography," *Optics Express*, vol. 12, no. 25, pp. 6313–6318, 2004.
[22] F. Natterer, *The Mathematics of Computerized Tomography.* Philadelphia, PA: SIAM, 2001.
[23] L. A. Shepp and Y. Vardi, "Maximum likelihood restoration for emission tomography," *IEEE Trans. Med. Imaging*, vol. 1, pp. 113 – 122, 1982.
[24] M. Jiang and G. Wang, "Convergence studies on iterative algorithms for image reconstruction," *IEEE Trans. Medical Imaging*, vol. 22, no. 5, pp. 569 – 579, May 2003.
[25] ——, "Development of iterative algorithms for image reconstruction," *Journal of X-ray Science and Technology*, vol. 10, no. 1–2, pp. 77 – 86, 2002, invited Review.
[26] M. Piana and M. Bertero, "Projected Landweber method and preconditioning," *Inverse Problems*, vol. 13, pp. 441 – 463, 1997.

Exploiting Symmetry in Fan-Beam Tomography and Some Remarks on the Filtered Backprojection Algorithm

Adel Faridani

Exploiting symmetry in fan-beam tomography. The integral transforms of x-ray tomography have a inherent symmetry stemming from the fact that interchanging the positions of x-ray source and detector will lead to the same measured value. Taking a measurement at some point thus gives also knowledge of the transform at a 'reflected' point. For the parallel-beam geometry this symmetry is readily exploited, for example by restricting the directions of irradiation to a 180 degree range. On the other hand it has not been obvious how to conveniently exploit the symmetry when using the fan-beam geometry. Recently, Izen, Rohler, and Sastry [7] showed that if fan-beam measurements are taken at the points of the so-called standard sampling lattice (cf. [10, 4]) then the union of measured and reflected points is a so-called periodic sampling set, that is a union of shifted copies of a smaller lattice. While Izen et al. proceeded to develop a special reconstruction algorithm for such data, in this talk we report results obtained by using the theory and algorithms for periodic sampling developed in [3]. Using this sampling theory the data are first interpolated onto a denser lattice and then the reconstruction is performed using the standard filtered backprojection algorithm. Some of this work has been done jointly with Mitchell [9]. The results show that resolution can clearly be increased in this way. The method used here is more widely applicable than that of [7] but it also has its limitations as the number of cosets of the smaller lattice can become very large in some cases, rendering the method ineffective. For these cases one can consider using the sampling theory for unions of shifted lattices developed in [1, 2]. In this talk we present some key ideas underlying the new sampling theorems of [2]. Gratton [5] found an ingenious way to apply this

theory to fan-beam tomography, the advantage being that now the sampling set for the union of measured and reflected data can be treated as the union of just two shifted subgroups, albeit different ones.

When working with real data, increasing the resolution by exploiting the symmetry also leads to an increase in noise. This calls for post-processing with appropriate denoising methods. We present numerical results obtained jointly with Hass [6] that demonstrate that the now classical Rudin-Osher-Fatemi [12] denoising method already improves matters, and indicate that further exploration of the interaction of image reconstruction and post-processing is promising.

A contemporary introduction to the application of sampling theory to fan-beam tomography can be found in [4].

Some remarks on the filtered backprojection algorithm.

(1) The filtered backprojection algorithm has become somewhat of a commodity, as evidenced for example by its inclusion in MATLAB. For the research community this may raise the question if such widely distributed implementations are also the best ones. This remark concerns the implementation of the convolution step. The convolution

$$\int v(\langle x,\theta\rangle - s) Rf(\varphi, s) ds \tag{1}$$

$$= \int \hat{v}(\sigma)\, \widehat{Rf}(\varphi,\sigma) e^{i\sigma\langle x,\theta\rangle}\, d\sigma \tag{2}$$

(v as in [11, §5.1]) can be implemented by discretizing either integral. Which may be better? Discretizing (2) is convenient for implementing a variety of convolution kernels whose Fourier transform is known, and MATLAB's iradon does this. However, we present numerical experiments showing that for achieving high accuracy discretizing (1) appears superior. A heuristic explanation is as follows. It can be shown that discretizing (1) gives

$$v * Rf(\varphi,\langle x,\theta\rangle) \;\simeq\; \int \hat{v}(\sigma) \sum_k \widehat{Rf}(\varphi, \sigma + 2\pi k/h) e^{i\sigma\langle x,\theta\rangle}\, d\sigma$$

while discretizing (2) yields

$$v * Rf(\varphi,\langle x,\theta\rangle) \;\simeq\; \pi \sum_j \hat{v}(\pi j) \sum_k \widehat{Rf}(\varphi, \pi j + 2\pi k/h) e^{i\pi j\langle x,\theta\rangle}$$

The second formula gives a trapezoidal rule, the first the corresponding integral. Heuristic interpretation: Since $\hat{v}(0) = 0$ the lowest frequencies contributing to the second formula correspond to $|\sigma| = \pi$. The first formula picks up more information about the very low frequencies (σ close to 0) and thus avoids the small nearly constant error that reconstructions based on discretizing (2) exhibit.

(2) For the fan-beam filtered backprojection algorithm we find two popular implementations in the literature which differ in the following aspect. The

first implementation as for example in [11, Formula (5.29)] has a sine in the argument of the convolution kernel v, while the implementation given in [8, p. 82] does not. The mathematical derivation for kernels other than the straight ramp filter appears more elegant in the first case, while our numerical results indicate that the second implementation may be more favorable with regard to ringing artifacts.

Acknowledgment. The author would like to express his best wishes and grateful appreciation to Professor Frank Natterer on the occasion of his retirement. Support from the National Science Foundation under award DMS-0206752 is gratefully acknowledged.

References

[1] H. Behmard and A. Faridani, *Sampling of bandlimited functions on unions of shifted lattices*, J. Fourier Anal. Appl. **8** (2002), 43–58.
[2] H. Behmard, A. Faridani, and D. Walnut, *Construction of sampling theorems for unions of shifted lattices*, to appear in Sampling Theory in Signal and Image Processing, **5** (2006).
[3] A. Faridani, *A generalized sampling theorem for locally compact abelian groups*, Math. Comp. **63** (1994), 307–327.
[4] A. Faridani, *Fan-beam tomography and sampling theory*, Proc. Sympos. Appl. Math., **63**, Amer. Math. Soc., Providence, RI, (2006), 43–66.
[5] L. A. Gratton, *Nonuniform Sampling Problems in Computed Tomography*, Ph.D. thesis, Dept. of Mathematics, Oregon State University, 2005.
[6] R. A. Hass, *De-noising tomography images through bounded variation*, M.S. paper, Dept. of Mathematics, Oregon State University, 2005.
[7] S. H. Izen, D. P. Rohler, and K.L.A Sastry, *Exploiting symmetry in fan-beam CT: Overcoming third generation undersampling*, SIAM J. Appl. Math. **65** (2005), 1027–1052.
[8] A. C. Kak and M. Slaney, *Principles of computerized tomographic imaging*, IEEE Press, New York, 1988.
[9] N. Mitchell, *Multi-dimensional sampling in fan beam tomography*, M.S. paper, Dept. of Mathematics, Oregon State University, 2005.
[10] F. Natterer, *Sampling in fan-beam tomography*, SIAM J. Appl. Math. **53** (1993), 358–380.
[11] F. Natterer and F. Wuebbeling, *Mathematical Methods in Image Reconstruction*, SIAM, Philadelphia, 2001.
[12] L.I. Rudin, S. Osher, and E. Fatemi, *Nonlinear total variation based noise removal algorithms*, Phys. D **60** 1-4 (1992), 259–268.

Sampling in helical fan beam CT using the reflected lattice

Laurent Desbat
(joint work with Larry Gratton)

Sampling conditions in helical parallel and fan beam tomography are known [7, 2]. This study concerns single sclice helical fan-beam CT or equivalently dynamic CT with a single row detector [8]. The fan beam geometry symmetry yields a reflected lattice associated to each sampling lattice. However, in fan beam CT, the union of the direct and the reflected lattices does not generally build a lattice. Thus, the classical sampling theory based on the Poisson formula does not apply.

In a recent work [5], Izen, Rohler and Sastry showed that the union of a standard fan beam lattice and its reflected lattice builds a union of shifted large standard lattices. Thus, generalized sampling theorems (see [3] or [6]) can be applied to exploit the reflected lattice for doubling the 2D resolution in fan beam CT with essentially only doubling the number of projections (the Quater Detector Offset [QDO] allows for the improvement of the sampling along the detector). However, this approach can lead to the resolution of a huge number of linear systems.

The recent work [1] is probably a better way to address this problem. In its PhD [4], Larry Gratton proposed adaptations of [1] to 2D fan-beam CT and further developments. In the present work (performed during this week at Oberwolfach) we propose a first simple generalization to helical fan-beam CT.
Notations and definitions: G denotes a LCA group, $\widehat{G}$ the dual group of G. In classical applications: $G = \mathbb{R}^n$ and $\widehat{G} = \mathbb{R}^n$ or $G = \mathbb{T}^n$ ($\mathbb{T} = \mathbb{R}/\mathbb{Z}$) and $\widehat{G} = \mathbb{Z}^n$ or $G = \mathbb{T}^m \times \mathbb{R}^n$ and $\widehat{G} = \mathbb{Z}^m \times \mathbb{R}^n$, then $x \in G, \xi \in \widehat{G}, \langle x, \xi \rangle = [x \cdot \xi]$, where $[a] = mod(a, 1)$ is the fractional part of $a \in \mathbb{R}$. The Fourier transform of $f \in L^1(G)$ is defined by:

$$\hat{f}(\xi) \stackrel{\text{def}}{=} \int_G f(x) e^{-2i\pi\langle x,\xi\rangle} dm_G(x) \text{ and } f(x) = \int_{\widehat{G}} \hat{f}(\xi) e^{2i\pi\langle x,\xi\rangle} dm_{\widehat{G}}(\xi) \left(= \tilde{\hat{f}}(x)\right)$$

holds for $f \in L^1(G)$ continuous and $\hat{f} \in L^1(\widehat{G})$. Let H a closed subgroup of G then the annihilator of H is $H^\perp = \left\{\eta \in \widehat{G}, \langle y, \eta\rangle = 0 \text{ for all } y \in H\right\}$. Examples: $G = \mathbb{R}^n$ and $H = W\mathbb{Z}^n = \{Wk, k \in \mathbb{Z}^n\}$ where W is a non singular matrix then $H^\perp = W^{-t}\mathbb{Z}^n$ (indeed $\langle Wk, W^{-t}l\rangle = [Wk \cdot (W^{-t}l)] = [k \cdot l] = 0$). A closed discrete subgroup of G such that $H^\perp$ is a closed discrete subgroup of $\widehat{G}$ is called a lattice. The (bounded) set $R \subset \widehat{G}$ is a fundamental domain of the lattice $H^\perp$ if $\bigcup_{\eta\in H^\perp}(R + \eta)$ is a partition of $\widehat{G}$.

The classical sampling conditions of a function f can be read in the Poisson formula: let H be a lattice and R a fondamental domain of $H^\perp$; let $f \in L^1(G)$, such that $y \to f(x_0 + y)$ belongs to $L^1(G)$ and $\sum_{y\in H} f(x_0 + y)$ is a continuous function on G/H and its Fourier transform is in $L^1(H^\perp)$ then

$$\sum_{y\in H} f(x_0 + y) e^{-2i\pi\langle x_0+y,\xi\rangle} = m_{\widehat{G}}(R) \left(\hat{f}(\xi) + \sum_{\eta\in H^\perp\setminus\{0\}} \hat{f}(\xi + \eta) e^{2i\pi\langle x_0,\eta\rangle} \right).$$

If $\hat{f}$ vanishes outside of a set $K \subset R$ then $\hat{f}(\xi)$ can be recovered by the multiplication by the indicator of K (or R).

In its PhD [4], Larry Gratton proposed the following adaptation to sampling on two shifted lattices of the results obtained in [1]. Let G be a LCA group ; let H_2 be a lattice and R a fundamental domain of its reciprocal lattice $H_2^\perp$; let $K = R \cup (\eta' + K')$, with $K' \subset R$ and $\eta' \in H_2^\perp, \eta' \neq 0$; let $f \in L^2(G)$ be a continuous function, $\hat{f}(\xi) = 0$ a.e. outside of K ; let H_1 be a lattice such that continuous functions $h \in L^2(G)$ with $\hat{h}(\xi) = 0$ a.e. outside of K' can be reconstructed from their sample on $h(x_1 + z'), z' \in H_1$. Assume that $\eta' \in H_2^\perp \cap$

$H_1^\perp, \eta' \neq 0$ and $\langle x_1 - x_2, \eta' \rangle \neq 0$. Then f can be reconstructed from its samples $f(z), z \in (x_2 + H_2) \cup (x_1 + H_1)$ with

$$Sf(x) = S_{x_2+H_2} f(x) + \frac{1 - e^{2i\pi\langle x - x_2, \eta' \rangle}}{1 - e^{2i\pi\langle x_1 - x_2, \eta' \rangle}} S_{x_1+H_1}(f - S_{x_2+H_2} f)(x)$$

with

$$S_{x_j+H_j} f(x) = \sum_{y \in H_j} f(x_j + y)\tilde{\chi}_{R_j}(x - x_j - y), j \in \{1, 2\}$$

and the following interpolation error bound holds:

$$|Sf(x) - f(x)| \leq \left(2 + \frac{4}{1 - e^{2i\pi\langle x_1 - x_2, \eta' \rangle}}\right) \int_{\widehat{G}\setminus K} |\hat{f}(\xi)| dm_{\widehat{G}}(\xi)$$

This results has been applied succesfully in fan-beam CT in order to enhance the resolution of the data (and of the reconstruction) by using the reflected lattice. We generelized this results to the 3D fan beam transform and helical fan-beam CT. The 3D fan beam transform is defined by $\mathcal{D}f(\beta, \alpha, t) = \int_{L_{\beta,\alpha,t}} f(x)dx,$, where $x \in \mathbb{R}^3$, $L_{\beta,\alpha,t}$ is the line in the plane perpendicular to $e_3 = (0, 0, 1)^T$ at abscissa t ($t \in \mathbb{R}$), intersecting the source located at $r(\cos\beta, \sin\beta, 0)^T + te_3$, with $\beta \in [0, 2\pi[$ and the detector at angular position $\alpha \in [-\pi/2, \pi/2[$, see [2]. As in [4] we parametrize $\mathcal{D}f$ by

$$g(u, v, t) = \mathcal{D}f\left(2\pi u, \pi(v - \frac{1}{2}), t\right)$$

so that $g \in L^1(\mathbb{T}^2 \times \mathbb{R})$ ($G = \mathbb{T}^2 \times \mathbb{R}$, and $\widehat{G} = \mathbb{Z}^2 \times \mathbb{R}$).

Assume from now that f is essentially b-band limited, $b > 0$. The essential support of $\mathcal{D}f$ and associated sampling conditions have been given in [2]. The essential support K_3 of $\hat{g}(k, m, t)$, the Fourier transform of g, can be easily derived

$$K_3 = \left\{(k, m, \tau) \in \mathbb{Z} \times \mathbb{Z} \times \mathbb{R}; |k - 2m|^2 + r^2\tau^2 < r^2b^2, |k|r < |k - 2m|\rho\right\}$$

where r and ρ are respectively the radius of the source trajectory and the radius of the cylindric reconstruction region.

Helical FB sampling is just samplingthe 3D fan-beam transform under the helical constraint $t = \frac{T}{P}u$, where $T \in \mathbb{R}^+$ is the helical pitch and P the number of projection each turn. The standard lattice H_S and its reciprocal $H_S^\perp$ are generated by

$$W_S = \begin{bmatrix} \frac{1}{P} & 0 & 0 \\ 0 & \frac{1}{N} & 0 \\ \frac{T}{P} & 0 & T \end{bmatrix}, W_S^{-T} = \begin{bmatrix} P & 0 & -1 \\ 0 & N & 0 \\ 0 & 0 & 1/T \end{bmatrix}.$$

where $N \in \mathbb{N}$ is the number of fan angles at each projection. The symmetry relation reads now $g(u, v, t) = g(u + v, 1 - v, t)$. This yields the reflected lattice H_R and $H_R^\perp$ generated by

$$W_R = \begin{bmatrix} \frac{1}{P} & -\frac{1}{N} & 0 \\ 0 & \frac{1}{N} & 0 \\ \frac{T}{P} & 0 & T \end{bmatrix}, W_R^{-T} = \begin{bmatrix} P & 0 & -1 \\ P & N & -1 \\ 0 & 0 & 1/T \end{bmatrix}.$$

Let $\eta' = (0, -P/2, 0)^t$, then $\eta' \in H_S^\perp \cap H_R^\perp$. Just as in 2D FB CT, if x_2 corresponds to the QDO, $\langle x_1 - x_2, \eta' \rangle \neq 0$. Let us call R_{2FB}, resp. R_{1FB}, be the corresponding 2D constructed region in 2D FB, see [4], can be generalized to

$$R_2 = R_{2FB} \times [-\frac{b}{2\pi}; \frac{b}{2\pi}], R_1 = R_{1FB} \times [-\frac{b}{2\pi}; \frac{b}{2\pi}]$$

Thus, the interpolation formulas $S_{x_2+H_2} f(x) = \sum_{y \in H_2} f(x_2 + y) \tilde{\chi}_{R_2}(x - x_2 - y)$ reads with $x_2 = (u_2, v_2, t_2)^t$

$$S_{x_2+H_2} f(u, v, t) = \sum_{z \in H_{2FB}} \left(\sum_{y \in \frac{\pi}{b}\mathbb{Z}} f(x_2 + (z, y)) \mathrm{sinc}_b(t - t_2 - y) \right) \tilde{\chi}_{R_{2FB}}((u - u_2, v - v_2)^t - z)$$

and the same for $S_{x_1+H_1}$. This reduces essentially the use of the reflected lattice in helical CT to 2D CT through the so called "2π" interpolation along the t-axis, followed by the 2D fan-beam CT interpolation using the reflected lattice.

References

[1] H. Behmard, A. Faridani, and D. Walnut. Construction of sampling theorems for unions of shifted lattices. *To appear in Sampling Theory in Signal and Image Processing*, 2006.

[2] L. Desbat, S. Roux, P. Grangeat, and A. Koenig. Sampling conditions of 3D Parallel and Fan-Beam X-ray CT with application to helical tomography. *Phys. Med. Biol.*, 49(11):2377–2390, 2004.

[3] A. Faridani. A generalized sampling theorem for locally compact abelian groups. *Math. Comp.*, 63(207):307–327, 1994.

[4] L. Gratton. *Nonuniform Sampling Problems in Computed Tomography*, PhD thesis, Oregon State University, 2005.

[5] S.H. Izen, D.P. Rohler, and K.L.A. Sastry. Exploiting symmetry in fan beam CT: Overcoming third generation undersampling. *SIAM J. Appl. Math.*, 65(3):1027–1052, 2005.

[6] S.H. Izen, D.P. Rohler, and K.L.A. Sastry. Generalized Sampling Expansion on Lattices. *IEEE Trans.Sig. Proc.*, 53(6):1949–1963, 2005.

[7] F. Natterer. Sampling in fan-beam tomography. *SIAM J. Appl. Math.*, 53(2):358–380, 1993.

[8] S. Roux, L. Desbat, A. Koenig, and P. Grangeat. Exact reconstruction in 2D dynamic CT: compensation of time-dependent affine deformations. *Phys. Med. Biol.*, 49(11):2169–82, June 2004.

Inverse Problems for the Radiative Transport Equation and Optical Tomography

John C. Schotland
(joint work with Vadim Markel)

Optical tomography (OT) is an emerging biomedical imaging modality which uses scattered light to probe tissue structure and function. The usual approach to the inverse problem of OT makes use of the diffusion approximation (DA) to the radiative transport equation (RTE). Using the DA, it is possible to formulate the linearized inverse problem in terms of the inversion of a suitably defined Fourier-Laplace transform which relates the optical absorption of a random medium to the intensity of light transmitted through the medium. Here we describe analogous results which hold beyond the diffusion approximation. In particular, it is shown that by making use of the plane-wave expansion for the Green's function of the RTE, a generalized Fourier-Laplace structure arises in the inverse medium problem for the RTE.

The steady-state RTE

$$\hat{\mathbf{s}} \cdot \nabla I(\mathbf{r}, \hat{\mathbf{s}}) + (\mu_a + \mu_s) I(\mathbf{r}, \hat{\mathbf{s}}) = \mu_s \int d^2 s' p(\hat{\mathbf{s}}, \hat{\mathbf{s}}') I(\mathbf{r}, \hat{\mathbf{s}}') \ , \tag{1}$$

is a conservation law for the specific intensity $I(\mathbf{r}, \hat{\mathbf{s}})$ at the point $\mathbf{r}$ propagating in the direction $\hat{\mathbf{s}}$. Here μ_a is the absorption coefficient, μ_s is the scattering coefficient, and the phase function p is normalized so that $\int p d^2 s = 1$. Consider an experiment in which light from a point source at $\mathbf{r_1}$ in the direction $\hat{\mathbf{s}}_\mathbf{1}$ is incident on an infinite inhomogeneous medium with absorption $\mu_a(\mathbf{r}) = \mu_a^0 + \delta\mu_a(\mathbf{r})$, where μ_a^0 is constant. Within the accuracy of the weak scattering approximation, the intensity of light $\phi(\mathbf{r_1}, \hat{\mathbf{s}}_\mathbf{1}; \mathbf{r_2}, \hat{\mathbf{s}}_\mathbf{2})$ measured by a point detector at $\mathbf{r_2}$ in the direction $\hat{\mathbf{s}}_\mathbf{2}$, relative to a reference medium with absorption μ_a^0, obeys the integral equation

$$\phi(\mathbf{r_1}, \hat{\mathbf{s}}_\mathbf{1}; \mathbf{r_2}, \hat{\mathbf{s}}_\mathbf{2}) = \int d^3 r d^2 s G(\mathbf{r_1}, \hat{\mathbf{s}}_\mathbf{1}; \mathbf{r}, \hat{\mathbf{s}}) G(\mathbf{r}, \hat{\mathbf{s}}; \mathbf{r_2}, \hat{\mathbf{s}}_\mathbf{2}) \delta\mu_a(\mathbf{r}) \ , \tag{2}$$

where G is the Green's function for the RTE in the reference medium [1]. It has recently been shown that G is representable as a decomposition into plane waves and spherical functions of the form

$$G(\mathbf{r}, \hat{\mathbf{s}}; \mathbf{r}', \hat{\mathbf{s}}') = \int d^2 q \sum_\mu \sum_{lm, l'm'} e^{i(\mathbf{q}\cdot\boldsymbol{\rho} + \mathbf{q}'\cdot\boldsymbol{\rho}')} Y_{lm}(\hat{\mathbf{s}}) Y^*_{l'm'}(\hat{\mathbf{s}}') \times \langle lm | \Psi_\mu(\mathbf{q}) | l'm' \rangle \, e^{-Q_\mu(\mathbf{q})|z - z'|} \ , \tag{3}$$

where Ψ_μ and Q_μ are obtained from the solution to an eigenproblem and we use the notation $\mathbf{r} = (\boldsymbol{\rho}, z)$ [2]. This expansion can be obtained for any rotationally invariant phase function of the form $p(\hat{\mathbf{s}} \cdot \hat{\mathbf{s}}')$. Suppose that the sources and detectors are located on the planes $z = z_1$ and $z = z_2$, respectively. Then it can be seen that the Fourier transform of ϕ with respect to the source and detector coordinates is

given by the expression

$$\tilde{\phi}(\mathbf{q_1}, z_1; \mathbf{q_2}, z_2) = \sum_{\mu,\mu'} M_{\mu\mu'}(\mathbf{q_1}, \mathbf{q_2}) \int d^3r \exp\left[i(\mathbf{q_1} - \mathbf{q_2}) \cdot \boldsymbol{\rho}\right] \times \exp\left[-(Q_\mu(\mathbf{q_1}) + Q_{\mu'}(\mathbf{q_2}))z\right] \delta\mu_a(\mathbf{r}) \ , \tag{4}$$

where $\hat{\mathbf{s}}_\mathbf{1}, \hat{\mathbf{s}}_\mathbf{2}$ are chosen to be in the normal directions to the source and detector planes, M can be computed in term of Ψ_μ, and $\mathbf{q_1}, \mathbf{q_2}$ are conjugate to the source and detector coordinates. The inverse problem in OT consists of reconstructing $\delta\mu_a$ from ϕ. The Fourier-Laplace transform (4) can be inverted following the methods described in [1]. In the DA, only the lowest order mode contributes and the results presented in [3] are recovered.

References

[1] Markel, V. and Schotland, J. Symmetries, Inversion Formulas, and Image Reconstruction for Optical Tomography. Phys. Rev. E **70**, 056616 (2004)

[2] Panasyuk, G., Schotland, J. and Markel, V. Radiative Transport Equation in Rotated Reference Frames. J. Phys. A **39**, 115 (2006)

[3] Schotland, J. Continuous-Wave Diffusion Imaging. J. Opt. Soc. Am. A **14**, 275 (1997)

Reporter: Andreas Groh

Participants

Prof. Dr. Mark Agranovsky
Department of Mathematics
Bar-Ilan University
52900 Ramat Gan
ISRAEL

Prof. Dr. Jan Boman
Slottsvaegen 88
S-18352 Taeby

Prof. Dr. Alexander A. Boukhgueim
Schlumberger
Aslakveien 14A
N-0753 Oslo

Prof. Dr. Alexandre L. Boukhgueim
Department of Mathematics
and Statistics
Wichita State University
Wichita, KS 67260-0033
USA

Prof. Dr. Les Butler
Department of Chemistry
Louisiana State University
232 Choppin Hall
Baton Rouge, LA 70803
USA

Prof. Dr. Emmanuel Candes
Applied Mathematics 217-50
California Institute of Technology
Pasadena, CA 91125
USA

Prof. Dr. Rolf Clackdoyle
Lab.Traitement du Signal et
Instrum. (CNRS UMR 5516)
Campus du Pole Opt. et Vision-Bat.F
10, rue Barrouin
F-42000 St. Etienne

Prof. Dr. Laurent Desbat
TIMC - IMAG
Institut Albert Bonuiot
Faculte de Medicine
F-38706 La Tronche Cedex

Dr. Oliver Dorn
Departamento de Matematicas
Campus de Leganes
Universidad CarlosIII de Madrid
Avda. de la Universidad 30
E-28911 Leganes Madrid

Prof. Dr. Adel Faridani
Dept. of Mathematics
Oregon State University
Kidder Hall 368
Corvallis, OR 97331-4605
USA

Prof. Dr. David V. Finch
Dept. of Mathematics
Oregon State University
Kidder Hall 368
Corvallis, OR 97331-4605
USA

Prof. Dr. Larry Gratton
Department of Mathematics
Berea College
Berea, KY 40404
USA

Andreas Groh
Universität des Saarlandes
Institut für Angewandte Mathematik
Postfach 151150
66041 Saarbrücken

Denis Gruenhagen
Fachbereich 10 - Mathematik und Informatik
Universität Münster
Einsteinstr. 62
48149 Münster

Prof. Dr. F. Alberto Grünbaum
Department of Mathematics
University of California
Berkeley, CA 94720-3840
USA

Prof. Dr. Martin Hanke-Bourgeois
Fachbereich Mathematik/Informatik
Johannes-Gutenberg-Universität
55099 Mainz

Prof. Dr. Steven H. Izen
Dept. of Mathematics
Case Western Reserve University
10900 Euclid Avenue
Cleveland, OH 44106-7058
USA

Prof. Dr. Ming Jiang
School of Mathematical Sciences
Peking University
Beijing 100871
P.R. CHINA

Prof. Dr. Alexander Katsevich
Department of Mathematics
University of Central Florida
Orlando, FL 32816-1364
USA

Prof. Dr. Peter Kuchment
Department of Mathematics
Texas A & M University
College Station, TX 77843-3368
USA

Prof. Dr. Leonid Kunyansky
Department of Mathematics
University of Arizona
617 N. Santa Rita
Tucson AZ 85721-0089
USA

Dr. Aref Lakhal
Universität des Saarlandes
Institut für Angewandte Mathematik
Postfach 151150
66041 Saarbrücken

Prof. Dr. Alfred K. Louis
Universität des Saarlandes
Institut für Angewandte Mathematik
Postfach 151150
66041 Saarbrücken

Prof. Dr. Peter Maaß
Universität Bremen
FB3 Mathematik und Informatik
Zentrum für Technomathematik
MZH 2250
28344 Bremen

Prof. Dr. Bernard A. Mair
Dept. of Mathematics
University of Florida
358 Little Hall
P.O.Box 118105
Gainesville, FL 32611-8105
USA

Prof. Dr. Dr. h.c. Frank Natterer
Institut für Numerische und
Angewandte Mathematik
Universität Münster
Einsteinstr. 62
48149 Münster

Dr. Clifford Nolan
Dept. of Mathematics and Statistics
University of Limerick
Limerick
IRELAND

Prof. Dr. Frederic Noo
CAMT
729 Arapeen Drive
Salt Lake City, UT 84108-1218
USA

Steven Oeckl
Fraunhofer Institut IIS
Projektgruppe Ultrafeinfokus
Röntgentechnologie
Dr.-Mack-Str. 81
90762 Fürth

Prof. Dr. Viktor P. Palamodov
School of Mathematical Sciences
Tel Aviv University
Ramat Aviv
Tel Aviv 69978
ISRAEL

Dr. Sarah Patch
Department of Physics
University of Milwaukee
PO Box 413
Milwaukee, WI 53201
USA

Prof. Dr. Eric Todd Quinto
Dept. of Mathematics
Tufts University
503 Boston Ave.
Medford, MA 02155
USA

Prof. Dr. Ronny Ramlau
Johann Radon Institute for Comput.
and Applied Mathematics (RICAM)
Austrian Academy of Sciences
Altenbergstrasse 69
A-4040 Linz

Prof. Dr. Andreas Rieder
Institut für Praktische Mathematik
Universität Karlsruhe
76128 Karlsruhe

Prof. Dr. Erik L. Ritman
Dept. of Physiology and Biomedical
Engineering, Alfred Bldg.
Mayo Clinic College of Medicine
200 First Street
Rochester MN 55905
USA

Dr. Hans Rullgard
Department of Mathematics
Stockholm University
S-10691 Stockholm

Prof. Dr. Pierre C. Sabatier
Laboratoire de Physique Theorique
and Astroparticules
Universite de Montpellier II
Pl. E. Bataillon - Case 70
F-34095 Montpellier Cedex 05

Prof. Dr. John C. Schotland
Dept. of Bioengineering
University of Pennsylvania
Philadelphia, PA 19104
USA

PD.Dr. Thomas Schuster
Universität des Saarlandes
Institut für Angewandte Mathematik
Postfach 151150
66041 Saarbrücken

Prof. Dr. Jan-Olov Strömberg
Dept. of Mathematics
Royal Institute of Technology
Lindstedtsvägen 25
S-100 44 Stockholm

PD Dr. Gerd Teschke
Konrad-Zuse-Zentrum für
Informationstechnik Berlin (ZIB)
Takustr. 7
14195 Berlin

Dr. Frank Wübbeling
Institut für Numerische und
Angewandte Mathematik
Universität Münster
Einsteinstr. 62
48149 Münster